

Louisiana Tech University

Louisiana Tech Digital Commons

Doctoral Dissertations

Graduate School

Summer 8-16-2018

Development and Analysis of Engineered Brain Cell Microenvironments Mimicking Healthy and Diseased Neuronal Circuits

Kahla St. Marthe
Louisiana Tech University

Follow this and additional works at: <https://digitalcommons.latech.edu/dissertations>

Recommended Citation

St. Marthe, Kahla, "" (2018). *Dissertation*. 26.
<https://digitalcommons.latech.edu/dissertations/26>

This Dissertation is brought to you for free and open access by the Graduate School at Louisiana Tech Digital Commons. It has been accepted for inclusion in Doctoral Dissertations by an authorized administrator of Louisiana Tech Digital Commons. For more information, please contact digitalcommons@latech.edu.

Summer 8-16-2018

Development and Analysis of Engineered Brain Cell Microenvironments Mimicking Healthy and Diseased Neuronal Circuits

Kahla St. Marthe
Louisiana Tech University

Follow this and additional works at: <https://digitalcommons.latech.edu/dissertations>

Recommended Citation

St. Marthe, Kahla, "" (2018). *Dissertation*. 26.
<https://digitalcommons.latech.edu/dissertations/26>

This Dissertation is brought to you for free and open access by the Graduate School at Louisiana Tech Digital Commons. It has been accepted for inclusion in Doctoral Dissertations by an authorized administrator of Louisiana Tech Digital Commons. For more information, please contact digitalcommons@latech.edu.

**DEVELOPMENT AND ANALYSIS OF ENGINEERED BRAIN
CELL MICROENVIRONMENTS MIMICKING HEALTHY
AND DISEASED NEURONAL CIRCUITS**

by

Kahla St. Marthe, B.S., M.S.

A Dissertation Presented in Partial Fulfillment
of the Requirements for the Degree
Doctor of Philosophy

COLLEGE OF ENGINEERING AND SCIENCE
LOUISIANA TECH UNIVERSITY

August 2018

LOUISIANA TECH UNIVERSITY

THE GRADUATE SCHOOL

JUNE 28, 2018

Date

We hereby recommend that the dissertation prepared under our supervision by

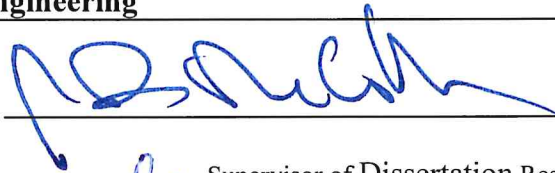
Kahla St. Marthe, B.S., M.S.

entitled Development and Analysis of Brain Cell Microenvironments

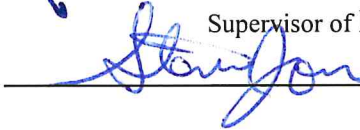
Mimicking Healthy and Diseased Neuronal Circuits.

be accepted in partial fulfillment of the requirements for the Degree of

Doctor of Philosophy in Biomedical Engineering



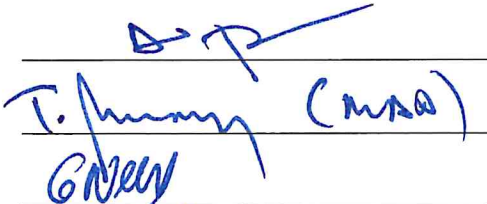
Supervisor of Dissertation Research



Head of Department

Department

Recommendation concurred in:



T. Jimmy (MSA)

Advisory Committee

Approved:



Director of Graduate Studies

Approved:



Dean of the Graduate School



Dean of the College

ABSTRACT

Astrocytes and microglia (glial cells) are active elements of the brain maintaining numerous homeostatic functions. Disturbances result in worsening of neuro-inflammation, traumatic brain injury, and various stages of brain tumors. Glial cells contribute to homeostasis for dynamic second messengers in the CNS, including intracellular calcium concentration ($[Ca^{2+}]_i$). Calcium is a central secondary messenger which signals for example, through the N-methyl-D-aspartate (NMDA) glutamate receptor on the neuronal membrane. A large, dynamic Ca^{2+} influx ensues after glutamate binds to the NMDA receptor. This influx initiates several molecular mechanisms within the cell. Disturbances in calcium homeostasis can lead to neurological diseases such as epilepsy and major depressive disorder.

In this project, we set out to gain a better understanding of the effect of glial density on neural signalling. This was done by accomplishing four main objectives:

1. Develop neural micro-environments with quantifiable variations in glial cell densities.
2. Use calcium imaging methods to analyze the calcium information processing capacity of the various neural micro-environment developed.
3. Develop mathematical tools for testing calcium dynamics

4. Study short term and interactions of novel biomaterial (CuHARS) used for tissue engineering in brain cell micro-environments (Ca^{+2} signaling as an indicator of cell “health”)

To do so, tissue engineered microenvironments were constructed to test the effects of the glial cell density have on calcium information processing. We investigated the response of glia rich, mildly glia depleted, partially depleted, and severely depleted neuronal cultures to sub-maximal (nM to μM) glutamate concentrations using calcium imaging. This was used to assist in predicting and interpreting chaotic neural networks experimentally. Anti-mitotic agents, cytosine arabinoside (AraC), or 2-deoxy-5-fluorouridine (FdU) were used to inhibit proliferating glia and develop the three classes of glia density. Imaging was done with Fluo 3/AM, nine to fourteen days after plating. Neuronal cultures severely depleted (greater than sixty percent depletion) of glia responded to increasing glutamate additions with large, slightly unsynchronized responses with the greatest area under the curve (AUC) observed which returned to baseline the slowest of the three micro-environments developed. Cultures partially depleted (thirty to sixty percent depletion) of glia, responded to increasing glutamate addition with mid-sized, synchronized responses with lower AUC than cultures with severely depleted glial cells. Mildly depleted cultures behaved similarly to glia rich cultures. The difference between their AUC was not statistically significant. Studying how the brain behaves in altered systems, such as in glia depleted micro-environments will help us explore cell loss in the brain and develop more targeted protective strategies.

APPROVAL FOR SCHOLARLY DISSEMINATION

The author grants to the Prescott Memorial Library of Louisiana Tech University the right to reproduce, by appropriate methods, upon request, any or all portions of this Dissertation. It is understood that “proper request” consists of the agreement, on the part of the requesting party, that said reproduction is for his personal use and that subsequent reproduction will not occur without written approval of the author of this Dissertation. Further, any portions of the Dissertation used in books, papers, and other works must be appropriately referenced to this Dissertation.

Finally, the author of this Dissertation reserves the right to publish freely, in the literature, at any time, any or all portions of this Dissertation.

Author _____

Date _____

DEDICATION

I dedicate this to my mother “Teacher Pearl”, your example of unwavering resilience has given me the strength to overcome every obstacle faced in my academic pursuits. I also dedicate this to my dear deceased cousin Jamal, my first research partner. I know you would be proud to see your “twin towel” graduate with her doctoral degree.

TABLE OF CONTENTS

| | |
|---|------|
| ABSTRACT..... | iii |
| APPROVAL FOR SCHOLARLY DISSEMINATION | v |
| DEDICATION | vi |
| LIST OF TABLES | xi |
| LIST OF FIGURES | xii |
| ACKNOWLEDGMENTS | xvii |
| CHAPTER 1 INTRODUCTION | 1 |
| 1.1 Project Overview | 1 |
| 1.2 Overview of the Nervous System | 2 |
| 1.3 Neural Circuits | 3 |
| 1.4 Neuron-Glia Interactions | 9 |
| 1.4.1 Glia and Glutamate Transmission..... | 11 |
| 1.5 Neural Calcium Dynamics..... | 12 |
| 1.5.1 Voltage Gated Calcium Channels..... | 15 |
| 1.5.2 Ligand Gated Calcium Channels | 16 |
| 1.5.3 Glutamate Receptors involved in Calcium Signalling..... | 17 |
| 1.5.4 Calcium Mediated Cell Death..... | 18 |
| 1.5.5 Calcium Dependent Excitotoxicity | 21 |
| 1.5.6 Glutamate Induced Calcium Fluorescence | 23 |
| 1.5.7 Calcium Imaging..... | 23 |
| 1.6 Neurological Diseases Associated with Glial Anomalies..... | 27 |

| | | |
|---|--|----|
| 1.6.1 | Epilepsy..... | 27 |
| 1.6.2 | Parkinson’s Disease | 29 |
| 1.6.3 | Major Depressive Disorder | 30 |
| CHAPTER 2 TISSUE ENGINEERED MICROENVIRONMENTS | | 31 |
| 2.1 | Overview..... | 31 |
| 2.2 | Background..... | 31 |
| 2.3 | Primary Cortical Culture Protocol | 32 |
| 2.4 | Development of Quantifiable Neural Cell Micro-Environments | 33 |
| 2.4.1 | Developing severely depleted micro-environments using cytosine arabinoside | 34 |
| 2.4.2 | Developing Micro-environments using novel method | 43 |
| 2.4.3 | Assessing Metabolic Activity of Various Brain Cell Micro-environments.. | 44 |
| CHAPTER 3 CALCIUM IMAGING | | 48 |
| 3.1 | Overview..... | 48 |
| 3.2 | Calcium Fluorescence Imaging | 48 |
| 3.2.1 | Preparation and Loading of Calcium Dye | 50 |
| 3.2.2 | Measuring and Analyzing Calcium Fluorescence Intensity | 52 |
| 3.3 | Image Analysis | 67 |
| 3.3.1 | Area Under the Curve | 67 |
| CHAPTER 4 MATHEMATICAL TOOLS | | 74 |
| 4.1 | Introduction..... | 74 |
| 4.2 | Modeling each phase after glutamate stimulation | 75 |
| | | 77 |
| CHAPTER 5 CELLULAR INTERACTION WITH NOVEL BIOMATERIALS..... | | 82 |
| 5.1 | Introduction..... | 82 |
| 5.2 | Biomaterials Used in Neuroscience | 83 |

| | | |
|--|--|-----|
| 5.2.1 | Quantum Dots | 83 |
| 5.3 | Copper Homeostasis in the CNS | 85 |
| 5.3.1 | Copper containing High Aspect Ratio Structures | 88 |
| 5.3.2 | Biocompatibility of CuHARS..... | 89 |
| 5.3.3 | Functionalization of CuHARS using Layer by Layer Assembly..... | 91 |
| CHAPTER 6 CONCLUSIONS AND FUTURE WORK..... | | 100 |
| 6.1 | Conclusions..... | 100 |
| 6.2 | Future Work | 101 |
| APPENDIX A..... | | 104 |
| A1 | Rat Primary Cervical Disarticulation: IACUC Approved | 105 |
| A2 | Fluo3/AM Loading: | 108 |
| APPENDIX B | | 115 |
| APPENDIX C | | 125 |
| C.2 | Dynamic Models of Neuron: Astrocyte Interaction..... | 126 |
| C2.1 | The Neuron Model | 126 |
| C2.2 | The Astrocyte Model..... | 128 |
| C2.3 | Modeling Astrocyte Interactions with Two Coupled Neurons | 130 |
| C2.4 | Computational Analysis of Neural Synchrony..... | 132 |
| C2.4 | Neural Population Model | 133 |
| C2.5 | Astrocyte model for the neural population..... | 135 |
| C2.6 | Astrocyte -Neuron interaction for the neural population | 136 |
| Bibliography | | 139 |

LIST OF TABLES

| | |
|--|----|
| Table 2-1: Neural Microenvironment Classification..... | 60 |
| Table 4-1: Parameter values used in the simulations..... | 84 |
| Table 4-2: Parameters used in the simulation of the extended neural population model..... | 91 |

LIST OF FIGURES

| | |
|---|----|
| Figure 1-1: Diagram showing different types of neurons. (Left) A purkinke cells of the cerebral cortex and (right) a pyramidal neuron of the neocortex..... | 4 |
| Figure 1-2: A simplified schematic illustrating the positive: negative feedback system of glutamate transmission and re-uptake within the synapse..... | 7 |
| Figure 1-3: Dynamic interaction of microglial processes with tripartite synapse. (A) Microglial processes (red) dynamically contact the cellular compartments of the synapse pre- and postsynaptic neuronal terminals (in brown) as well as the enwrapping perisynaptic astroglial process (in blue). (B) The electron micrograph (EM) specifically shows a microglial process (m) contacting both the pre- and postsynaptic compartment... .. | 8 |
| Figure 1-4: Diagram showing one example of the coordinated action of neuron-glia interaction in the CNS..... | 10 |
| Figure 1-5: Diagram showing signal transduction by voltage gated Ca^{2+} channels..... | 13 |
| Figure 1-6: Diagram highlighting subunits of voltage gated calcium channels. | 15 |
| Figure 1-7: Diagram showing HVA and LVA channel subunit compositions..... | 16 |
| Figure 1-8: Diagram showing receptors involved in calcium signaling on neuronal and glial membranes: purple (NMDA), blue (AMPA), green (KA), pink (GABA), green (mGLUR 1/5), blue (mGLUR2/3), and burgundy (mGLUR 4/7/8). Calcium is a key signaling ion involved in memory and learning with NMDA receptors on the neuronal membrane..... | 18 |
| Figure 1-9: Diagram showing the involvement of calcium/ calpain in AIF processing | 20 |
| Figure 1-10: A schematic representation of Ca^{2+} homeostasis in neurons. | 22 |
| Figure 1-11: Calcium deregulation leading to neurodegenerative diseases | 27 |
| Figure 1-12: Diagram depicting some of the major metabolic pathways and tissue compartments involved in normal homeostasis of brain glu. The dashed frames indicate areas being affected in epilepsy | 29 |
| Figure 2-1: Schematic outlining the different steps used to develop various brain cell microenvironments. | 34 |

| | |
|--|----|
| Figure 2-2: Structure of Cytosine Arabinoside (AraC). | 35 |
| Figure 2-3: Image showing mixed cortical neuronal cultures with and without AraC treatment. A: Phase image of primary cortical cultures high in glia (No AraC treatment) B: Phase image of primary cortical cultures low in glia (AraC treatment). | 36 |
| Figure 2-4: Graph showing the effect of adding AraC on the number of cells within the mixed glial (astrocytes and microglia) cell cultures field of analysis. Data is shown as mean plus standard deviation (sd). | 37 |
| Figure 2-5: Overview of the protocol for preparing mixed glial cell cultures and isolation of primary astrocytes..... | 38 |
| Figure 2-6: Phase-contrast microscopy of: (A) primary astrocytes; (B) primary microglia; (C) mixed culture of astrocytes and microglia. | 38 |
| Figure 2-7: Graph showing the effect of adding AraC to the number of cells within the pure astrocyte culture's field of analysis. (Error bars = Standard Deviation) | 40 |
| Figure 2-8: Graph showing the effect of adding AraC on the number of cells within mixed neuronal culture's (neurons, astrocytes, and microglia) field of analysis. (Error bars = Standard Deviation) | 41 |
| Figure 2-9: Graph showing percent depletion of astrocytes treated with different concentrations of 2-deoxy-5-fluorouridine (FdU). These values have been normalized to the % of the cell density of untreated cells. The data is given as the mean± sd of three independent experiments. Since the sample size varied for each experiment, the significance of changes in the treatment responses was assessed using the Tukey-Kramer multiple comparison test; differences were considered statistically significant at P<0.05. | 43 |
| Figure 2-10: Schematic showing the conversion of MTT (yellow) to Formazan (blue/purple) via mitochondrial reductases..... | 44 |
| Figure 2-11: Graph showing survival percent of mixed glial cultures treated with different concentrations of FdU. These values have been normalized to the percent of the cell density of untreated cells. The data is given as the mean± sd of three independent experiments. Since the sample size varied for each experiment, the significance of changes in the treatment responses was assessed using the Tukey-Kramer multiple comparison test; differences were considered statistically significant at P<0.05, n=18. | 45 |
| Figure 3-1: Stimulation protocol for most experiments. Glutamate is added into the experiment at equally defined times and at three concentrations. Each concentration is added at a set treatment number without washing the glutamate out of the well. | 48 |
| Figure 3-2: Structure of Ionomycin. | 51 |

| | |
|---|----|
| Figure 3-3: One example of the line tracings derived from a calcium imaging experiment..... | 52 |
| Figure 3-4: Line tracings of primary neuronal cortical cultures high in glia response to additions of 250nM, 500nM and 750nM glu additions. Top Panel: Each line represents individual cells (ROIs). Bottom Panel: Average of all ROIs..... | 54 |
| Figure 3-5: Line tracings of primary neuronal cortical cultures with mildly depleted glia response to additions of 250nM, 500nM and 750nM glu. Top Panel: Each line represents individual cells (ROIs). Bottom Panel: Average of all ROIs. | 55 |
| Figure 3-6: Line tracings of primary neuronal cortical cultures with partially depleted glia response to additions of 250nM, 500nM and 750nM glu. Top Panel: Each line represents individual cells (ROIs). Bottom Panel: Average of all ROIs | 56 |
| Figure 3-7: Line tracings of primary neuronal cortical cultures with severely depleted glia response to additions of 250nM, 500nM and 750nM glu. Top Panel: Each line represents individual cells (ROIs). Bottom Panel: Average of all ROIs. | 57 |
| Figure 3-8: : Line tracings of primary mixed glial cortical cultures responses to additions of 100 μ M glu. Top Panel: Each line represents individual cells (ROIs). Bottom Panel: Average of all ROIs. | 58 |
| Figure 3-9: Line tracings of mildly depleted primary mixed glial cortical cultures responding to additions of 100 μ M glu. Top Panel: Each line represents individual cells (ROIs). Bottom Panel: Average of all ROIs | 59 |
| Figure 3-10: Line tracings of partially depleted primary mixed glia cortical cultures responding to an addition of 100 μ M glu. Top Panel: Each line represents individual cells (ROIs). Bottom Panel: Average of all ROIs..... | 60 |
| Figure 3-11: Line tracings of severely depleted primary mixed glia cortical cultures responding to an addition of 100 μ M glu. Top Panel: Each line represents individual cells (ROIs). Bottom Panel: Average of all ROIs..... | 61 |
| Figure 3-12: Line tracings of pure astrocyte cortical cultures responding to an addition of 100 μ M glu. Top Panel: Each line represents individual cells (ROIs). Bottom Panel: Average of all ROIs. | 62 |
| Figure 3-13: Line tracings of mildly depleted primary pure cortical astrocyte cultures response to additions of 100 μ M glu concentrations. Top Panel: Each line represents individual cells (ROIs). Bottom Panel: Average of all ROIs..... | 63 |
| Figure 3-14: Line tracings of partially depleted primary pure cortical astrocyte cultures response to additions of 100 μ M glu concentrations. Top Panel: Each line represents individual cells (ROIs). Bottom Panel: Average of all ROIs..... | 64 |

| | |
|--|----|
| Figure 3-15: Line tracings of severely depleted primary cortical pure astrocyte cultures response to additions of 100 μ M glu concentrations. Top Panel: Each line represents individual cells (ROIs). Bottom Panel: Average of all ROIs..... | 65 |
| Figure 3-16: Area under the curve (AUC) in response to glutamate treatments to mixed neuronal cultures high in glia (control), mildly glia depleted (MD) and partially depleted (PD).. | 67 |
| Figure 3-17: Area under the curve (AUC) in response to glutamate treatments to mixed neuronal cultures severely glia depleted (SD). | 68 |
| Figure 3-18: Area under the curve (AUC) in response to glutamate treatments to mixed glial cultures high in astrocyte (control), mildly depleted (MD) and partially depleted (PD)..... | 69 |
| Figure 3-19: Area under the curve (AUC) in response to glutamate treatments to pure astrocyte cultures high in astrocyte (control), mildly depleted (MD) and partially depleted (PD). | 70 |
| Figure 4-1: Plots of (a) averaged baseline response, (b) baseline response modeled by $x_{t+1}=3.7x_t(1-x_t)+0.3$. For all equations, x_t is the fluorescence at any given time, t , and t_i is the time since the introduction of the stimulus. | 73 |
| Figure 4-2: Plots (a) averaged immediate response to the glutamate, (b) response to glutamate modeled by $x_t=13t_i-12$. For all equations, x_t is the fluorescence at any given time, t , and t_i is the time since the introduction of the stimulus..... | 74 |
| Figure 4-3: Plots (a) averaged fluorescence during the recovery period, and (b) recovery period modeled by $x_t=14e^{-0.14t_i}+1$. For all equations, x_t is the fluorescence at any given time, t , and t_i is the time since the introduction of the stimulus..... | 75 |
| Figure 4-4: Graph showing waveform derived from Eqn. 4-49 . | 76 |
| Figure 4-5: Graph showing wave- form derived from Eqn. 4-50..... | 77 |
| Figure 5-1: Diagram showing structure of semiconductor fluorescent quantum dot nanocrystal (86) | 79 |
| Figure 5-2: Diagram showing summary of copper uptake in astrocytes (93) | 82 |
| Figure 5-3: Diagram of proposed model of astrocytic copper supply to neurons (93).... | 83 |
| Figure 5-4: Effect of varying CuHARS concentration on mitochondrial toxicity of PC12 cells A) Copper Nanoparticle (CuNP) treatment. B) CuHARS treatment. Y: Axis values=Relative Absorbance normalized to the controls (no treatment). | 85 |

- Figure 5-5:** Schematic illustrating distribution of CuHARS throughout individual wells in the 48 well cell culture treated plate. Left) PLL coated CuHARS, Right) Uncoated CuHARS..... 86
- Figure 5-6:** Images showing PLL coated and uncoated CuHARS association with edge of the well in a 48 well cell culture treated well. Left) (Top and bottom) Uncoated CuHARS, Right) (Top and bottom) PLL coated CuHARS. White arrows indicate edges. Scale Bar = 100 μ m. 87
- Figure 5-7:** Diagram showing the structure of A23187 at the free acid. The two structures are in “open and closed” conformation, respectively (top to bottom) (101).... 88
- Figure 5-8:** Images illustrating Uncoated CuHARS and their association with CRL 2303 cells. Left (Top and bottom) Bright Field images highlighting CuHARS; Right (Top and Bottom) Phase contrast images of the same area of highlighting cells. Scale Bars = 100 μ m..... 89
- Figure 5-9:** Images illustrating PLL-coated CuHARS and their association with CRL 2303 cells. Left (Top and bottom) Bright Field images highlighting CuHARS; Right (Top and Bottom) Phase contrast images of the same area of highlighting cells. Scale Bars = 100 μ m..... 90
- Figure 5-10:** I Zoomed in Phase image of uncoated CuHARS and their association with CRL 2303 cells. Scale Bars = 100 μ m. White Arrows = CuHARS
..... 91
- Figure 5-1:** I Zoomed in Phase image of PLL-coated CuHARS and their association with CRL 2303 cells. Scale Bars = 100 μ m. White Arrows = CuHARS
..... 92
- Figure 6-1:** Schematic illustrating the steps needed to successfully functionalize and confirm ionophore coated CuHARS. Blue lines have been completed and red lines will be done in future work.. 93

ACKNOWLEDGMENTS

Graduate school has been a fascinating experience and there are several people who have contributed to this journey. None of this work would have been possible without the support of my advisor, Dr. Mark A. DeCoster and I thank him for his exemplary scientific training, advice, expertise and mentoring. I leave this lab a competent scientist in and out of the lab as a result. I am grateful to my committee members: Dr. Theresa Murray, Dr. Bryant Hollins, Dr. Prabhu, Dr. David Mills and Dr. Gergana Nestorova for their scientific insight and support.

I would like to thank my lab-mates for all their help and for consistently prioritizing collaboration over competition. I am hugely indebted to Nam Nguyen for always finding time to assist me with planning and executing many of my experiments. Nam has been an in-lab confidante and I will be forever grateful for his assistance throughout my time in the lab. I would like to express my gratitude to my immediate family members: George, Pearl, Kahlil and Kahleen Ste Marthe for their continued support and encouragement during my educational pursuits. I also thank my closest friends Kerneisha Murphy, Grace Joseph and Tiffany Victor, for being supportive and believing in me when I had lost faith in myself. I thank my boyfriend, Jan Durand for being an unlimited vault for my many venting sessions. Unbeknownst to him, having to explain what happened during my day taught me to communicate my research in the most concise manner without losing necessary technical detail. I also thank him for fulfilling his designated nag duties

during the writing process. With his constant reminders, I was able to write my dissertation in a timely manner and reach my personal deadline.

I end by thanking the one who made this all possible, my heavenly father. I thank him for my health, strength, and the ability to understand, learn and complete this project.

CHAPTER 1

INTRODUCTION

1.1 Project Overview

Disorders of the brain and central nervous system account for more hospitalizations and loss of productivity than any other group of diseases including cancer and heart disease. In 2006, the World Health Organization (WHO) estimated that over one billion persons were affected directly or indirectly by neurological disorders ranging from epilepsy and Alzheimer's disease to migraine headaches and stroke (1).

The uniqueness and variance of each higher brain makes neuroscience a very widely studied scientific field. A precise pre-specified point to point description of the wiring of each section of the brain has yet to be discovered. There are generalities however, which are currently being studied. Anatomical and physiological interactions between neuronal and non-neuronal cells, like astrocytes (2) and microglia (3) are being studied, and many insightful discoveries have been made in recent years. Our lab has been using calcium signaling as an indicator of interactions between brain cells in culture. This project is a continuation of our long-standing interest in brain cell calcium dynamics with engineered environments coupled with applied mathematical tools and computerized programs which will assist in broadening our understanding of processing dynamics in the

neuronal circuit. We wish to gain insight into neurological diseases linked to altered glial cell densities and the resulting deregulated homeostatic calcium levels.

1.2 Overview of the Nervous System

Studies of the nervous system date back to the middle of the nineteenth century when neuroanatomists studied the morphology, cellular structure, and circuitry of the brain. Scientists were also interested in understanding the chemical composition and bioelectric properties of the nervous system with the goal of linking all these properties to specific phenotypic expressions. Over time and many experiments later, neuroscience is now described as a data rich and theory poor discipline (4). Many breakthroughs have been made, but we have not been able to develop molecule to behavior definitions for behavioral expressions and neurological conditions such as Alzheimer's and Parkinson's disease. Although lots of data has been generated, the neuronal network level of neuroscience is data poor (4). To make some headway in understanding the many complexities of the nervous system at micro and macro scales requires new computational and experimental techniques and tools. These tools will be vital for obtaining and analyzing data at the various levels.

Our nervous system consists of many connections that send signals throughout the body to control several voluntary and involuntary actions. The nervous system is made up of the central and peripheral nervous system. The central nervous system (CNS) comprises the brain and spinal cord and the peripheral nervous system (PNS) consist of nerves and ganglia outside of the brain and spinal cord. The brain serves as the central organ of the nervous system and is involved in regulating many significant processes needed for the healthy functioning of the human body.

1.3 Neural Circuits

The brain is made of copious interconnected neural microcircuits, each made up of neurons, glial cells, and synapses. The neurons are the major processing units of the brain and glial cells perform many regulatory and supportive functions in the central nervous system (CNS). These heterogeneously shaped, highly secretory active cells are sometimes referred to as the basic building blocks of the nervous system. Neurons are interconnected, highly differentiated, bioelectrically driven, cellular units that communicate via electrochemical signals that are generated and propagated via several mechanisms.

These cells are classified in many ways ranging from their function (sensory, motor, interneuron) to the neurotransmitter synthesized and released by that cell (cholinergic or glutaminergic neurons) to something as simple as their morphology (pyramidal neurons). Typically, neurons can be separated into three main groups: inhibitory neurons (e.g. GABA interneurons), excitatory neurons (e.g. pyramidal neurons using glutamate) and neuromodulatory neurons that are involved in neurotransmission. Neurons are polarized (consist of various sub-cellular domains with varied functions) cells made up of three main components, the cell body, axon, and dendrites.

There are precise cytological characteristics associated with the secretory property of neurons such as large nuclei, substantial amounts of Golgi clusters and many smooth and rough endoplasmic reticulum. Each component of the neuron (axon, cell body and dendrites) are rich in microtubules that support the elongated structures (axons and dendrites) and facilitate the movement of essential substrates between the cell body and the elongated structures. The dendrites are branched treelike structures extending at the end of the axons or cell body which ramify over certain volume of grey matter. Figure 1.1 shows

three distinct types of neurons classified by morphology and location (pyramidal and purkinje, respectively)

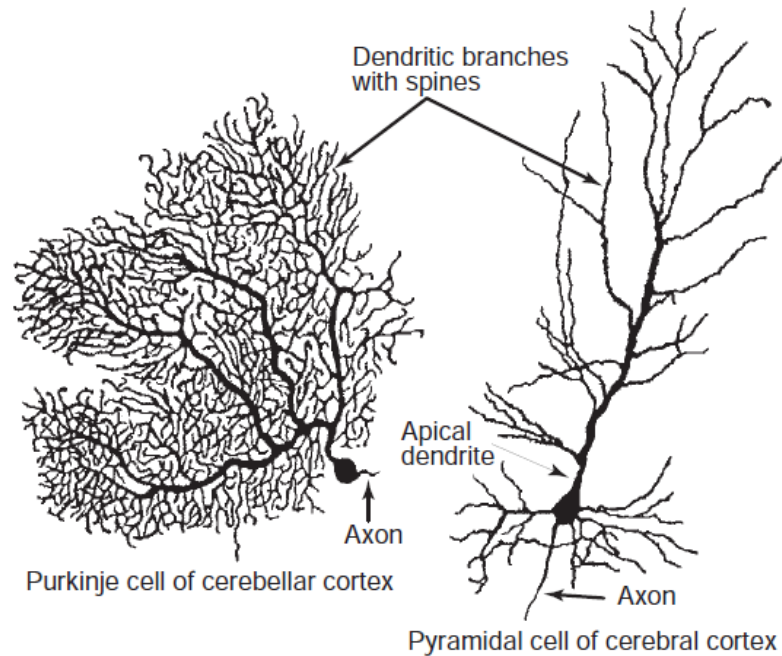


Figure 1-1: Diagram showing different types of neurons. (Left) A purkinje cell of the cerebellar cortex and (right) a pyramidal neuron of the neocortex. (5).

Non-neuronal cells include microglia, astrocytes, cells that make up the vasculature of the brain, cells of the choroid plexus, and meninges, the sheets of connective tissue that cover the surface of the brain and comprise the cerebrospinal fluid-containing envelope that protects the brain within the skull. There are many glial cells in the brain, with many estimates indicating at least as many as the number of total neurons (5). The main types of glial cells found in the CNS are astrocytes, oligodendrocytes, and microglia. Schwann cells are the predominant glial cells in the

PNS. The two most abundant glial cells in the CNS are astrocytes and microglia. The first description of glial cells was made in 1846 by a German Rudolf Virchow, who named them neuroglia meaning “nerve glue”. For decades, these glial cells were thought to play passively supportive roles to neurons, however, recent evidence strongly suggest that these cells are actively involved in signal transmission and processing(6). This evidence has introduced a new idea that the brain is not only an array of interconnected neural networks but numerous integrated circuits of neurons and glia(7).

Astrocytes are the most abundant multifunctional glial cells in the CNS (8); collectively called astroglia and are found mostly between the vasculature and the neuron or surrounding synapses. They play a significant role in brain homeostasis, via several metabolic processes established with neurons such as, removal of excessive extracellular neurotransmitter via uptake, break-down and recycling; and supplying neurons with energy metabolites. Gap junctions extensively couple these astroglia to form a functional syncytium that facilitates exchange between neighboring cells. Astrocytes signal and sense changes in the synapse via regulated pathways of neurotransmitter release, they also control its ionic environment. One of these regulatory pathways is illustrated in Figure 1-2.

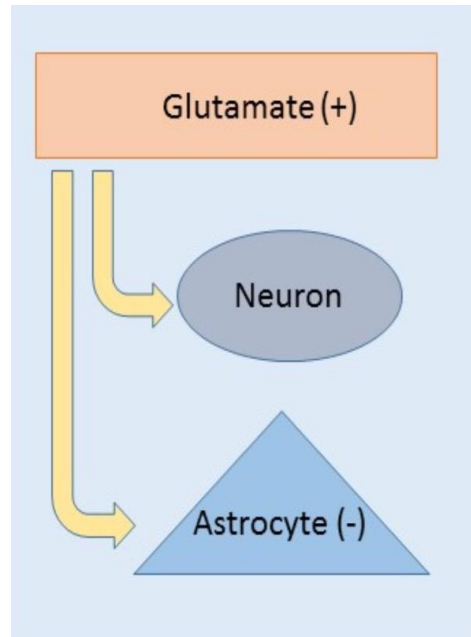


Figure 1-2: A simplified schematic illustrating the positive: negative feedback system of glutamate transmission and re-uptake within the synapse

Astrocytes also regulate neurotransmitter release and uptake by removing and recycling neurotransmitters that are released in the synapse which prevents excitotoxicity (uncontrolled neuronal stimulation). The uptake of neurotransmitter by astrocytes also modifies the signal strength from one neuron to the next. It is now known that astrocytes outnumber neurons within the brain; however, the ratio of the two cell types varies with location and species. Astrocytes are also known to have large glycogen deposits, which allow them to produce lactate, an energy source for neurons. Furthermore, astrocytes maintain proliferation abilities, making them easy to work with in cell culture. Recently, a growing number of researchers have found that astrocytes are also excitable cells (contrary to the belief that only neurons were excitable) and play an important role in brain information processing (9). The main mechanisms

modulating the tripartite synapse are as follows: neurotransmitters (glutamate), released from presynaptic neuron during its activation, are bound to the metabotropic glutamate receptors (mGluR) on the astrocytes adjacent to synaptic terminals. This causes the synthesis of the second messenger, inositol (1,4,5)-trisphosphate (IP₃) and the movement of calcium from the endoplasmic reticulum (ER) to the cytoplasm. The increased cytoplasmic calcium also takes place in nearby astrocytes as intercellular calcium waves that take place with the passage of second messengers through gap junctions. Due to the increased intracellular Ca²⁺ concentration, the astrocyte releases gliotransmitters, such as glutamate (glu) and ATP into the extracellular space and thereby can regulate pre- and postsynaptic neurons.

Microglia are not as well described as other brain cells; discoveries have shown that these cells are more than likely from mesodermal origin. Microglia are the resident macrophage-like cells in the brain and function as the endogenous immune system of the CNS. These cells originate from bone marrow derived monocytes that enter the brain during the developmental stage. Once the blood brain barrier is formed, they become the exclusive immune cells of the brain. Microglia are evenly dispersed throughout the brain and can phagocytose, migrate, and proliferate as the need arises. Microglia are typically in a quiescent state characterized by small processes. In this basal or resting condition, microglia survey the surrounding environment with their ramified morphologies used for dynamic surveying movements. During periods of intracerebral inflammation (e.g., infection, certain degenerative diseases, or traumatic injury), activated microglia extend more processes that are notably thicker, which aids the cell in detecting pathogens. Microglia also have an amoeboid-like state which is

associated with its role as a phagocytic cell. In addition to the recruitment of microglia to sites of intracerebral inflammation, circulating macrophages and other white-blood cells enter the brain via endothelial signals to remove necrotic tissue or to defend against the microbial infection. Under normal conditions, microglial surveilling processes interact with synaptic structures (Figure 1-3).

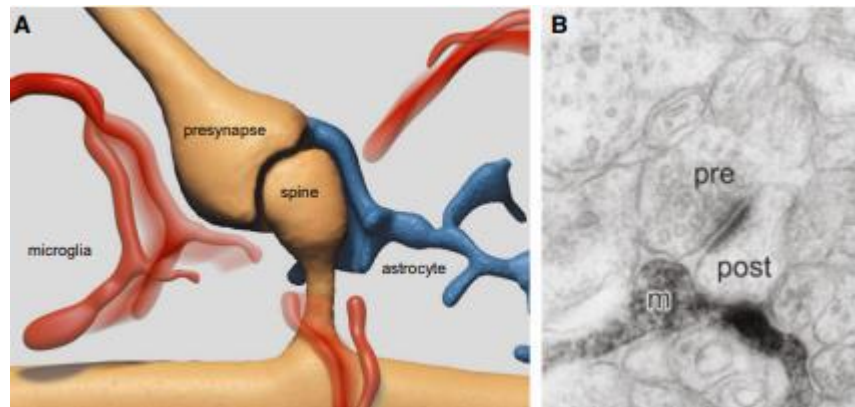


Figure 1-3: Dynamic interaction of microglial processes with tripartite synapse. (A) Microglial processes (red) dynamically contact the cellular compartments of the synapse pre- and postsynaptic neuronal terminals (in brown) as well as the enwrapping perisynaptic astroglial process (in blue) (10). (B) The electron micrograph (EM) specifically shows a microglial process (m) contacting both the pre- and postsynaptic compartment. The EM image is modified from (11).

The synapse is made up of three components: a pre-synaptic neuronal element, a post-synaptic neuronal element, and the synaptic cleft. The presynaptic element is a specialized portion of the pre-synaptic neuron's axon, the synaptic cleft is the space between the pre and post synaptic elements and the post synaptic element is a specialized portion of the post synaptic somato-dendritic membrane. The pre-synaptic part of the axon is identified by the formation of vesicles and thickening at the active

site, the post synaptic site is also identified by thickening. If the thickening at the pre and post synaptic membrane is equal the synapse is referred to as symmetric when the post synaptic active site is thicker it is called asymmetric. Astrocytes are generally described as synaptic support cells (12) as they remove neurotransmitters such as glutamate and ions from the synapse after synaptic transmission from neuron to neuron takes place. Recently, evidence suggests that they play a more active role in synaptic transmission. One study showed evidence of enhanced synaptic activity by retinal ganglion cells (RGC) cultured with astroglial cells as compared with RGCs grown in purified cultures. In fact, in the purified cultures, little synaptic activity occurred (12).

1.4 Neuron-Glia Interactions

Neuronal networks are the organizational matrix that connects neurons to larger organ systems and without understanding how these networks function, it is difficult to explain how the larger systems communicate. The cells in the brain form microcircuits that communicate via electrochemical signals. One example of this signal transduction is shown in Figure 1-4.

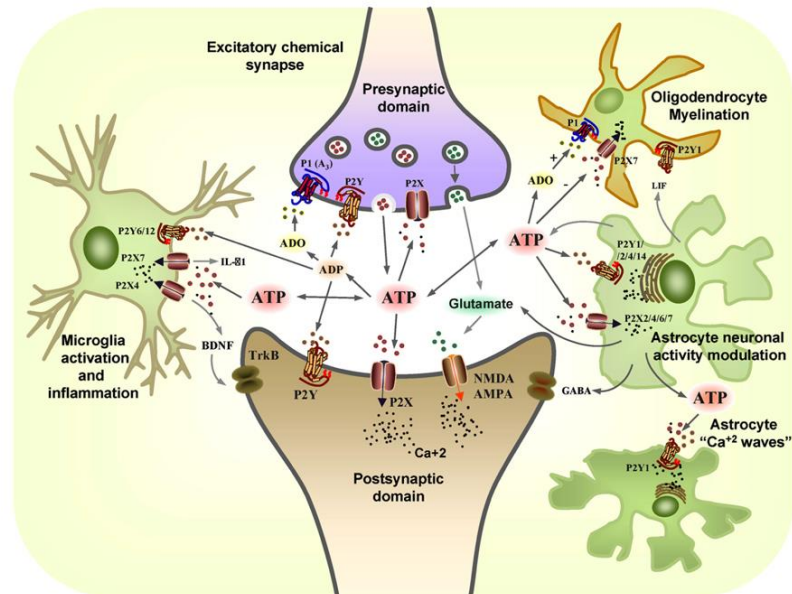


Figure 1-4: Diagram showing one example of the coordinated action of neuron-glia interaction in the CNS (13)

These circuits constitute the structural basis for brain function. Neural circuits can be categorized by the number of connections; macro-circuits comprise groups of neurons projecting from one part of the brain to another and micro-circuits involve local neuronal connections with a brain region. Detailed studies micro and macro circuits are essential in understanding the neural basis for cortical function in healthy and diseased brains. Mammalian brains contain neurons as numerous as one hundred million to one hundred billion depending on the species. Increasing evidence demonstrates the existence of bidirectional communication between neurons and their surrounding glial cells. Neurotransmission in neurons can illicit an increase in intracellular calcium concentration in adjacent glial cells. Activated glia can in turn release neurotransmitters that can feed

back to neuronal synaptic elements thus regulating the postsynaptic neuronal excitability and modulating neurotransmitter release from presynaptic terminals. Alterations in glial density may elicit profound changes on the functionality of their associated neuronal circuits and cause nerve cell damage.

1.4.1 Glia and Glutamate Transmission

Glutamate is one of the most important excitatory neurotransmitters responsible for brain homeostasis. It excites the neuron in part by causing large dynamic changes in intracellular calcium concentration. This neurotransmitter is clinically relevant because, elevated glutamate concentrations in the extracellular space are toxic.

One signaling pathway of interest is the release and uptake of glutamate and the cascade of electrochemical events that ensue. Upon release from the pre-synaptic membrane, glutamate is bound by receptors on the post synaptic membrane which causes an influx of calcium ions in the post synaptic neuron on which the glutamate is bound. This calcium influx, if sufficiently strong, initiates an action potential which relays an electrical signal to the post synaptic neuron. This signal can be propagated from neuron to neuron in very small to very large networks. The excess glutamate in the synapse is removed and recycled by the astrocytes. Astrocyte uptake and recycling prevents excitotoxicity which can cause seizures. Glutamate is also removed from the synapse via several high affinity glutamate transporters in presynaptic terminals. Approximately five to fifteen mmol of free glutamate per kg weight is present in the brain (14). This is more than one thousand times the amount needed to activate glu receptors therefore most of the glu in the brain is stored in intracellular compartments and there are many mechanisms to regulate extracellular glutamate levels.

As mentioned earlier, microglia are the innate immune cells of the brain and are involved in all CNS diseases. In pathological conditions, these cells are converted from their surveillant state to an activated state that operates within the diseased conditions. Microglial cells express various receptors for neurotransmitters, neuromodulators, and neuropeptides to sense neuronal activity. Scientists have found that cultured microglia express adrenergic receptors, metabotropic and ionotropic glutamate and γ -aminobutyric acid (GABA) receptors, dopamine receptors, bradykinin receptors, and several types of purinoceptors(10). In different pathological states, microglia gain distinct functional characteristics that change as the disease progresses. One such characteristic is their ability to contact injured neurons directly and remove synaptic connections in a process called synaptic stripping. This leads to desynchronization of neuronal circuits but also prevents the spread of the harmful effects. In some instances, entire dendritic trees can be removed. As part of the cascade of events taking place after microglial activation, substances such as reactive oxygen species, cytokines, or growth factors, which influence the pathological process during the acute and chronic phase as well as during subsequent regeneration are released. Even in their “resting” state, it has been shown that microglial processes are motile and as such, this state is better described as being a “surveillant” state. Fontainhas et al. found that activity mediated by GABAergic and glutamatergic mechanism regulate this movement of processes in the surveillant state (15).

1.5 Neural Calcium Dynamics

Calcium ions are involved in many functions of the nervous system, from neurotransmitter release to intracellular signal transduction (Figure 1-5) (16).

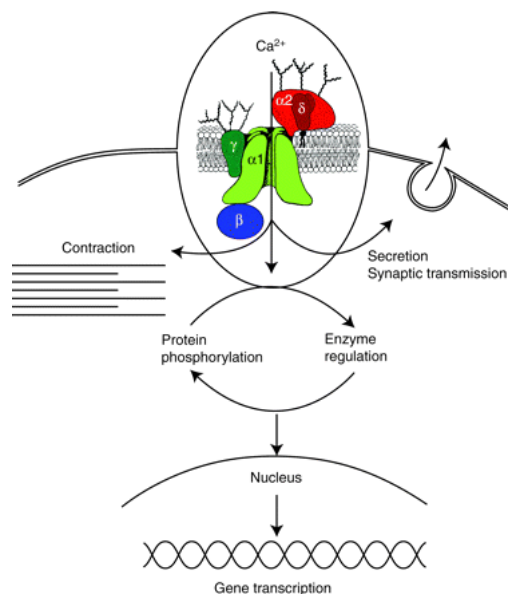


Figure 1-5: Diagram showing signal transduction by voltage gated Ca^{2+} channels (17)

These ions initiate specific intracellular signals that controls certain neuronal functions (18). Intracellular calcium concentrations lie in the 100 nM range under normal resting conditions due to calcium buffering molecules and sequestration into intracellular calcium stores (19). Electrochemical signals travelling along excitable cells are facilitated by calcium ion (Ca^{2+}) fluxes through calcium channels. This phenomenon translates into varying functional outcomes.

Calcium influx contributes to propagation of electrical signals and acts as a secondary messenger that activates several regulatory pathways. Many neuronal signaling pathways directly or indirectly increase cytosolic calcium concentration. Calcium in its ionic form is very dynamic, especially in excitable cells such as brain or muscle cells. These ions move from high extracellular concentrations to low intracellular concentrations where calcium ions are used as secondary messengers initiating G-protein dependent cascades.

These signals are involved in many biological processes within the neuronal circuit, including, gene expression, synaptic plasticity, neurotransmitter release, neurite outgrowth during development, learning, plasticity and apoptosis(20, 21) . Calcium imaging in the neuronal unit is essential since calcium signals are highly specific in well-defined cellular sub-compartments(18).

Ca^{2+} channels in many different cell types are activated by membrane depolarization and mediate Ca^{2+} influx in response to action potentials and sub-threshold depolarizing signals. Ca^{2+} entering the cell through voltage-gated Ca^{2+} channels serves as the second messenger of electrical signaling, initiating many different cellular events (17). In cardiac and smooth muscle cells, activation of voltage gated calcium channels results in contraction by increasing intracellular (cytosolic) calcium concentration. In skeletal muscle cells, these Ca^{2+} channels interact directly with ryanodine- activated Ca^{2+} release channels in the sarcoplasmic reticulum.(17).

Neuronal activity depends on a variety of voltage and ligand gated channels that are selectively permeable to ions such as sodium, potassium chloride, and calcium. Of the three aforementioned ions, calcium is the only one responsible for both altering membrane potential and cell signaling (22). Depolarization (voltage) induced calcium entry into neurons is primarily controlled by voltage gated calcium channels (Figure 1-6).

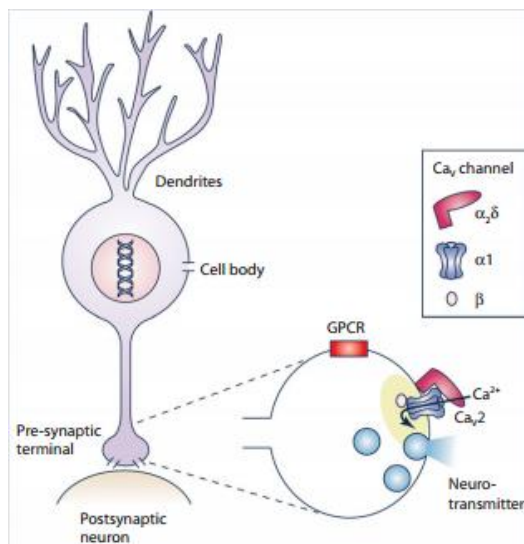


Figure 1-6: Diagram highlighting subunits of voltage gated calcium channels(17)

Calcium influx along the electrochemical gradient takes place whenever these voltage gated calcium ions are opened. This causes a localized increase in intracellular calcium concentration that triggers several calcium dependent processes that include gene expression, neurite outgrowth, neurotransmitter release and the activation of calcium dependent enzymes such as protein kinase C (23).

1.5.1 Voltage Gated Calcium Channels

There are two types of voltage gated calcium (Ca_v) channels: high voltage activated (HVA) channels and low voltage activated (LVA) channels. HVA channels are opened by large membrane depolarizations and LVA channels are opened by smaller depolarizations near the resting potential of the neuronal membrane. HVA channels are heteromultimers made up of a pore forming Ca_v - α_1 subunit that assemble with different Ca_v conjugates and calmodulin. LVA channels are made up of four major transmembrane domains that are connected by cytoplasmic linkers. These two Ca_v channels are shown in Figure 1-7.

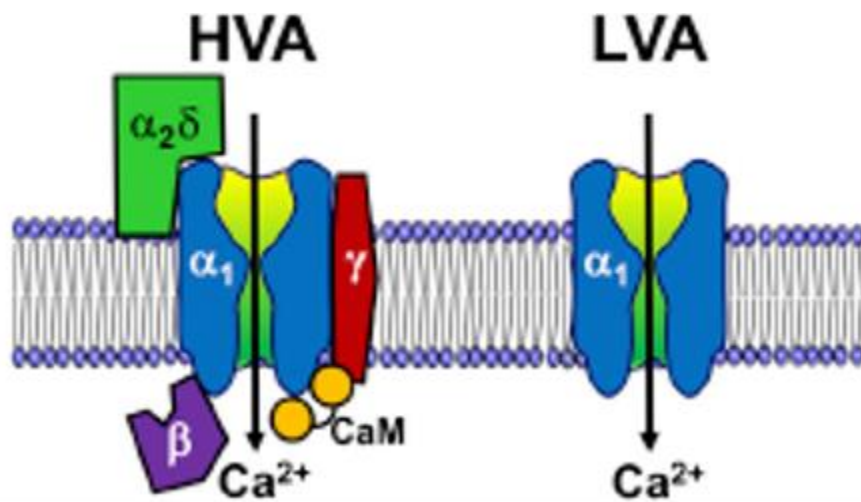


Figure 1-7 : Diagram showing HVA and LVA channel subunit compositions (19)

1.5.2 Ligand Gated Calcium Channels

Ligand gated calcium channels can be activated by excitatory neurotransmitters such as acetylcholine, glutamate, adenosine tri-phosphate (ATP) and serotonin. The primary excitatory neurotransmitter, glutamate, mediates excitatory synaptic transmission in many regions of the CNS. Glutamate activates ionotropic glu receptor (GluR) channels and causes increased channel permeability to Ca^{2+} ions. The three main types of GluRs are N-methyl-D-aspartate receptors (NMDARs), α -amino-3-hydroxy-5-methyl-isoxazolepropionate receptors (AMPA) and kainate receptors (KARs). The N-site in NMDARs controls channel conductance and calcium permeability. Glutamate – mediated calcium entry into neuronal cells increases intracellular calcium at a wide temporal and amplitude range.

While the exact mechanism is not fully understood, it is believed that NMDAR mediated intracellular calcium increases can induce long term potentiation (LTP) or long term depression (LTD) of the post synaptic response (24). Aside from initiating LTP and LTD, it has been discovered that NMDAR mediated intracellular Ca^{2+} elevation also affects the NMDAR channels themselves. Ca^{2+} entry facilitated by NMDARs is sufficient to provide feedback inhibition of slow excitatory post synaptic currents (EPSC)(25),(26, 27).

1.5.3 Glutamate Receptors involved in Calcium Signalling

Glutamate transporters are responsible for many important processes involved in synaptic signaling. These transporters rapidly clear the synaptic cleft of released neurotransmitter (28) and are therefore involved in the negative feedback loop responsible for preventing excitotoxicity. Many types of glutamate receptors are located on the neuronal cell membrane.

AMPA receptors on the post-synaptic membrane are responsible for plasticity and synaptic transmission. They can also be glutamate receptors and cation channels. Long Term Potentiation is one of the most studied aspects of plasticity and can be activated only when glutamate is bound to the AMPA and the NMDA receptors (29-31). The kainate receptor is found on both the pre- and post-synaptic membrane and acts as a modulatory factor on the inhibitory neurotransmitter Gamma-Aminobutyric acid (GABA) through the presynaptic membrane. This has been confirmed as selectively blocking glutamate transporters enhances metabotropic GluR EPSC.

Metabotropic receptors are indirectly linked to ion channels through signal transduction pathways which are usually G proteins. These receptors initiate a cascade of

events involving secondary messengers that opens specific ion channels. Neuronal and glial glutamate transporters are distributed on the membranes surrounding excitatory synapses. GLT-1 and GLAST are glutamate transporters found on astroglial cells and distributed at varying densities depending on the localized brain region. Figure 1-8 is a schematic of the different receptors involved in calcium signalling.

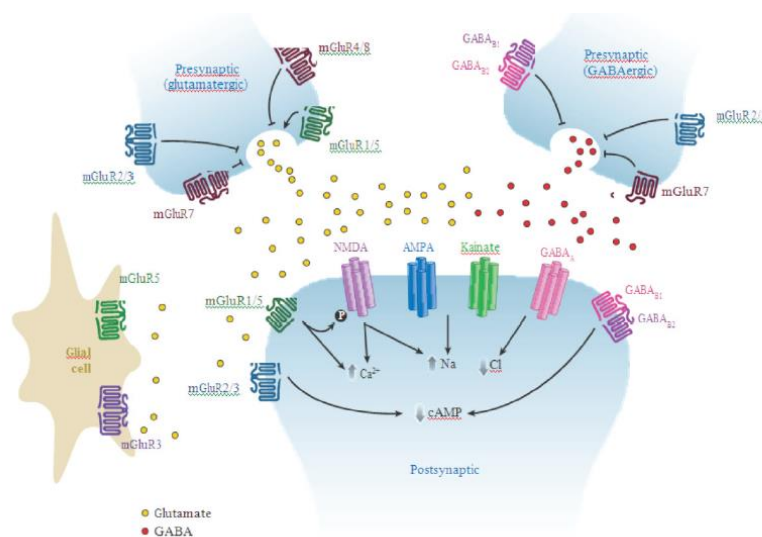


Figure 1-8 : Diagram showing receptors involved in calcium signaling on neuronal and glial membranes: purple (NMDA), blue (AMPA), green (KA), pink (GABA), green (mGLUR 1/5), blue (mGLUR2/3), and burgundy (mGLUR 4/7/8) (32). Calcium is a key signaling ion involved in memory and learning with NMDA receptors on the neuronal membrane (33).

1.5.4 Calcium Mediated Cell Death

There are many cellular mechanisms that precede cell death such as, necrosis and apoptosis. Each mechanism can be identified due to differences in their morphological and biochemical expression. In 2009, the Nomenclature Committee on Cell Death proposed criteria for the definition of twelve cell death modalities (34). These classifications are:

apoptosis, necrosis, autophagy, cornification, mitotic catastrophe, anoikis, excitotoxicity, Wallerian degeneration, paraptosis, pyroptosis, pyronecrosis and entosis. The most extensively described cell death modalities are apoptosis, necrosis, and autophagy. The term “apoptosis” was coined by Kerr et al. (35) and has been defined as a form of cell suicide since death is controlled by active intracellular processes. This is morphologically characterized by rounding up of the cell, retraction of pseudopodes, reduction of cellular volume (pyknosis), chromatin condensation, nuclear fragmentation, and plasma membrane blebbing. The cell fragments break up into membrane enclosed fragments which are then recognized and destroyed by macrophages or neighboring cells. Apoptosis is usually referred to as “programmed cell death” and occurs during development as a mechanism to control cell populations. The execution of this process is mediated by several enzyme-mediated systems that are activated through elaborate signaling pathways.

The calcium ion is a key player in homeostasis and has been implicated in both the initiation and effectuation of cell death (36) as well as cell growth (37). Perturbation of Ca^{2+} homeostasis in cancer cells has been linked with sustained cell proliferation and the inhibition of cell death through the modulation of Ca^{2+} signaling (37). Characterization of the signaling pathways involved in apoptosis revealed that a Ca^{2+} -calpain complex is significantly involved in the processing of the mitochondrially localized factor called Apoptosis Inducing Factor (AIF) (Figure 1-9).

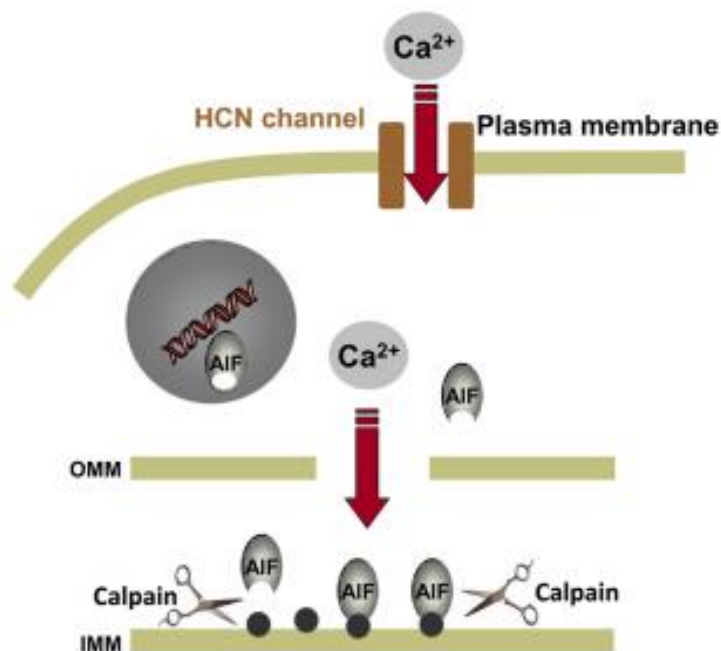


Figure 1-9 : Diagram showing the involvement of calcium/ calpain in AIF processing (36)

AIF is a key component in the death of certain cells such as neurons and some cancer cells (38). Compounds that perturb intracellular Ca²⁺ homeostasis make the AIF-mediated pathway the predominant mechanism of subsequent apoptosis. This event is a frequent component of cell death signaling, particularly in ischemia-reperfusion injury and after treatment with toxic drugs.

NMDARs are sometimes excessively stimulated by glutamate; this can lead to an increase in calcium influx which in turn causes neuronal damage and subsequent excitotoxicity. Glial cells are responsible for removing the excess glutamate from the surrounding environment but can only take up a specific amount of glutamate. Many diseases are caused by cell death triggered by excessive calcium influx such as, Alzheimer's disease (AD), Parkinson's disease (PD), and Huntington's disease (HD).

1.5.5 Calcium Dependent Excitotoxicity

Excitotoxicity is one of the key mechanisms underlying neuronal damage during CNS events such as ischemia, traumatic brain injuries and other neurological disorders. Ca^{2+} ions are ubiquitous intracellular messengers governing numerous cellular functions such as the control of cell growth and differentiation, membrane excitability, exocytosis, and synaptic activity (39). As a result, neurons need to efficiently regulate the intracellular Ca^{2+} to achieve a sufficiently high signal to noise ratio for proper calcium signaling to occur.

The free calcium concentration needs to be very low ($\sim 10\text{nM}$) when the neuron is not signalling so that small or localized calcium increases can trigger physiological events such as the activation of ion channels. To do so, neurons have developed complex homeostatic mechanisms that control both the concentration and the localization of calcium at any given time. These mechanisms consist of complex interactions between four broad categories of events namely: Ca^{+2} influx, buffering, internal storage, and efflux (shown in Figure 1-10).

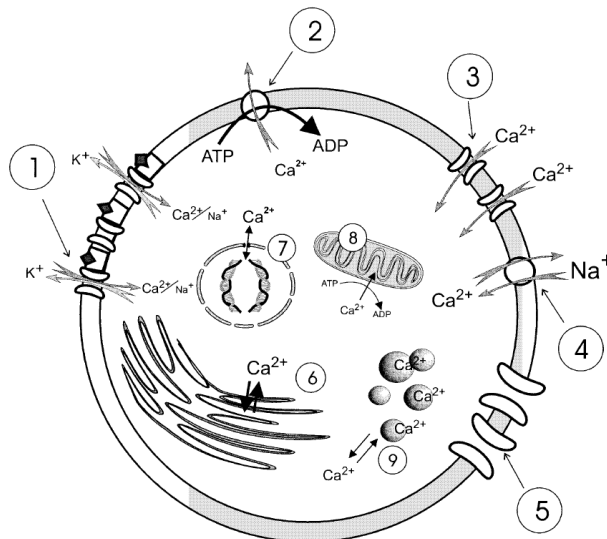


Figure 1-10: A schematic representation of Ca^{2+} homeostasis in neurons (39)

Under physiological conditions, a complex yet delicate connection between these processes allows the regulation of multiple Ca^{+2} dependent signaling cascades within one cell. Research shows that excessive Ca^{+2} , exceeding the capacity of these regulatory mechanisms can result in the over-activity of certain processes which would either be dormant or normally operate at low levels. When this happens, enzyme-mediated processes and other metabolic machinery damage neurons and subsequently leads to the formation of toxic products which leads to cell death.

Metabotropic receptors activated by glutamate are not directly associated with an ion channel pore but mediate their actions through guanine triphosphate (GTP) binding protein dependent mechanisms leading to a mobilization of Ca^{+2} ions from internal stores such as the endoplasmic reticulum by inositol triphosphate formation. Dr. Olney coined the term excitotoxicity when he observed neurodegeneration caused by EAAs such as glutamate (40). Since then, it has been discovered that excitotoxicity is a key mechanism

in many neuro-pathological states such as ischemia (stroke), nervous system trauma, epilepsy, and certain chronic neurodegenerative disorders.

Excitotoxicity is a consequence of excessive and sustained synaptic release of glutamate. Studies have shown that the use of glutamate receptor antagonists such as MK-801 and 2-amino-7-phosphonoheptanoic acid resulted in neuroprotective activity (16). Kass and Lipton reported that attenuating synaptic transmission and post synaptic receptor binding of glutamate via magnesium blocking resulted in a reduction of hypoxic/anoxic neuronal death (41). Practically, every glutamate receptor subtype has been implicated in mediating neurotoxicity. Although the entire molecular basis of glutamate toxicity has not been fully described, there is general agreement that it is largely Ca^{+2} dependent. It has also been discovered that the NMDA subtype of glutamate receptors plays a key role in mediating at least certain aspects of glutamate neurotoxicity, owing to their high Ca^{+2} permeability.

1.5.6 Glutamate Induced Calcium Fluorescence

Glutamate homeostasis involves neuronal release, neurotransmission, and glial uptake. Neuronal release of glutamate is stochastic and as a result exogenous glutamate is introduced to cells *in vitro*. When this is done, we expect calcium to enter the neurons as it is an excitatory neurotransmitter (42). There is a directly proportional relationship between glutamate stimulation and the probability that neurotransmission takes place. During calcium imaging experiments, calcium influx is expressed as an increase in fluorescence.

1.5.7 Calcium Imaging

Over the past few decades, much of the research on neuronal properties and overall brain function was derived from recording single neuron electrical signals. This method is

comparable to looking at a movie scene with a straw, many crucial details are left out and there are many opportunities for error as a result. Recently, optical methods have been developed to observe higher-order interactions between hundreds of cells and this facilitates studying neural networks as well as single cells simultaneously. One such method is calcium imaging. Calcium imaging is a common technique used to detect and measure calcium signals in cultured cells (43). This technique uses calcium indicator dyes which are mainly organic molecules that respond to binding Ca^{2+} ions by changing their spectral properties.

The calcium ion is a universal secondary messenger involved in specific and selective regulation of cellular process such as muscle contraction, fertilization, synaptic transmission, cell division and blood clotting. Calcium ions play a significant role in neuronal signaling and generate intracellular signals that elicit various responses. It has been shown that changes in intracellular calcium concentration is a mechanism for cell signaling in many brain cells (44). These intracellular changes are usually visualized as wave-like transient (small or brief), sustained (prolonged calcium increase) or oscillatory (repeated brief calcium increases) signals throughout specific cellular regions or between groups of adjacent cells. Ca^{2+} cannot be visualized directly in living cells as it does not have any intrinsic fluorescent properties. To image intracellular calcium changes, specific molecules expressing optical properties dependent on intracellular Ca^{2+} concentrations are used. Calcium signals differs in their timing, sub cellular location and amplitude and these properties are related to explicit functions. Calcium signaling is essential for normal brain function, however, excessive and sustained intracellular Ca^{2+} levels are associated to neuronal injury and cell death (45).

Calcium imaging is one of the most widely used techniques in neuroscience today as intracellular calcium concentration is associated with physiological and pathophysiological activity of neurons. Calcium sensitive dyes are used as tools for studying calcium signaling in various cell types. From their introduction by Tsien *et al* (46), calcium indicators have been used to study calcium signaling in a plethora of cell types and applications. There are two main types of Ca^{2+} indicators, genetically encoded fluorescent proteins and chemically engineered fluorophores (47). The fluorescent properties of the indicators are altered when bound to freely diffusible calcium and it is therefore possible to monitor intracellular calcium processing in live single cells and multi-cellular networks.

Many advances have been made since the introduction of these indicators. Our emphasis will be on fluorescent acetoxymethyl (Fluo-AM) dyes. The cell membrane is impermeable to most free Ca^{2+} indicators therefore varied methods are used to facilitate their entrance. Once inside the cell, esterases cleave the AM groups and release the hydrophilic fluorophore which can then bind to the free Ca^{2+} . To choose an appropriate indicator, the imaging hardware and software available, the importance of qualitative versus quantitative data and the potential problems that may be encountered should be considered. Fluo-AM dyes are single wavelength indicators that change their fluorescence properties when bound to free calcium.

One drawback of using these dyes is that it is difficult to distinguish between fluorescent intensity changes caused by a change in $[\text{Ca}^{+2}]$ or intensity variations caused by a disparity in dye loading. To combat this problem, the fluorescent signal (F) is typically expressed relative to the initial fluorescence intensity (F_0) denoted by F/F_0 or $\Delta F/F_0$ if the

change in fluorescence is measured. This approach does not account for changes in fluorescence caused by extrusion or bleaching and as such, care needs to be taken when performing an experiment.

The calcium concentration to be measured during the experiment needs to be considered when choosing a suitable indicator. The dissociation constant (denoted by K_d) of the indicator should be near the midpoint of the $[Ca^{2+}]$ range to be detected. For large concentration ranges, low affinity indicators are used, and high affinity indicators are used for minor changes in $[Ca^{2+}]$. Selecting an indicator that is excited by red or green light is preferred to UV because UV light has more energy than the visible spectrum. However, prolonged exposure to any type of light will result in cell death. Control experiments studying the impact of excitation light to the cells should be done. Before performing experiments with stimuli, an identical experiment with the same duration and light intensity should be done to ensure that the indicator-cell combination remains stable. Studies have shown that some indicators buffer Ca^{2+} therefore excessive loading of cells can significantly reduce the Ca^{2+} signal (48). Calcium imaging is a useful tool for studying signal transduction in neuronal cultures and typically works robustly for primary cells. The indicators used are sufficiently bright with exceptional signal to noise ratios. For this project Fluo3/AM dye was used. Fluo3/AM binds non-covalently to calcium and therefore has a dissociation constant. The free calcium concentration can be calculated using a single wavelength calcium indicator using the following formula (48):

$$[Ca^{2+}]_{free} = K_d \left[\frac{F - F_{min}}{F_{max} - F} \right] \quad \text{Eqn. 1-1}$$

where F is the fluorescence of the indicator at a certain time point, F_{\min} is the minimum fluorescence due to calcium chelation and F_{\max} is the fluorescence of the calcium saturated probe (found using calcium ionophores such as ionomycin).

1.6 Neurological Diseases Associated with Glial Anomalies

As mentioned throughout this chapter, we are interested in studying how glial density is involved in glutamate re-uptake and recycling as this relates to synaptic activity (calcium signalling). Since the brain comprises several interconnected networks, disturbances in one area leads to many secondary manifestations and the development of various neurological diseases (Figure 1-11).

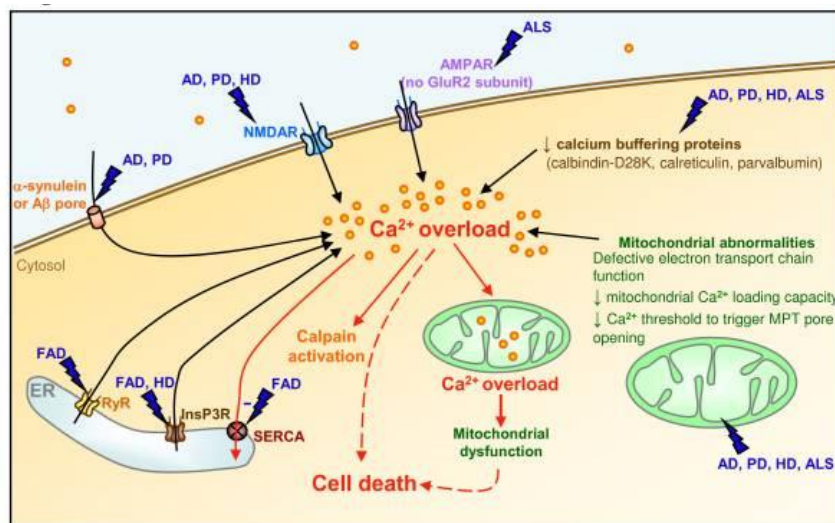


Figure 1-11: Calcium deregulation leading to neurodegenerative diseases (49).

1.6.1 Epilepsy

Astrocytes are critically important in the regulation of extracellular glutamate levels in the CNS due to the abundant expression of high affinity glutamate transporter proteins

on the cell membrane (50). It is estimated that approximately 80–90% of extracellular glutamate uptake is done by astrocytic glutamate transporters (51). Accumulation of this neurotransmitter has harmful effects on the function and survival of neurons. Many neurological diseases, particularly epilepsy, are accompanied by astrocyte dysfunction which leads to the development of over-excitabile neurons. Rapid growth of reactive astrocytes (gliosis) is a common feature of temporal lobe epilepsy (TLE). This gliosis is associated with delayed re-uptake of extra-cellular glu (52). Early studies evaluating the effects of glu and glu analogues on the development of epileptic seizures in lab animals indicated that glu is a critical player in the development of this pathophysiology (53). Numerous studies have been done subsequently and it is now generally accepted that glutamate dysregulation, specifically over-exposure of neurons to glu leads to excitotoxicity which if unregulated leads to epileptic seizures. Figure 1-12 shows some of the major metabolic pathways involved in normal brain glu homeostasis and some of the areas affected by epilepsy.

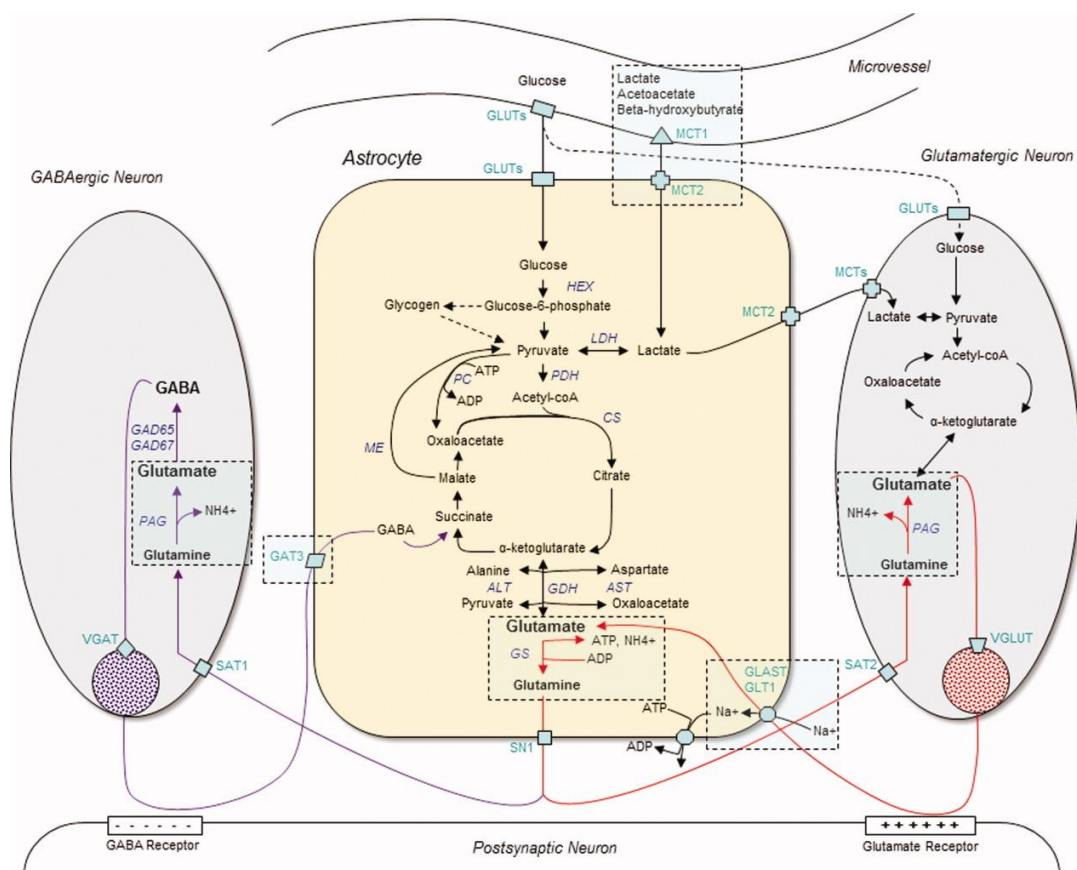


Figure 1-12: Diagram depicting some of the major metabolic pathways and tissue compartments involved in normal homeostasis of brain glutamate. The dashed frames indicate areas being affected in epilepsy (51).

1.6.2 Parkinson's Disease

Parkinson's disease (PD) is the second most common neurodegenerative disease worldwide (54). It is currently an incurable disease with symptomatic manifestations ranging from tremors, bradykinesia and rigidity to amnesia, dementia, and many others. The causes of this disease are not fully understood, and no formal treatment has been developed to slow down its progression. The core motor symptoms are attributed to the death of dopaminergic neurons located in the substantia nigra pars compacta (SNc), a small region in the mesencephalon. Several studies implicate disturbances in calcium signalling

as a cause. These studies link Ca^{2+} entry through Cav1 channels and the feed-forward control of mitochondrial metabolism to the development of PD (55).

1.6.3 Major Depressive Disorder

Major depressive disorder (MDD) is debilitating mental disorder that affects millions of individuals directly and indirectly (56). Postmortem studies have shown that reduction in astrocyte density and their related markers are key features in this disorder. This finding has also been found in rodent models of depressive-like behavior (57). As mentioned earlier, astrocytes are crucial in the uptake, metabolism and recycling of glutamate and glutamate transporters located on the astrocytic membrane (used as markers for astrocyte function) are also down-regulated in postmortem studies of patients with MDD.

CHAPTER 2

TISSUE ENGINEERED MICROENVIRONMENTS

2.1 Overview

The goal of this chapter is to describe the methods used to develop neural circuits with quantifiable variations in glial cell densities. These variations are separated into three distinct categories: severely depleted, moderately depleted, and mildly depleted glial cell neural micro-environments. We hypothesize that the glial density will be reduced using anti-mitotic agents leading to fewer cells and changes in cell morphology.

2.2 Background

It is virtually impossible to look at all the neurons in the brain simultaneously, and as a result, scientists have begun exploring the idea of looking at neuronal circuits where the number of neurons in a circuit ranges between a few to many thousand cells. Many of the breakthroughs made in neuroscience are because of the piecemeal reconstruction of many neuronal circuits. Miniscule changes in neuronal circuits can elicit drastic physiological changes in an individual. For decades, immortalized cell lines have been used as a tool in basic research. Over time, continuous passaging of cell lines facilitates genetic or phenotypic variations and the cells lose the original tissue properties. Primary cells are more biologically relevant as they are derived directly from the human or animal

tissue via enzymatic or mechanical methods. These cells are physiologically and phenotypically more closely related to the tissue that they are extracted from than immortalized cell lines. The cells can be grown either suspension or adherent. Throughout this study, adherent primary brain cells were utilized. Unlike cell lines, primary cells have limited lifetimes before reaching senescence. Also, neurons are very delicate cells therefore it is easier to perform experiments with the less fragile, pure glial cultures before the neuronal cultures. Dissociated cortical neuronal cultures possess many distinct benefits for studying chemical and electrical signaling between neurons. The applications of these benefits include (but are not limited to) neural circuit models of development, memory, aging and disease.

2.3 Primary Cortical Culture Protocol

Cortical cells were obtained by performing cervical disarticulation of outbred Sprague-Dawley newborn rat pups (age \leq 48hours) in adherence to protocols approved by Louisiana Tech University's Institutional Animal Care and Use Committee (IACUC). Rat pups were decapitated, and the brain tissue was quickly removed and placed into dissecting solution consisting of Basal Media Eagle, (BME, Sigma) and 0.5% Penicillin Streptomycin (PS, Sigma).

The cerebellum and meninges were removed, and the cortical lobes were then stored in an ice-cold dissecting solution. (An average of n=seven newborn rat pups were used for each culture set). After dissection was completed, the brain tissue was then aspirated with a 5ml pipette and placed into a 15ml conical tube with a complementing volume of Trypsin EDTA (volume determined by number of rat pups, Sigma) and inverted five times. Trypsin was then neutralized with Neuronal Culture Medium (NCM. Appendix

A) comprised of BME, Ham's F-12K (ATCC), 10% Horse Serum, 10% Fetal Bovine Serum (FBS), glucose, glutamine and PS. The cells were then mechanically dissociated by trituration and allowed to form a brain cell supernatant for ten minutes. The supernatant was then aspirated and stored in a 15ml ice-cold conical tube. NCM was then re-introduced to the brain tissue and the process repeated thrice in total. The brain cell supernatant was centrifuged at 160 relative centrifugal force (rcf) at eight degrees Celsius for seven minutes to form a pellet.

2.4 Development of Quantifiable Neural Cell Micro-Environments

To study the effect of glial density on the calcium signalling capacity of neurons within a cell culture platform, we have employed the use of certain anti-mitotic agents to deplete the mixed culture harvested from brain tissue. We will be studying the effect of two specific chemicals, namely, Cytosine Arabinoside and 2-deoxy-5-fluorouridine (FdU). To establish cultures with varied cell densities, we performed several preliminary experiments using various concentrations to find the optimal concentrations needed to develop the three levels of depletion outlined above. Figure 2-1 is a schematic briefly outlining each step in this process.

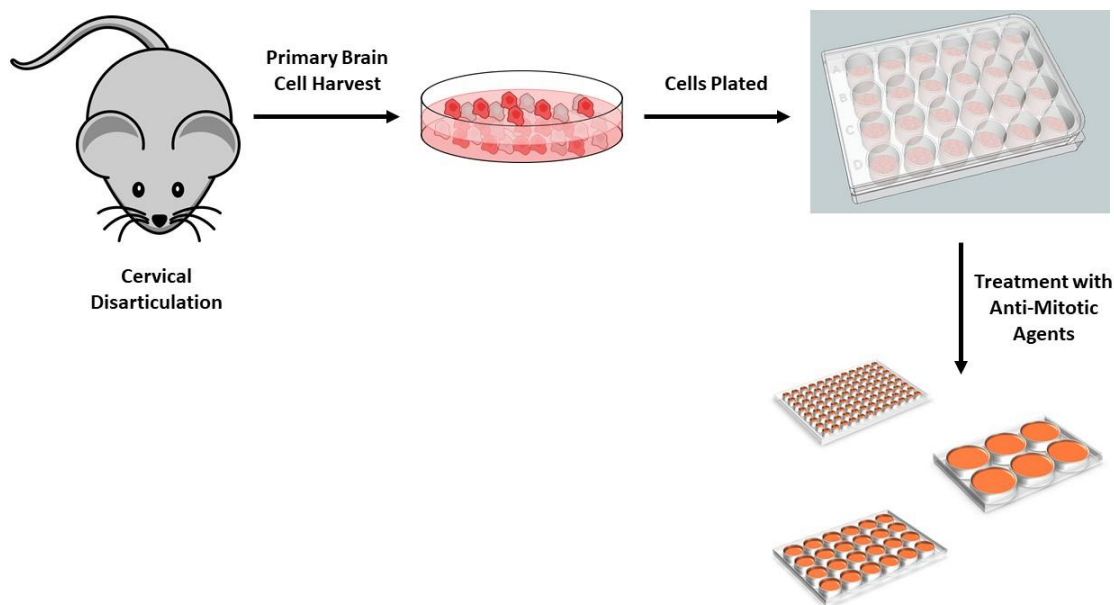


Figure 2-1: Schematic outlining the different steps used to develop various brain cell microenvironments.

2.4.1 Developing severely depleted micro-environments using cytosine arabinoside

Cytosine Arabinoside (AraC) is a chemotherapeutic drug used to treat certain brain cancers by slowing down the growth and spread of rapidly dividing cancer cells. This drug has also been used traditionally to establish primary cultures of neurons by killing the dividing, non-neuronal brain cells. This method is useful in mixed cultures, as neurons are post-mitotic and are therefore not targeted; thus, it can be used to eliminate the glial cells and establish “pure” neuronal cultures. AraC is a pyrimidine anti-metabolite that depletes proliferating cells by inhibiting deoxyribonucleic acid (DNA) synthesis (structure shown in Figure 2-2).

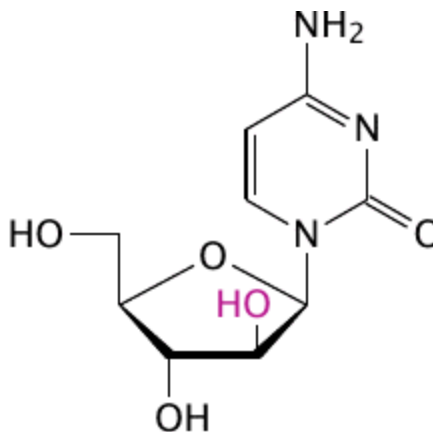


Figure 2-2: Structure of Cytosine Arabinoside (AraC) (58),

Our lab uses an established protocol to develop severely depleted neural cell micro-environments (59). After following the primary cortical culture protocol, the cells were treated with a 100x dilution of the anti-mitotic, AraC (1mM, Sigma) to deplete glial cells from cultures at four *days in vitro*. Cell cultures prepared using this method were determined to be at minimum, eighty percent depleted using a combination of staining methods and Image Pro Plus software for cell counting. The number of cells is recorded by calculating the average (mean) number of cells in ten images taken from the same well and this is done in thirty-two wells per experiment. These images are taken using a Leica inverted microscope and the coordinates for each image is retrieved using the Leica Application Suite software to ensure that each image is taken from a different area in the well. Four plates were used for each experiment and the experiment was repeated three times to ensure that the results were reproducible. Representative images of mixed cortical brain cell cultures with and without AraC are shown in Figure 2-3.

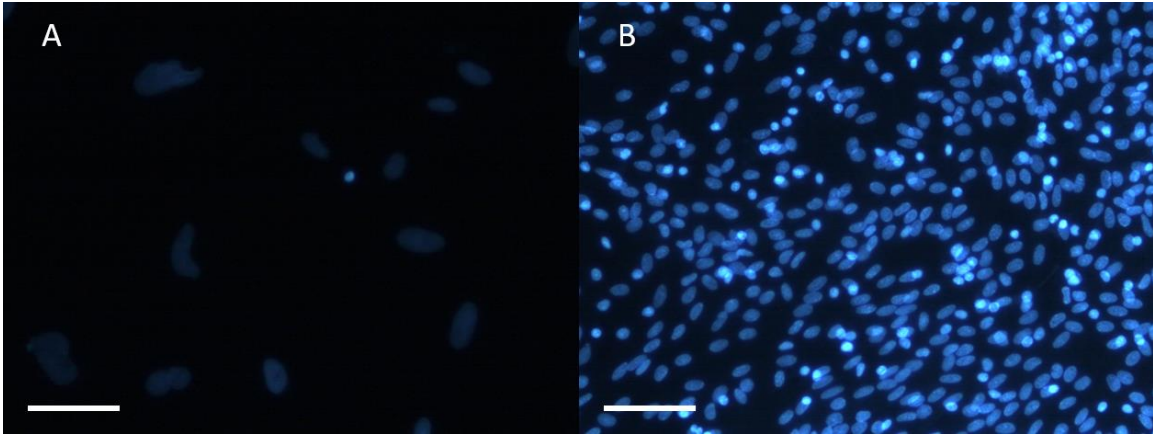


Figure 2-3: Images showing mixed cortical neuronal cultures with and without AraC treatment. A: Primary cortical cultures low in glia (AraC treatment) B: Primary cortical cultures high in glia (no AraC treatment). Error Bars = 100 μ m

The images reveal an increase in the cell area on the plate after treatment with AraC. The cells are less balled up and are spread out over the plate therefore increasing the area on the plate without increasing the cell volume. Each experiment was done in eight wells on a forty-eight well plate with four wells per condition. The data in Figure 2-4 is representative of one of the experiments. The average number of cells recorded in cultures treated and untreated with AraC were 27 and 269 cells respectively, with standard deviations of 5.24 and 24.38 respectively. Each bar represents the average number of cells from a total of sixteen wells per condition.

Effect of adding 100 μ M AraC to Mixed Glial Cultures

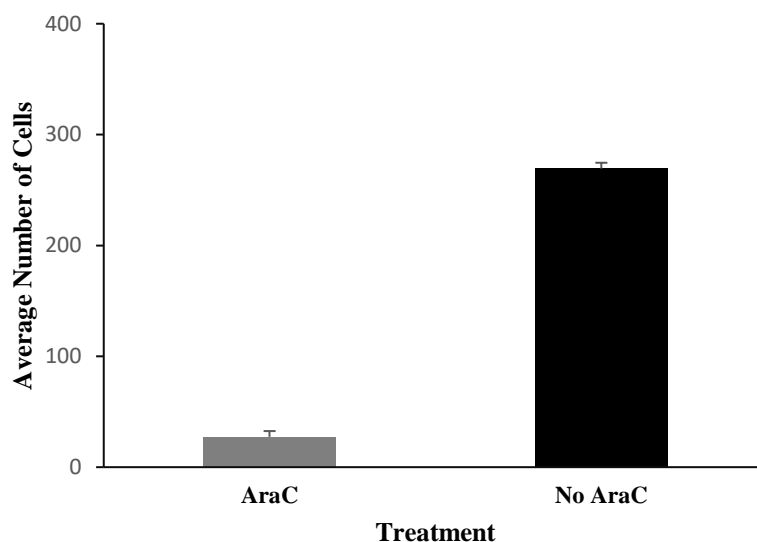


Figure 2-4: Graph showing the effect of adding AraC on the number of cells within the mixed glial (astrocytes and microglia) cell cultures field of analysis. Data is shown as mean plus standard deviation (Error Bars = sd).

This protocol was then repeated with pure astrocyte cultures which were derived using the method outlined in Figure 2-5.

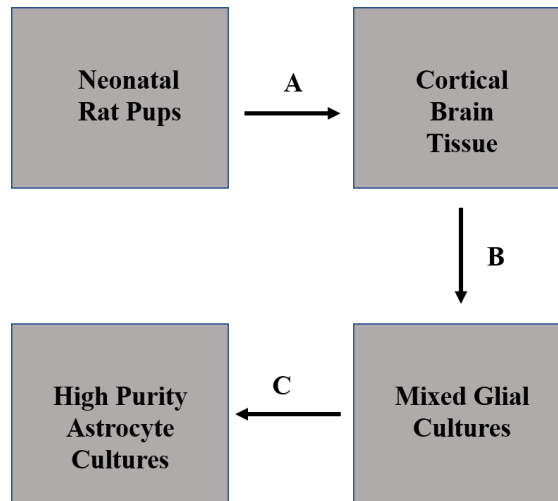


Figure 2-5: Overview of the protocol for preparing mixed glial cell cultures and isolation of primary astrocytes.

The mixed glial cell culture was checked using an inverted phase-contrast microscope fourteen to seventeen days after the initial plating, when astrocytes reach ~90% confluence. The microglia are growing above the single layer of astrocytes as small rounded cells. *(Adjusting the fine focus of the microscope assists in distinguishing the different cell layers)* as shown in Figure 2-6.

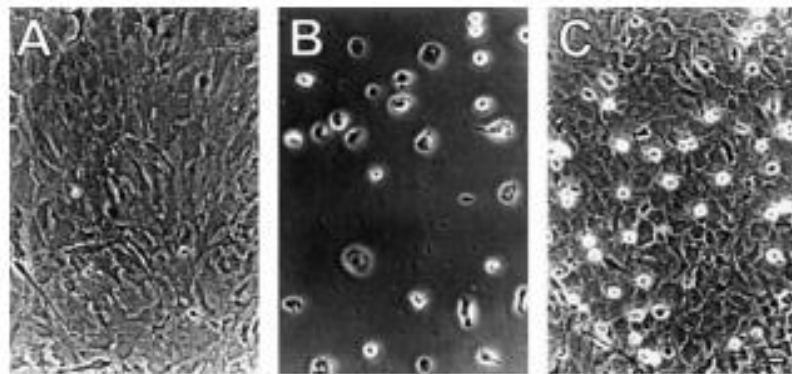


Figure 2-6: Phase-contrast microscopy of: (A) primary astrocytes; (B) primary microglia; (C) mixed culture of astrocytes and microglia (41).

The cell culture flask was then placed on a flattened surface and gently tapped on the sides at the speed of forty-five times per minutes (*Try to minimize the amount of foam generated when shaking the cell culture flasks*). While tapping and shaking the cell culture flask, the centrifuge was prepared by setting the temperature to four degrees Celsius (Other settings used: 160rcf for 8 minutes). Using a centrifuge, it takes about twenty minutes to cool down from room temperature to four degrees Celsius. This may vary based on the type of centrifuge available, so it is important to ensure that it is ready for use at the appropriate temperature as you are isolating the cells to prevent any delays. The cell culture flask was then checked under the inverted phase- contrast microscope every three minutes to ensure that the monolayer astrocytes remained undisturbed and continued to adhere to the substratum of the flask. The detached microglia float in the media, while the astrocytes remain attached to the bottom.

If attached microglia are observed, keep shaking the flasks until most microglia are floating. Using this method, after gentle shaking of the flasks for nine to twelve minutes, most of the microglia were removed without disturbing the adherent astrocytes. Note: If astrocytes are sheared from the bottom, immediately stop shaking the flasks. If the harvested cells are contaminated with significant amounts of astrocytes, this may be caused by two reasons: 1) shaking is too rigorous; 2) astrocytes are not sufficiently healthy to remain attached to the substratum of the flask. If astrocytes readily detach from the flask, consider changing fresh culture media more frequently (three rather than two times per week).

After most microglia detach, the shaking (tapping) was stopped and the culture media was carefully aspirated and placed into a 15 or 50 ml conical tube (depending on the amount of media used) for culturing primary microglia if needed (Primary microglia media protocol: Appendix A). Fresh media was then added to the astrocytes attached to the surface of the flask and placed in the incubator. The cells were then placed in the incubator for about twenty-four hours then removed and passaged by trypsinization. This protocol is ideal for the concomitant isolation of both microglia and astrocytes. The cells are then counted and re-plated for treatment or imaging. Using a combination of staining and Image Pro Plus software for cell counting the isolated astrocyte culture was found to be ~95% pure astrocytes.

The pure astrocyte cultures were treated with 10 μ M AraC and Figure 2-7 shows the results. Like the mixed glial cultures, the pure astrocyte cultures were depleted by at least 90% overall after addition of AraC. The average number of cells recorded in cultures treated and untreated with AraC were 24 and 234 cells respectively, with standard deviations of 2.22 and 14.60 respectively.

Effect of adding 100 μ M AraC to Pure Astrocyte Cultures

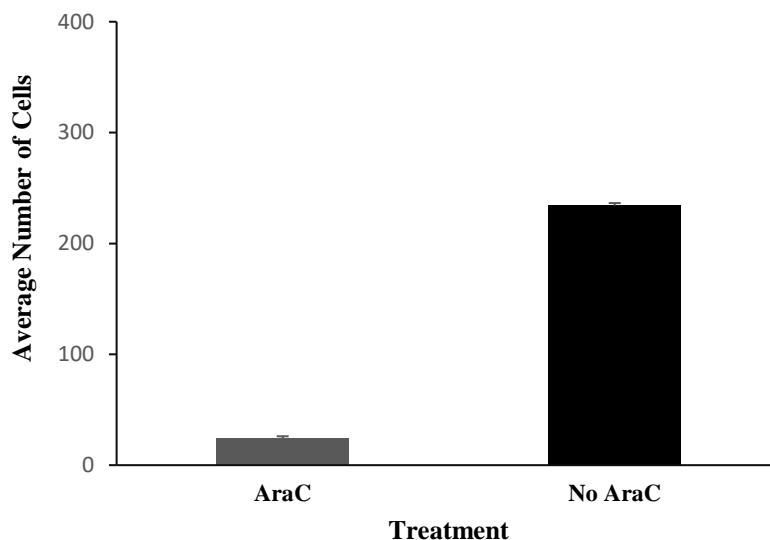


Figure 2-7: Graph showing the effect of adding AraC to the number of cells within the pure astrocyte culture's field of analysis. (Error bars = Standard Deviation). n=16

As a last step for developing glia- depleted micro-environments mixed cultures with neurons and glia were also treated with AraC as follows. Briefly, once the cells were harvested from the cortical region of the rat pup brains and resuspended in fresh NCM, a cell count was obtained with a hemocytometer, the cells were then plated in a poly-L-lysine (PLL, Sigma) coated, 48 multi-well plates (cell culture treated, CellStar) at an optimal density of 100,000 cells per well. The cell cultures were maintained in 37 degrees Celsius ($^{\circ}$ C), five percent carbon dioxide, and humidified incubation. At four days in vitro, the cells were treated with AraC and media was changed every three to four days until nine days in vitro when the cells were stained and counted. The average number of cells recorded in mixed neuronal cultures treated and untreated with AraC were 140 and 349 cells respectively, with standard deviations of 20.28 and 47.63 respectively. Each bar

represents the average number of cells from a total of sixteen wells per condition. The results obtained are shown in Figure 2-8.

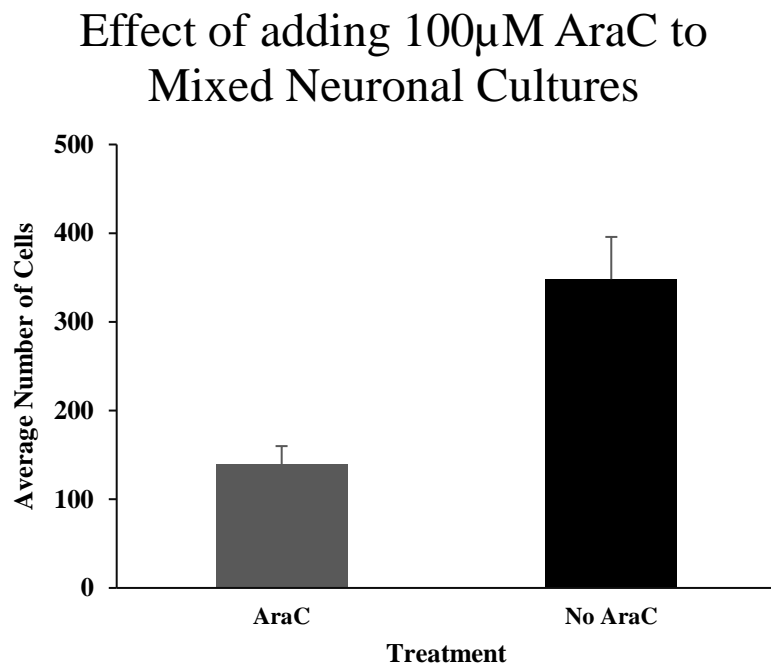


Figure 2-8: Graph showing the effect of adding AraC on the number of cells within mixed neuronal culture's (neurons, astrocytes, and microglia) field of analysis. (Error bars = Standard Deviation) n=16.

It is important to note that AraC does not affect neurons, thus the number of cells in this last step will always be higher. To confirm that the AraC depleted the astrocytes in the mixed neuronal cultures as expected (same as pure astrocyte cultures), concurrent staining with 4,6-diamidino-2-phenylindole (DAPI) and glial fibrillary acidic protein (GFAP) was used to count the astrocytes only.

The astrocytes depletion was found to be at least 85% in the mixed neuronal cultures.

2.4.2 Developing Micro-environments using novel method

Literature indicates that the use of AraC to produce pure neuronal cultures may have harmful effects on the post mitotic neurons in a similar fashion to nerve growth factor (NGF) deprivation of neurons (60). A recently published article by Hui et al. described a method used to deplete astrocytes within the mixed cultures with minimal effects on neurons using fluoro deoxyuridine (61). FdU is an antineoplastic drug that inhibits thymidylate synthetase, blocks DNA synthesis and kills proliferating cells (62). We have developed a novel method using a modified version of this protocol to develop brain cell microenvironments categorized as mildly, moderately, and severely depleted. After preliminary experiments were completed to find the optimal concentrations to develop these quantifiable micro-environments, a modified protocol was developed. For our modified protocol, 0.01 μ M, 0.5 μ M, 1 μ M, 2 μ M and 4 μ M concentrations of FdU was added at four *days in vitro* and incubated for twenty-four hours to kill the proliferating cells. Medium containing FdU was then replaced with fresh medium without FdU (old to new NC medium in a one to one ratio). Half of the medium was then replaced every five days until at least 14 days *in vitro* (DIV) before any treatment staining and cell counting was done. Figure 2-9 shows the percent (%) depletion of astrocytes within mixed brain cell cultures treated with different concentrations of fluoro deoxyuridine.

The % depletion recorded in mixed neuronal cultures treated with 0.01, 0.5, 1, 2, and 4 μM FdU are 23, 42, 63, 61, and 94 respectively, with standard deviations of 3.46, 2.46, 1.74, 1.63, and 0.20 respectively.

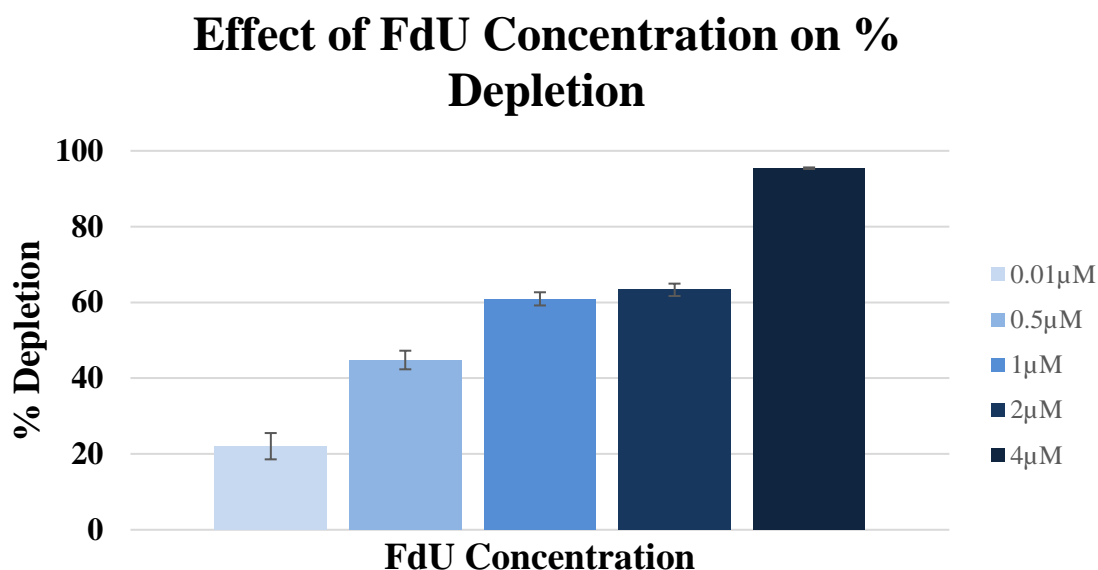


Figure 2-9: Graph showing percent depletion of mixed neuronal cultures treated with different concentrations of 2-deoxy-5-fluorouridine. These values have been normalized to the % of the cell density of untreated cells. The data is given as the mean \pm sd of three independent experiments. Since the sample size varied for each experiment, the significance of changes in the treatment responses was assessed using the Tukey-Kramer multiple comparison test; differences were considered statistically significant at $P < 0.05$, $n = 18$.

2.4.3 Assessing Metabolic Activity of Various Brain Cell Micro-environments

The MTT assay is a colorimetric assay which is used as a relatively high throughput (96-well plates) method of measuring cell viability by assessing the cell's metabolic activity. This method has been accepted as a reliable way to examine cell proliferation and is based on the principle that most viable cells have constant mitochondrial activity. The

mitochondrial activity is measured by the cell's ability to reduce the yellow tetrazolium salt MTT to purple formazan crystals (Figure 2-10) which are then dissolved for homogeneous measurement (63).

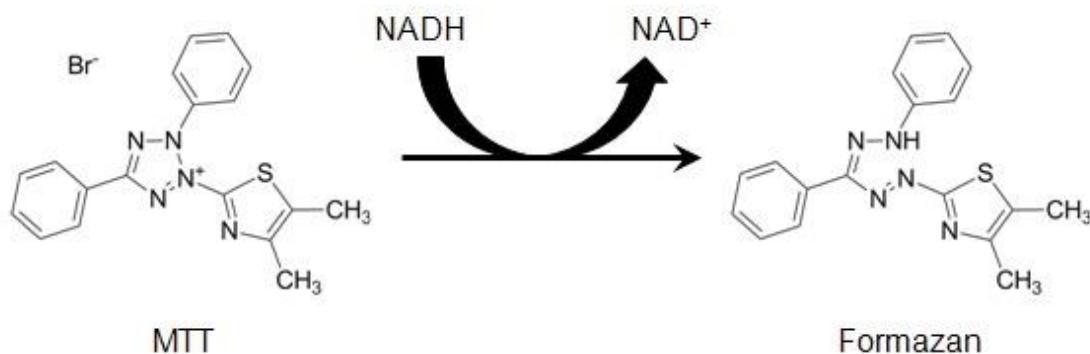


Figure 2-10: Schematic showing the conversion of MTT (yellow) to Formazan (blue/purple) via mitochondrial reductases (64).

After successfully developing the quantifiable brain cell micro-environments, the metabolic activity of each brain cell culture was evaluated using the MTT (3-(4,5-Dimethylthiazol-2-yl)-2,5-Diphenyltetrazolium cell viability assay. This was done first with mixed glial cultures then pure astrocyte cultures and finally with mixed neuronal cultures. The results of these experiments are shown in Figure 2-11. The protocol for the MTT assay can be found in Appendix A.

Cell survival was calculated using the following formula (63):

$$\text{Survival \%} = (100) * \frac{\text{Absorbance of treated cells} - \text{Absorbance of culture medium}}{\text{Absorbance of untreated cells} - \text{Absorbance of culture medium}}$$

Eq. 2-1

Any change in mitochondrial activity can then be quantified using various spectrophotometric means. The survival % recorded in mixed neuronal cultures treated with 0.01, 0.5, 1, 2, and 4 μM FdU are 86.7, 69, 40, 39, and 5 respectively, with standard deviations of 5.58, 2.67, 3, 2.25, and 1.33 respectively

The data in Figure 2-11 is given as the mean plus sd of three independent experiments.

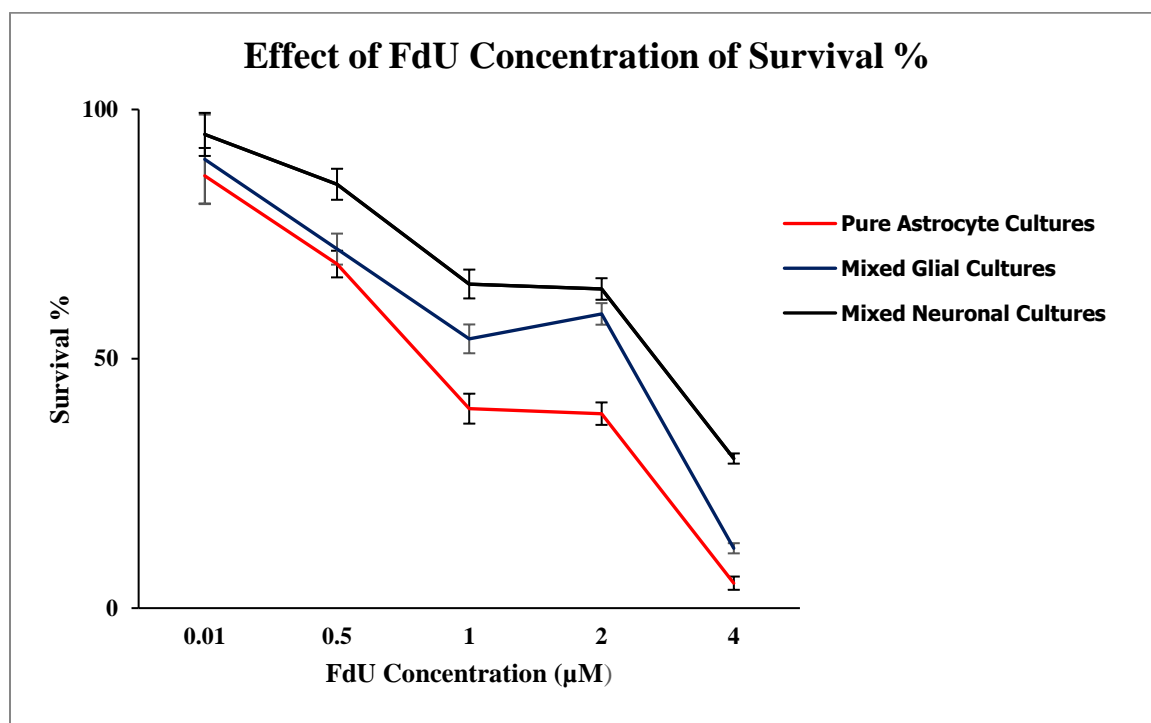


Figure 2-11: Graph showing survival percent of mixed glial cultures treated with different concentrations of FdU. These values have been normalized to the percent of the cell density of untreated cells. Error bars = sd.

Since the sample size varied for each experiment, the significance of changes in the treatment responses was assessed using the Tukey-Kramer multiple comparison test;

differences were considered statistically significant at $P < 0.05$, $n = 18$. After assessing the MTT and the % depletion results, the microenvironments were categorized as follows (Table 2-1).

Table 2-1: Neural Microenvironment Classification

| | Mildly Depleted | Partially Depleted | Severely Depleted |
|---|------------------------|---------------------------|--------------------------|
| FdU Concentration (μM) | 0.01 | 0.5 | 1,2,4 |
| % Depletion(x) | $x < 30$ | $30 < x < 60$ | $x > 60$ |

The hypothesis that the glial density will be reduced using anti-mitotic agents leading to fewer cells and changes in cell morphology was supported. Glial density was assessed using percent depletion after treatment with FdU and the cultures were categorized into three conditions: mildly, partially, and severely depleted cell cultures. The MTT assay was used to assess and quantify the metabolic activity of each condition and the results indicated that metabolic activity decreased as percent depletion increased as expected. The calcium imaging techniques used to study the calcium information processing of cultures in each category is discussed in the following chapter.

CHAPTER 3

CALCIUM IMAGING

3.1 Overview

This chapter describes the accomplishment of the second goal of the overall project which is to use calcium imaging methods to analyze the calcium dynamics of various neural micro-environments. As previously mentioned, calcium imaging techniques were used to analyze the signal processing capacity of the quantified micro-environments described in chapter two. Calcium imaging is a widely used technique to investigate the calcium signal processing in neuronal cultures. We hypothesize that decreasing the glial cell density will affect neuronal calcium dynamics by increasing the amount of glutamate to which the neurons are exposed, and increasing the time taken for recovery.

3.2 Calcium Fluorescence Imaging

The goal of this procedure is to gain a better understanding of the effect that glial density has on the neuron's capacity to recover from glutamate stimuli. An example of the raw data is given in Appendix B. Multiple experiments were performed utilizing different protocols. The protocols utilized were dependent on the substrate, cell type and stimulus added during imaging. During the experiments, primary cortical cells were on polystyrene surfaces with the Fluo3/AM calcium indicator and a 20X objective. The cells were imaged using an Olympus CKX31 inverted microscope with a 488nm excitation wavelength filter

over real-time at four seconds per frame with the InCyt Basic Im™ Imaging System (Intracellular Imaging Inc., Cincinnati, OH). A baseline recording (spontaneous oscillations prior to addition of stimulus) was obtained for 80 seconds, various glutamate concentrations were added to the imaged wells typically at intervals of 80 seconds, but this could be changed depending on the experiment without washing out the media between addition (illustrated in Figure 3-1)

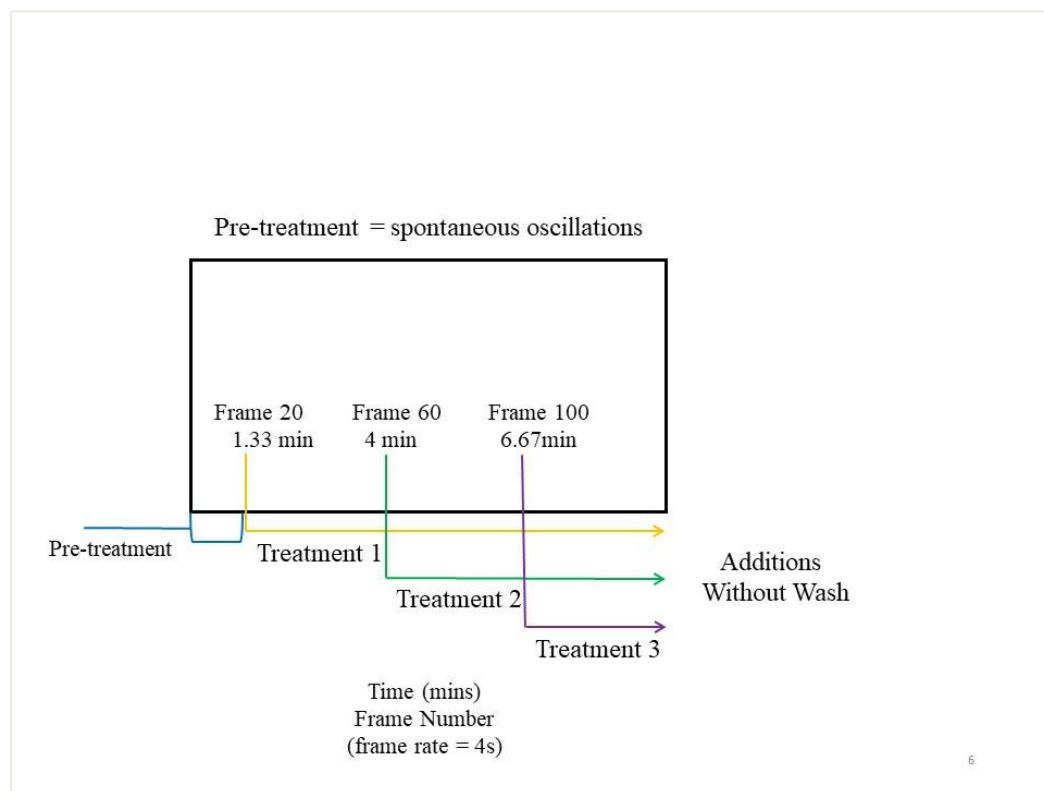


Figure 3-1: Stimulation protocol for most experiments. Glutamate is added into the experiment at equally defined times and at three concentrations. Each concentration is added at a set treatment number without washing the glutamate out of the well.

3.2.1 Preparation and Loading of Calcium Dye

The cortical cultures were images eight to nine *days in vitro* (DIV), by incubating the cells in a loading solution (Appendix A) for 45 minutes to an hour. The cells were then washed and recovered in pre-warmed Locke's solution and re-incubated for 30 minutes. While the cells were recovering, fresh glutamic acid solutions of three concentrations 250, 500, 750nM (Sigma Aldrich) were prepared in Locke's solution.

Locke's Solution:

Locke's solution is a solution used in fluorescence experiments because it lacks serum and phenol red (found in complete media) thus eliminating auto-fluorescence or quenching of the calcium dye (43). Locke's solution is made up of sodium chloride, potassium chloride, calcium chloride, calcium bicarbonate, glucose, Hepes buffer and sterile deionized water (Appendix A).

Glycine Bath:

Glycine is a co-agonist of the NMDA receptor and assists in preventing excitotoxicity of neuronal cells (65). A 10 μ M glycine (Sigma) bath (also called recovery solution) was prepared with Locke's solution as the solvent. This solution was warmed and introduced to the experimental wells after the cell had fully recovered from exposure to the loading solution. The cells were recovered in the glycine bath for 30 minutes then the live cells were imaged.

Glutamate

Three different glutamate (Sigma) concentrations were utilized throughout the main experiments namely: 250, 500 and 750nM. These are the final concentrations after the 20X dilution factor on addition of 25 μ l of the stimulus to the well containing 475 μ l Locke's solution. These glutamate aliquots are made fresh for each experiment by dissolving in Locke's solution. Other concentrations used in experimentation were 1 μ M, 10 μ M and 100 μ M.

Ionomycin

Determining the essential function of Ca^{2+} in controlling numerous cellular pathways has been significantly aided by Ca^{2+} ionophores such as Ionomycin. Ionomycin is an antibiotic that serves as a relatively specific calcium ionophore (Figure 3-2) (66,67). This compound perforates the cell membrane to facilitate rapid calcium influx across the cell membrane into the cytosol, maximizing the fluorescence calcium intensity. Ionomycin was frozen in a -80°C freezer in aliquots solubilized in dimethyl sulfoxide (DMSO) at a stock concentration of 665 μ M until it was ready to be used during experimentation, in which the stock concentration is then mixed with Locke's solution to obtain a working concentration. DMSO is a commercial solvent that is sometimes used to preserve organs and other tissues. The structure of ionomycin is shown in Figure 3-2.

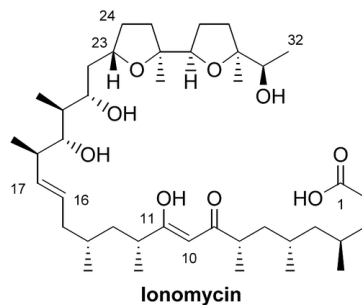


Figure 3-2: Structure of Ionomycin (68)

Potassium Chloride. (KCl, Sigma). KCl is known to produce a transient increase in calcium influx. The KCl solution is dissolved in Locke's solution to obtain a desired working concentration of 50mM. When testing the calcium imaging system, it is often useful to use stimuli like high concentrations of KCl or Ionomycin that are known to cause an increase in the intracellular calcium concentration and calcium free extracellular solutions such as EGTA, BAPTA or bicuculline that will reduce the calcium concentration.

3.2.2 Measuring and Analyzing Calcium Fluorescence Intensity

After the experiments were done, InCyt Basic Im™ Imaging System software was used to create regions of interest (ROIs) around every neuron that responded dynamically to glutamate by calcium influx (illustrated by fluorescence increase). In the experiments done with mixed neuronal cultures, the neurons are the main cells that respond to the subthreshold glu concentrations. GFAP staining was done to estimate the glial depletion category for each experiment. The morphology of the cells was also used to determine the glial depletion category of each cell culture. Astrocytes require higher glu concentrations to cause calcium influx and the calcium response tends to be slower and more sustained than in neurons. The ROIs were then used to measure fluorescence intensity over time in

the specified area. The ROIs were then normalized to their starting values for correlation between the cells within the experiment and other experiments. The data is then represented using line tracings and the average is then calculated by averaging all ROIs for triplicate experiments. An example of the line tracings derived from an experiment is shown in Figure 3-3.

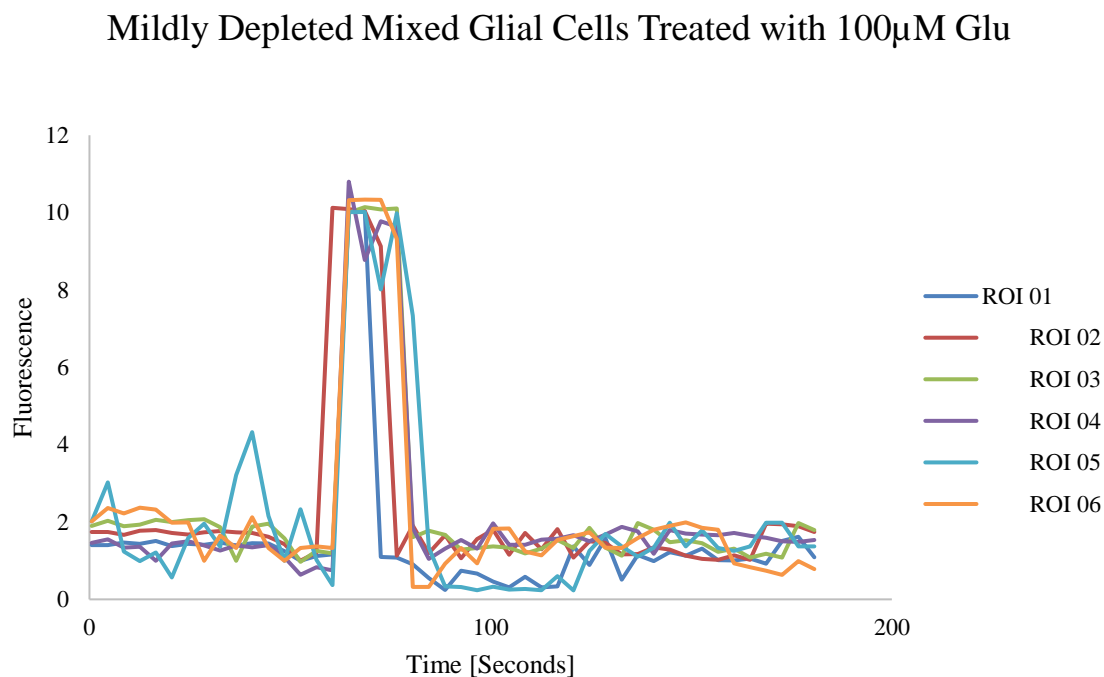


Figure 3-3: One example of the line tracings derived from a calcium imaging experiment

Under normal resting conditions, the cytosolic calcium concentration is in the nanomolar region, when the cells are stimulated, this concentration can reach micromolar amounts. Extracellular glutamate concentrations are in micromolar quantities around the synapse and millimolar quantities in the synaptic and intracellular vesicles. Research has shown that exogenous concentrations of L-glutamate greater than one micromolar have an electro-desensitizing effect on the NMDA receptor (69,70).

The calcium imaging experiments done in this project will test for calcium signalling in the presence of glu concentrations less than one micromolar to prevent NMDA desensitization and excitotoxicity. This will be done to ensure that glial density is the main contributor to changes in signal processing as this will be the only variable changed. To determine the effect that changes in glial density have on the calcium signalling capacity of neuronal cells, normal (glia rich) primary cortical cell micro-environments must be tested to obtain a control of calcium signalling under healthy conditions. These healthy (undisturbed) cortical cultures can maintain calcium influx due to glu stimulation by the action of specific homeostatic mechanisms (mentioned in Chapter One). It is important to note that the spikes shown in the data set are caused exclusively by neurons because higher (millimolar) concentration of glutamate are needed to induce calcium spiking in glial cells. Figure 3-4 displays glutamate induced calcium fluorescence in undisturbed (control) cortical cultures stimulated by increasing submaximal glu concentrations 250, 500, 750 nM.

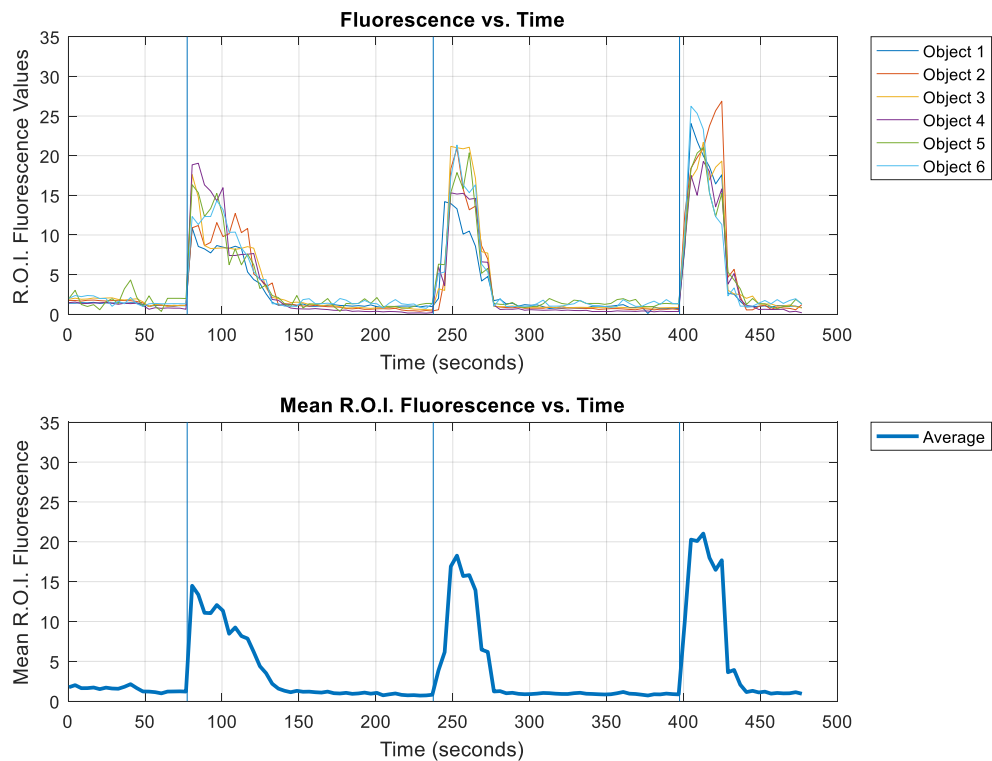


Figure 3-4: Line tracings of primary neuronal cortical cultures high in glia response to additions of 250nM, 500nM and 750nM glu additions. Top Panel: Each line represents individual cells (ROIs). Bottom Panel: Average of all ROIs

Each colored line represents a single neuron's response to glutamate stimulation and was chosen randomly. The average of the neuronal population is depicted by the blue line in the graph at the bottom. Each spike illustrates the initial baseline readings followed by a rise in intracellular calcium concentration followed by a return to baseline levels. It is possible that intracellular calcium levels can be elevated by release from intracellular stores, however this is a slower, more sustained process, this is not the case in these experiments as the spikes take place within seconds. Biochemical calcium responses are slower than electrical responses and require multiple seconds to produce a spike. The

length of time that the cell takes to recover from stimulation is dependent on the negative feedback mechanism provided by the glu re-uptake functionality of astrocytes.

Once the control is established, the effect of glial density on calcium signalling is then studied. This is done by performing identical experiments to the distinct micro-environments discussed in chapter two. The results of these experiments are shown in Figures 3-5 to 3-14.

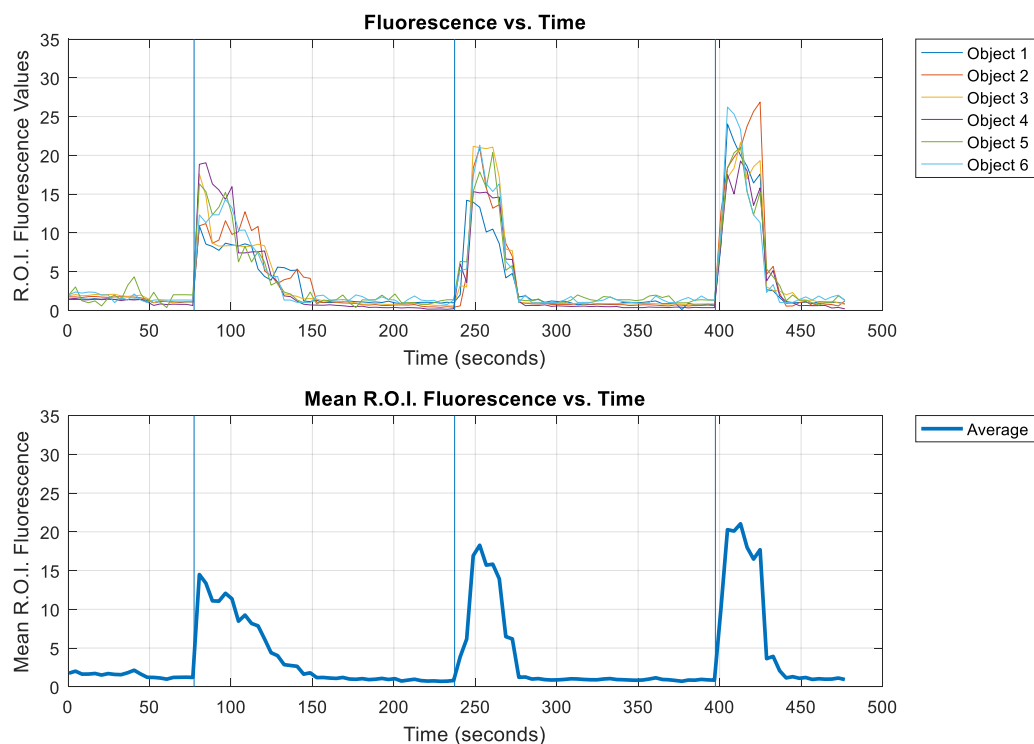


Figure 3-5: Line tracings of primary neuronal cortical cultures with mildly depleted glia response to additions of 250nM, 500nM and 750nM glu. Top Panel: Each line represents individual cells (ROIs). Bottom Panel: Average of all ROIs.

The individual ROIs in Figure 3-6 represent typical calcium signaling which should be observed in cultures with partially depleted glia. The average depicts how glia uptake the exogenous glutamate with decreasing calcium influx after each stimulation.

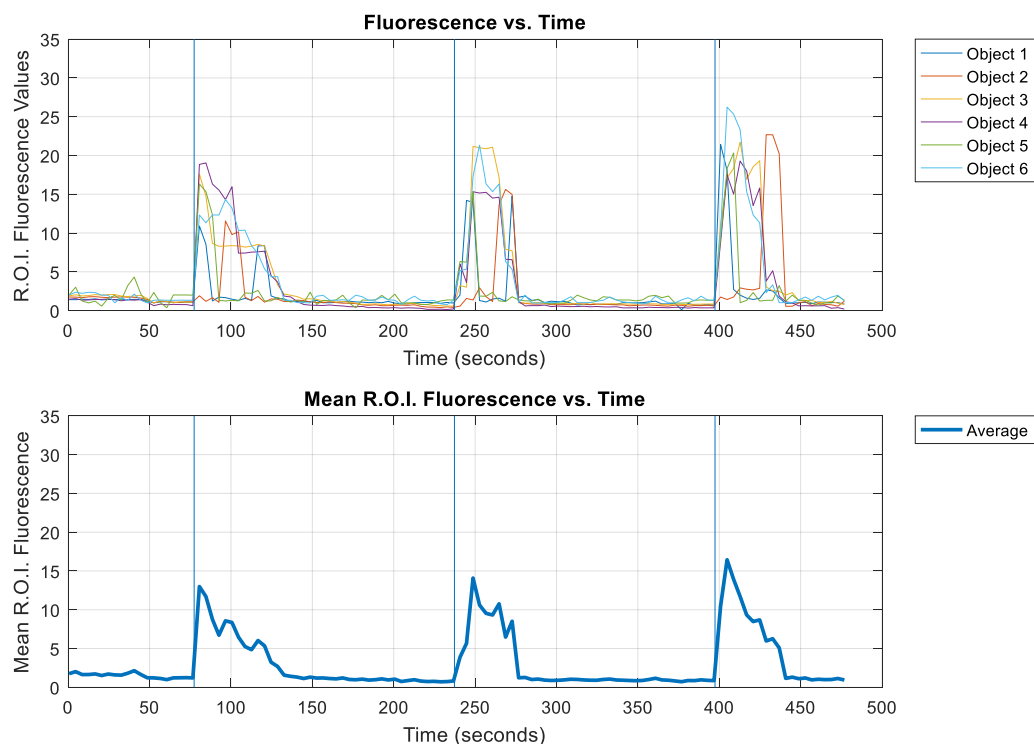


Figure 3-6: Line tracings of primary neuronal cortical cultures with partially depleted glia response to additions of 250nM, 500nM and 750nM glu. Top Panel: Each line represents individual cells (ROIs). Bottom Panel: Average of all ROIs

When exposed to glutamate, the cultures severely depleted of glia display very broad and high amplitude response to calcium influx, see Figure 3-7.

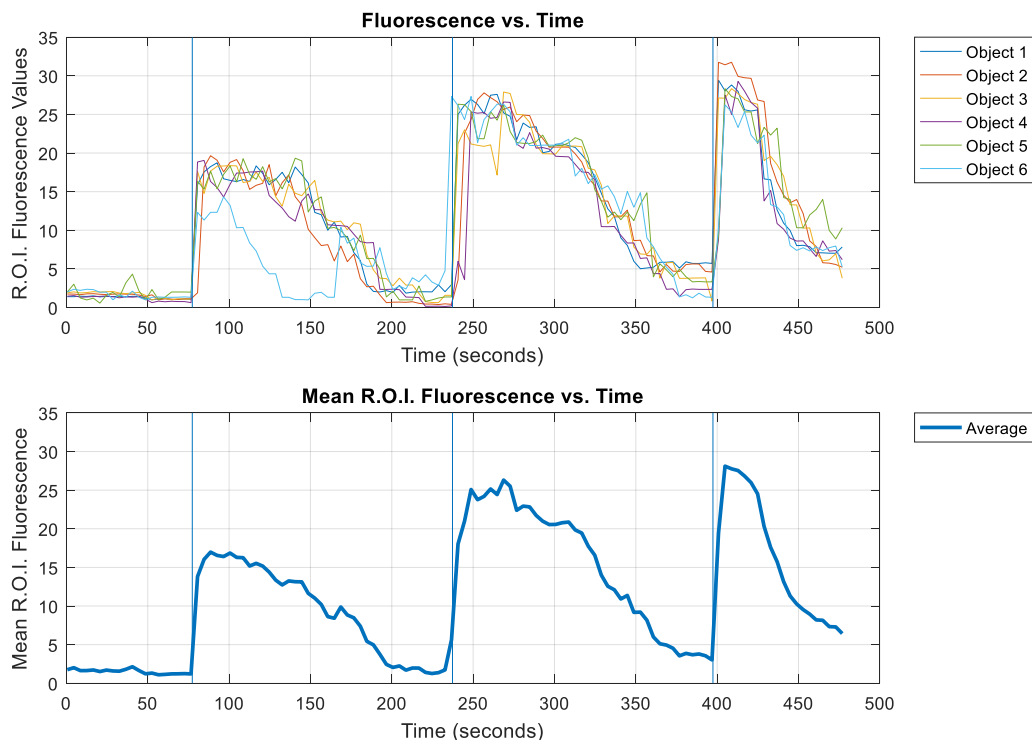


Figure 3-7: Line tracings of primary neuronal cortical cultures with severely depleted glia response to additions of 250nM, 500nM and 750nM glu. Top Panel: Each line represents individual cells (ROIs). Bottom Panel: Average of all ROIs.

These broad peaks are also indicators of excitotoxicity; line tracings of excitotoxic responses plateau, meaning the tracing does not return to baseline. The excitotoxic response in calcium signaling to glutamate could infer spillover of glutamate onto the dendritic NMDA receptors.

Mixed glial cultures containing astrocytes and microglia require higher concentrations of glu to elicit fluorescence calcium responses. When exposed to glutamate, the mixed glial cultures display narrow peaks with high amplitude response to calcium influx, see Figure 3-8.

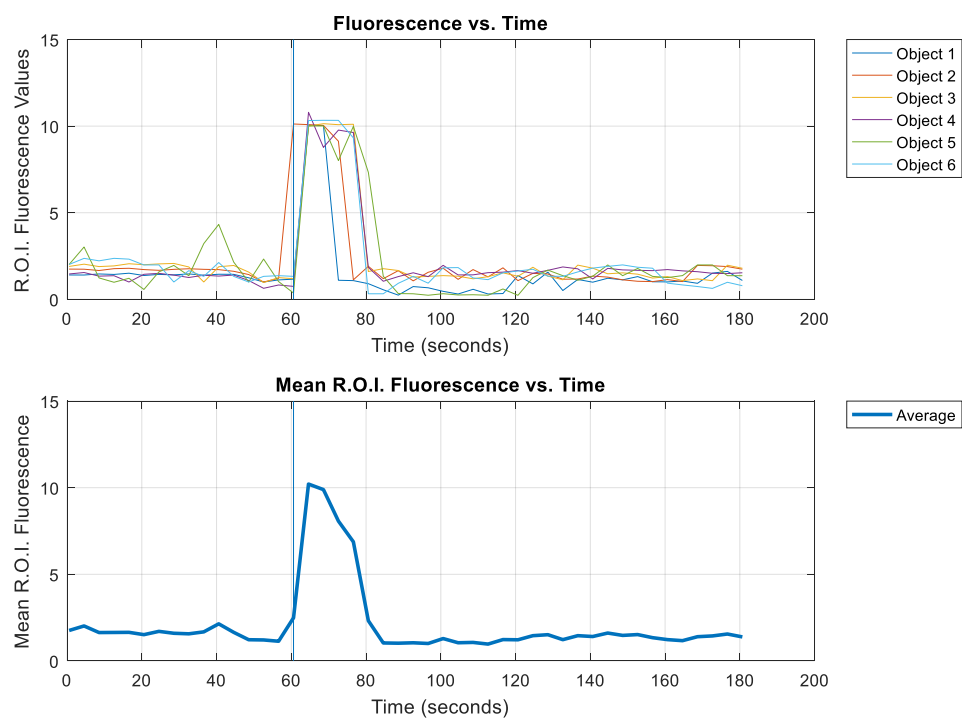


Figure 3-8: Line tracings of primary mixed glial cortical cultures responses to additions of 100 μ M glu. Top Panel: Each line represents individual cells (ROIs). Bottom Panel: Average of all ROIs

When exposed to glutamate, the mildly depleted mixed glial cultures also displayed narrow peaks with high amplitude response to calcium influx, see Figure 3-9.

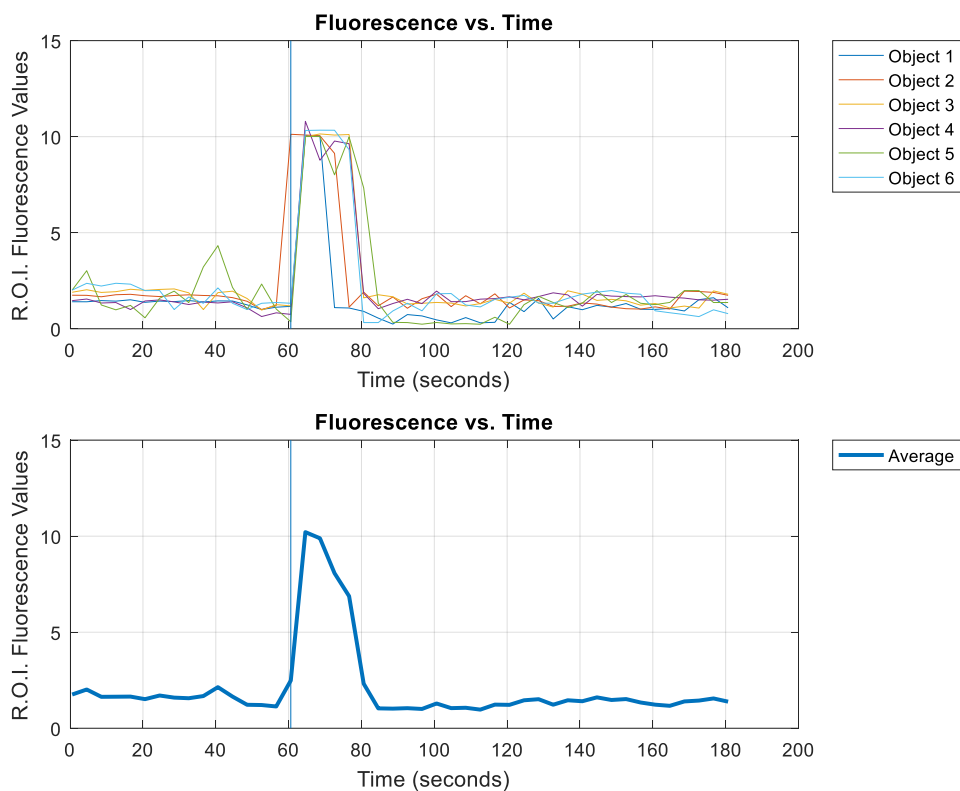


Figure 3-9: Line tracings of mildly depleted primary mixed glial cortical cultures responding to additions of 100 μ M glu. Top Panel: Each line represents individual cells (ROIs). Bottom Panel: Average of all ROIs

The partially depleted cultures behaved similarly to the mixed and mildly depleted cultures in displaying narrow peaks with high amplitude response to calcium influx (Figure 3-10).

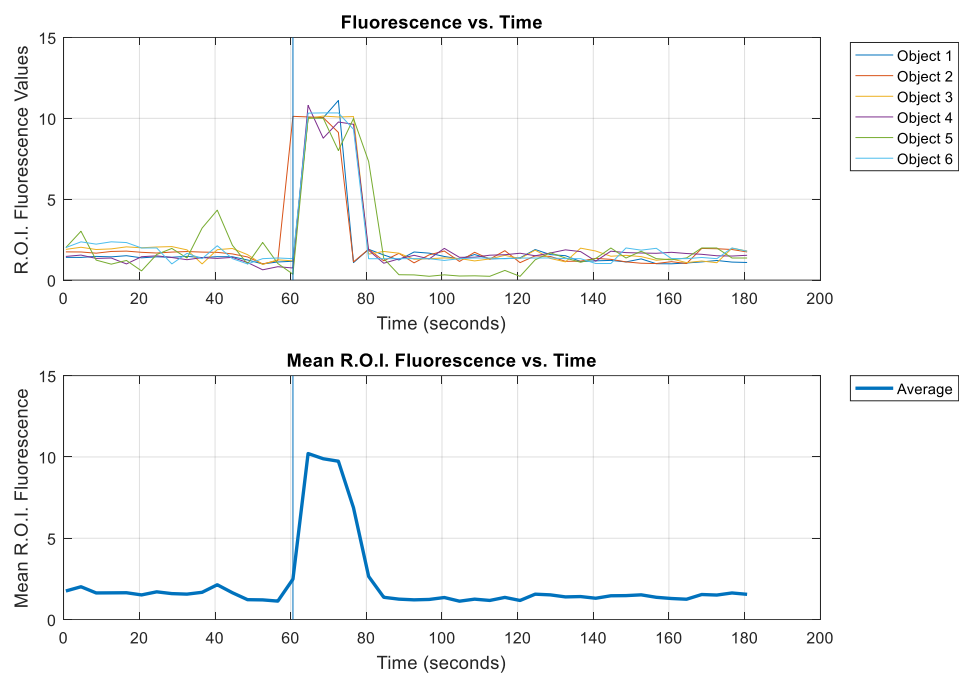


Figure 3-10: Line tracings of partially depleted primary mixed glia cortical cultures responding to an addition of $100\mu\text{M}$ glu. Top Panel: Each line represents individual cells (ROIs). Bottom Panel: Average of all ROIs

The severely depleted cultures responded to glu stimulation with high amplitude response to calcium influx without returning to baseline levels as seen in excitotoxic micro-environments (Figure 3-11).

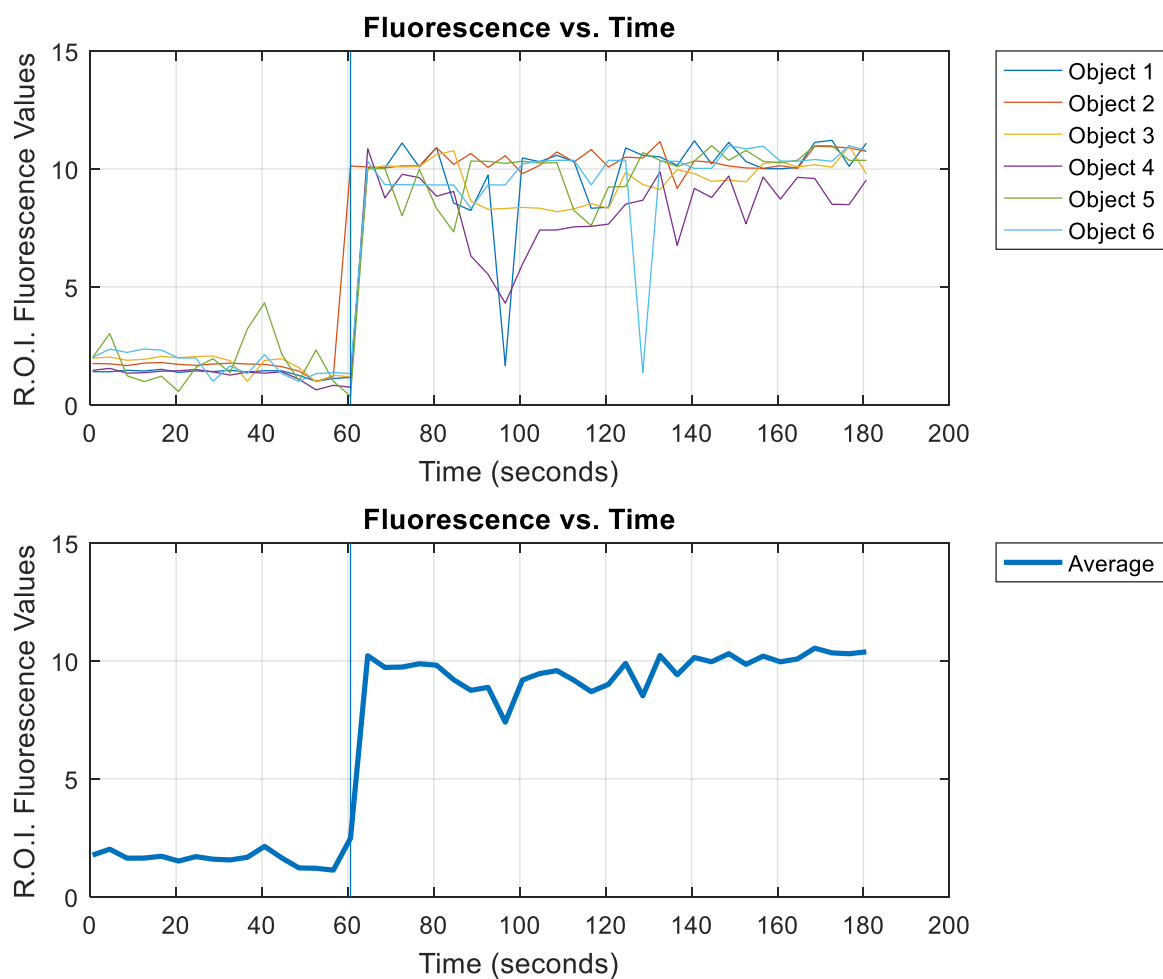


Figure 3-11: Line tracings of severely depleted primary mixed glia cortical cultures responding to an addition of $100\mu\text{M}$ glu. Top Panel: Each line represents individual cells (ROIs). Bottom Panel: Average of all ROIs

Astrocytes also require high concentrations of glu to elicit fluorescence calcium responses, and the calcium response tends to slowly increase with time. The pure astrocyte cultures also tend to respond with broader peaks as expected. The brain functions optimally in with functioning microenvironments containing neurons and glial cells. Although pure astrocyte cultures look completely healthy under the microscope, we have observed that these cells take longer to recover from glu stimulations that mixed cultures (Figure 3-12).

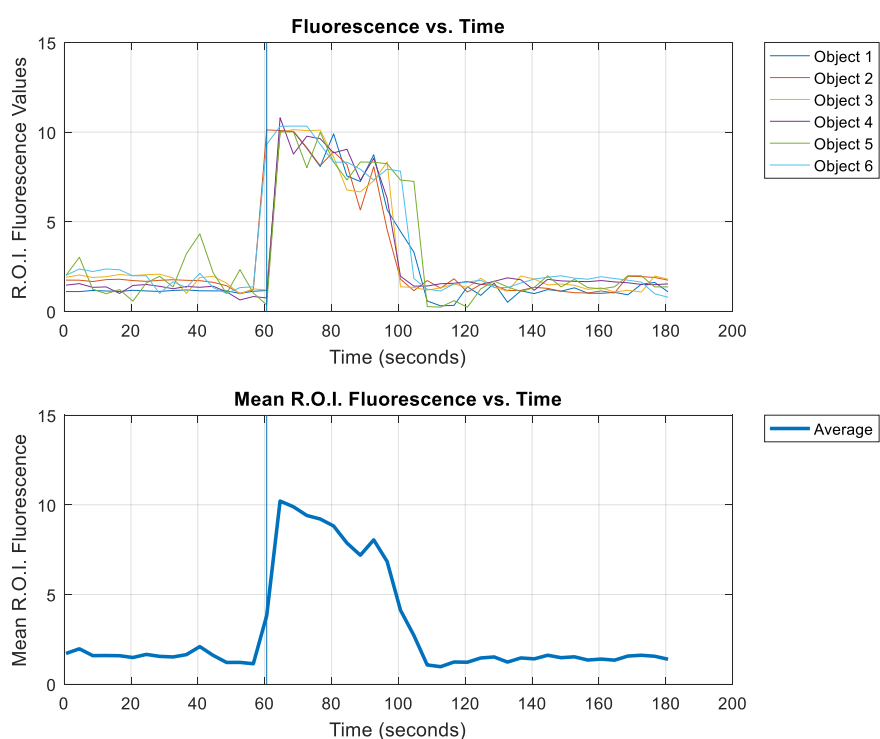


Figure 3-12: Line tracings of pure astrocyte cortical cultures responding to an addition of 100 μ M glu. Top Panel: Each line represents individual cells (ROIs). Bottom Panel: Average of all ROIs

When exposed to glutamate, the mildly depleted pure astrocyte cultures respond with broad, high amplitude peaks indicating very high calcium influx (Figure 3-13).

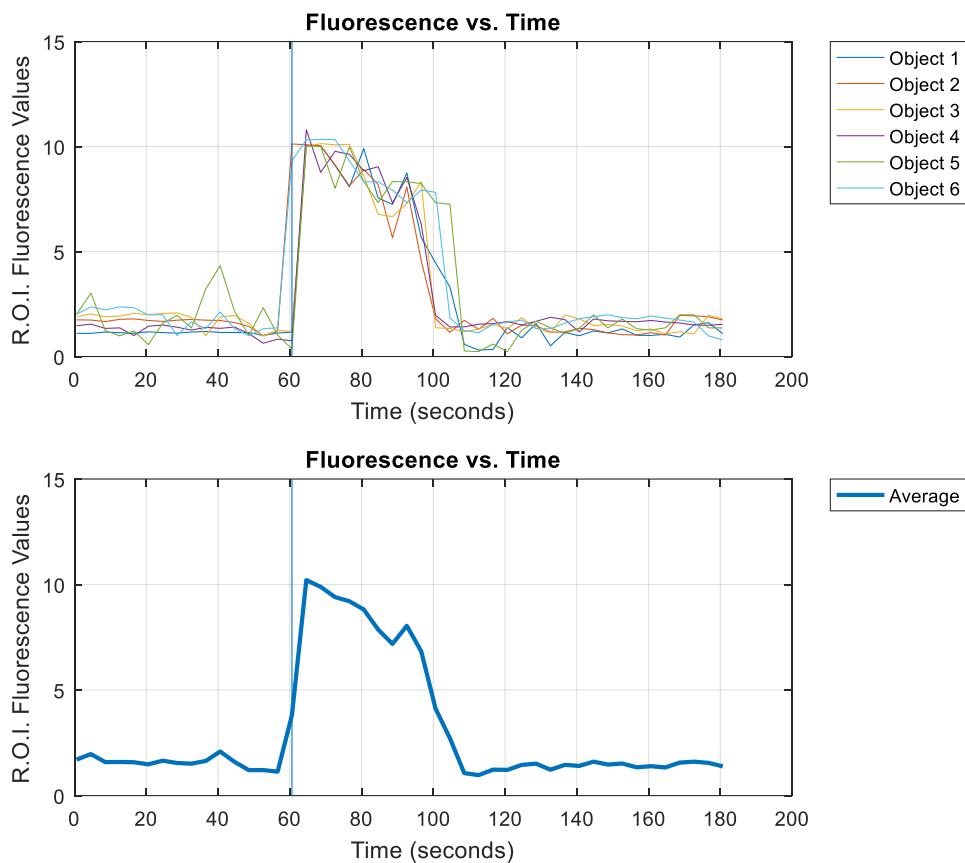


Figure 3-13: Line tracings of mildly depleted primary pure cortical astrocyte cultures response to additions of $100\mu\text{M}$ glu concentrations. Top Panel: Each line represents individual cells (ROIs). Bottom Panel: Average of all ROIs

When exposed to glutamate, the partially depleted pure astrocyte cultures respond with broader, high amplitude peaks indicating an even higher calcium influx than the mildly depleted cultures (Figure 3-14).

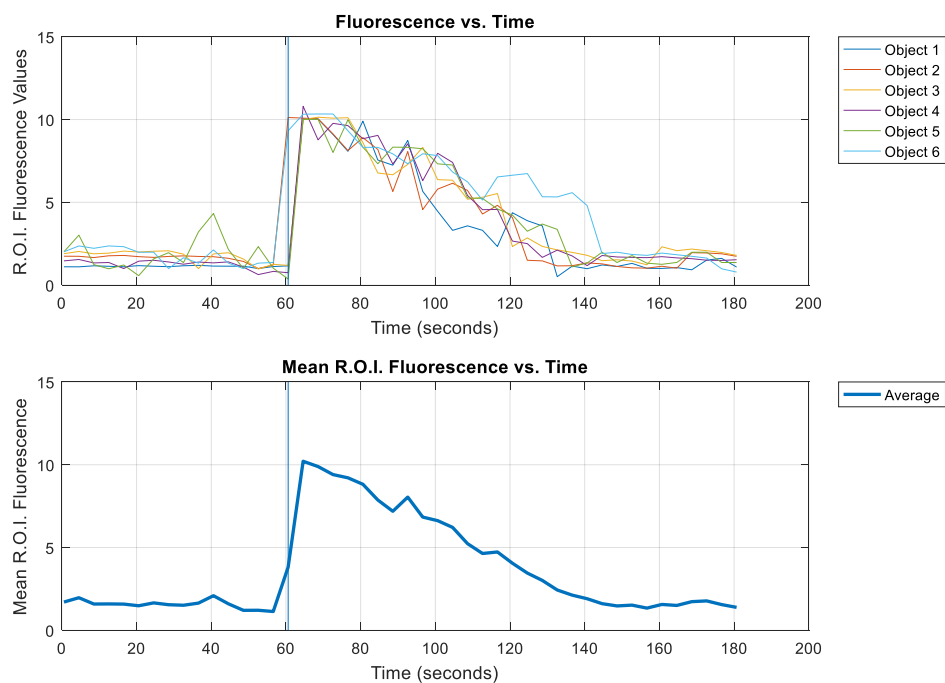


Figure 3-14: Line tracings of partially depleted primary pure cortical astrocyte cultures response to additions of 100 μ M glu concentrations. Top Panel: Each line represents individual cells (ROIs). Bottom Panel: Average of all ROIs

Like the severely depleted mixed glial cultures, the severely depleted pure astrocyte cultures responded to glu stimulation with a high amplitude response to calcium influx without returning to baseline levels as seen in excitotoxic micro-environments (Figure 3-15).

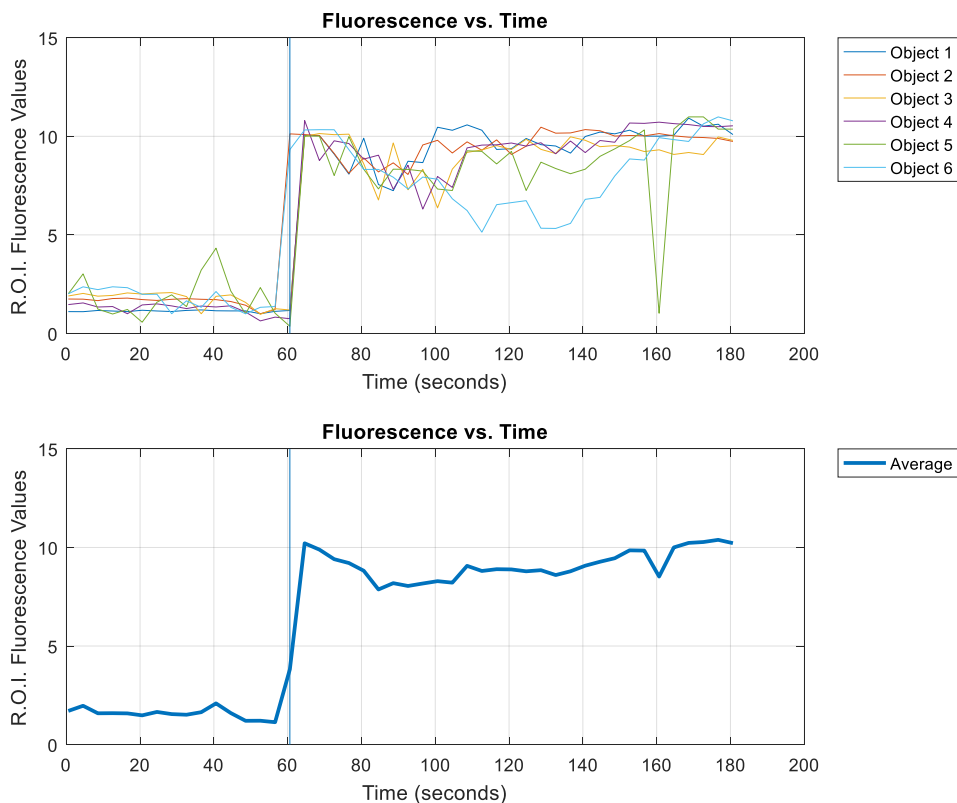


Figure 3-15: Line tracings of severely depleted primary cortical pure astrocyte cultures response to additions of $100\mu\text{M}$ glu concentrations. Top Panel: Each line represents individual cells (ROIs). Bottom Panel: Average of all ROIs

In summary, the different conditions resulted in the following findings. The mildly and partially glia depleted cultures behaved similarly to glia rich cultures with narrow width responses (peaks) to calcium influx. It is important to note that although the range for partially glia depleted cultures was between thirty and sixty percent depleted, the cultures used in these experiments were between thirty-five and forty-five percent depleted. The severely depleted cultures using both FdU and AraC displayed very broad and high amplitude responses to glu stimulation. The broad peaks are indicative of excitotoxicity; line tracings of excitotoxic responses do not return to baseline. The excitotoxic response in calcium signaling to glutamate may be caused by glutamate also binding to the dendritic

NMDA receptors after over-exposure due to the altered negative feedback component (glia density).

3.3 Image Analysis

This work is a continuation of Dr. Kinsey Kelly's dissertation research (45). In her studies, she concluded that the area under the curve was the best predictor of neuronal response to glutamate stimulation. We have therefore continued using the area under the curve (AUC) as the defining characteristic indicating the strength of the signal induced by glutamate stimulation. This parameter is essential for determining calcium information processing and will be used throughout the upcoming chapter. The final parameter used in this analysis was the number of cells responding to a stimulus. This will be used to determine the level of synchrony within the culture.

3.3.1 Area Under the Curve

The trapezoidal rule was used to determine the AUC for the fluorescence intensity curve, f. The trapezoidal equation used is as follows:

$$\int_a^b f(x)dx \approx (b - a) \frac{f(a) + f(b)}{2}$$

Where time (s) is a and b, and their corresponding fluorescence intensities are f(a) and f(b) at the time interval's end points. An average of evaluated areas is then compiled for every ROI. To improve analysis, we developed a MATLAB code to measure area under the curve using trapezoidal Riemann sums. The MATLAB code and instructions for using the code are found in Appendix C.

AUC elucidates the effects of altered glial cell density on calcium signaling when trying to determine the amount of calcium which has permeated into the cytosol. As

expected, severely depleted glial cultures have increased AUC as glu concentrations increase. In contrast, partially and mildly depleted glial cultures have very low AUC per treatment and a slight decrease in AUC with increasing treatment additions (not statistically significant). In mixed neuronal cultures, the AUC for the calcium response curves at baseline and after treatment with 250, 500 and 750 nM glu for the control (untreated) are 51, 385, 230, and 412 respectively, with standard deviations of 27.38, 12.32, 15.92, and 57.12 respectively. The AUC for the calcium response curves at baseline and after treatment with 250, 500 and 750 nM glu for the mildly depleted cultures are 58, 258, 240, and 367 respectively, with standard deviations of 23.45, 20.154, 36.12, and 45.23 respectively. The AUC for the calcium response curves at baseline and after treatment with 250, 500 and 750 nM glu for the partially depleted cultures are 40, 358, 400, and 425 respectively, with standard deviations of 11.36, 28.56, 21.33, and 36.21 respectively. These results are shown in Figures 3-16 to 3-19.

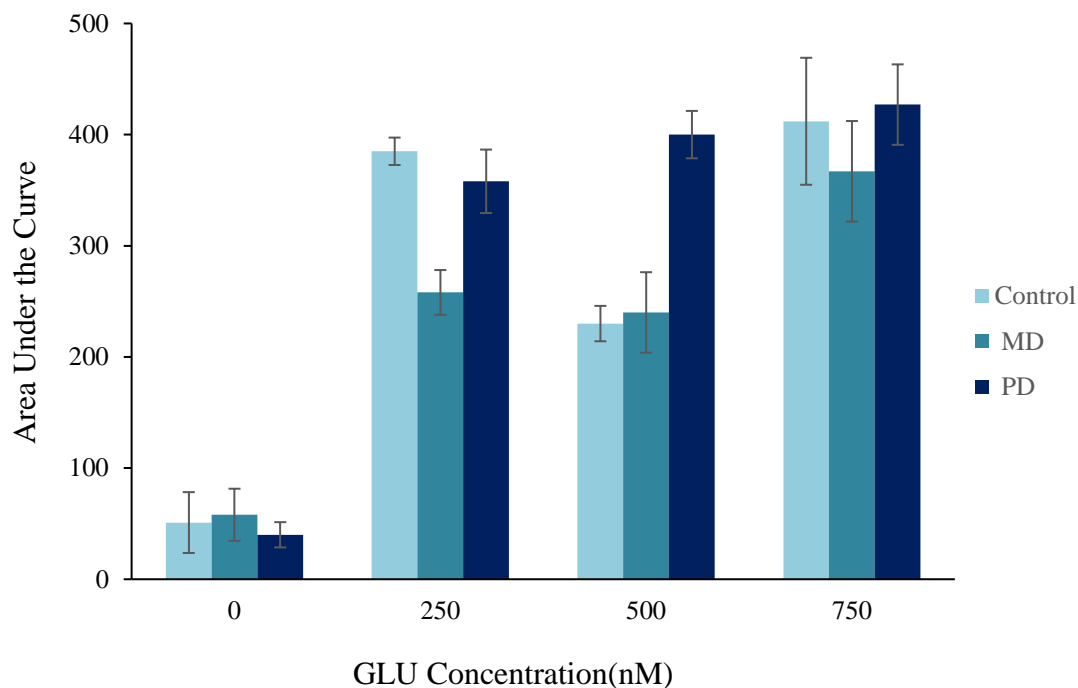


Figure 3-16: Area under the curve (AUC) in response to glutamate treatments to mixed neuronal cultures high in glia (control), mildly glia depleted (MD) and partially depleted (PD). Error bars = sd, n=18.

The area under the curve in mixed neuronal cultures severely depleted of glia was at least ten times greater than the other conditions. The AUC for the calcium response curves at baseline and after treatment with 250, 500 and 750 nM glu for the severely depleted cultures are 20, 2374, 6125, and 8236 respectively, with standard deviations of 2.36, 112.47, 231.885, and 212.36 respectively. This indicates that the severely depleted microenvironments recover from subthreshold (physiological) glutamate concentrations at a much lower rate than the other two conditions (Figure 3-17).

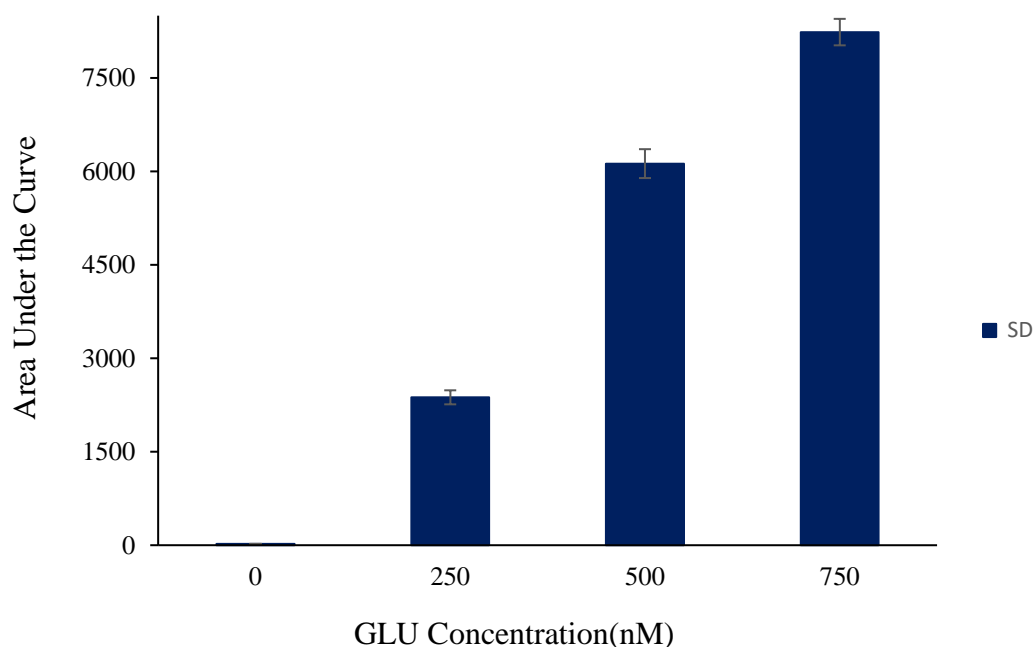


Figure 3-17: Area under the curve (AUC) in response to glutamate treatments to mixed neuronal cultures severely glia depleted (SD). Error bars = sd, n=18.

In mixed glial cultures, the AUC for the calcium response curves at baseline and after treatment with 100 μ M glu for the control (untreated) are 17, and 321 respectively, with standard deviations of 5.5, and 72.112 respectively. The AUC for the calcium response curves at baseline and after treatment with 100 μ M glu for the mildly depleted cultures are 13 and 397 respectively, with standard deviations of 3.47 and 63.24 respectively. The AUC for the calcium response curves at baseline and after treatment with 100 μ M glu for the partially depleted cultures are 5 and 356 respectively, with standard deviations of 1.21, and 54.21 respectively. The AUC could not be measured in severely depleted cultures as the fluorescence values remained elevated. There were no statistical differences in AUC of mixed glial cultures in each microenvironment (Figure 3-18).

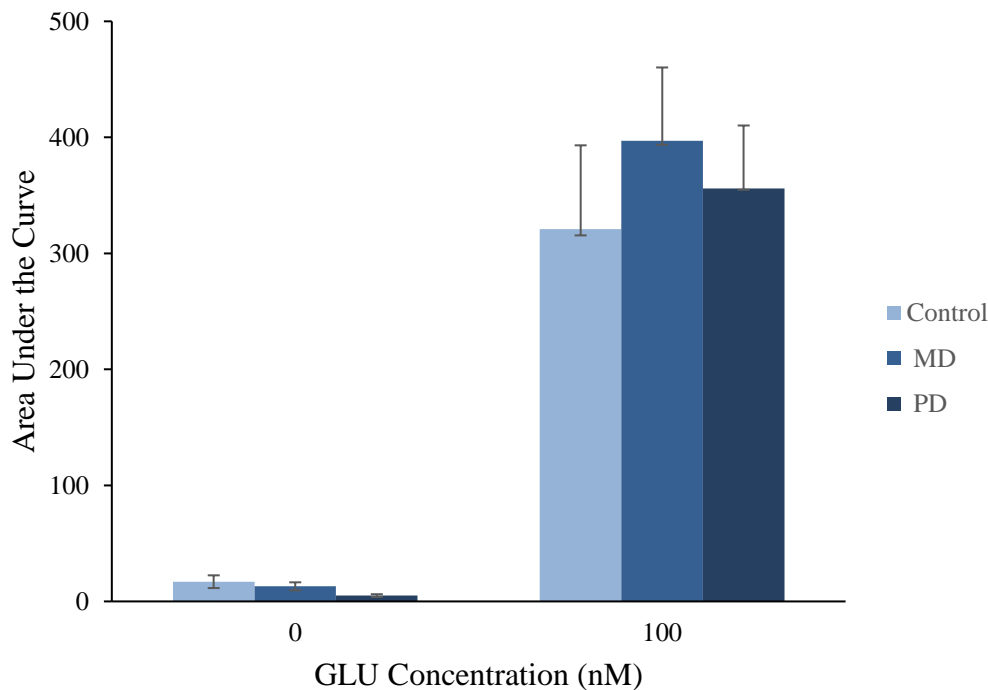


Figure 3-18: Area under the curve (AUC) in response to glutamate treatments to mixed glial cultures high in astrocyte (control), mildly depleted (MD) and partially depleted (PD). Error bars = sd, n = 18.

In pure astrocyte, the AUC for the calcium response curves at baseline and after treatment with 100 μ M glu for the control (untreated) are 15, and 852 respectively, with standard deviations of 5.5, and 57.8 respectively. The AUC for the calcium response curves at baseline and after treatment with 100 μ M glu for the mildly depleted cultures are 13 and 1200 respectively, with standard deviations of 4.63, and 355.37 respectively. The AUC for the calcium response curves at baseline and after treatment with 100 μ M glu for the partially depleted cultures are 7 and 2020 respectively, with standard deviations of 2.11, and 334.17 respectively. Like the mixed glial cultures, there was also no statistical difference observed in the AUC of the pure astrocyte cultures in each microenvironment (Figure 3-19). The

AUC could not be measured in severely depleted cultures as the fluorescence values remained elevated.

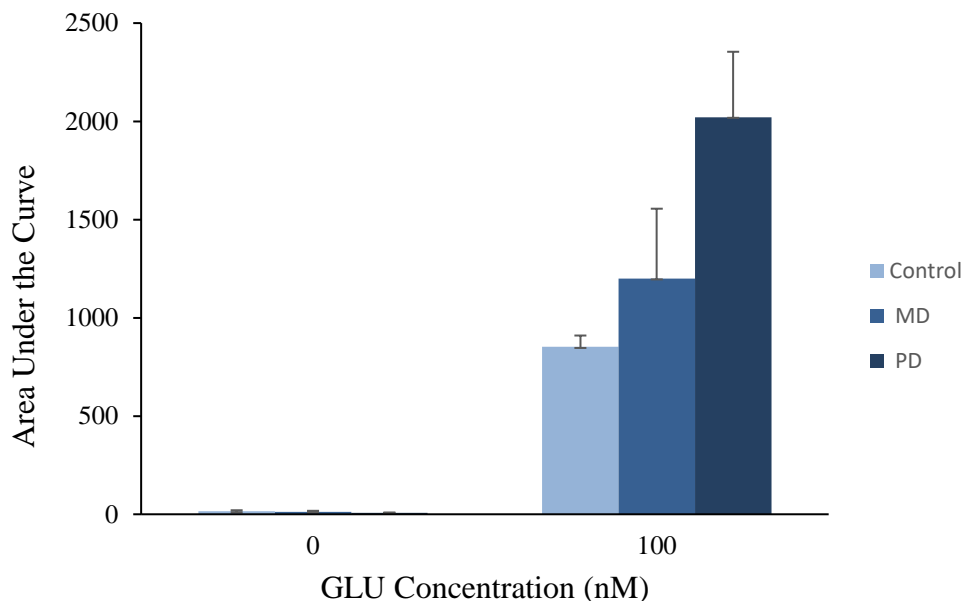


Figure 3-19: Area under the curve (AUC) in response to glutamate treatments to pure astrocyte cultures high in astrocyte (control), mildly depleted (MD) and partially depleted (PD). Error bars = sd, n=18.

Calcium imaging was used to visualize and analyze calcium influx due to cellular exposure to exogenous glu. In these experiments, the cells are stimulated by different glu concentrations and the calcium influx is detected by calcium indicators loaded in the cytosol. Calcium response curves are then developed by imaging software measuring changes in fluorescence (when the indicator is bound to calcium). These experiments were done in mixed neuronal, mixed glial and pure astrocyte cultures. Subthreshold (physiological) concentrations of 250, 500 and 750 nM glu were used to stimulate the mixed neuronal cultures and 100 μ M glu was used to stimulate the mixed glial and pure

astrocyte cultures. The results indicate that severely depleted cultures recover at a much slower rate than any other condition and our hypothesis that decreasing the glial cell density will increase the amount of glutamate to which the neurons are exposed was supported.

To further study the calcium dynamics, this project is also geared towards the development of mathematical tools to model each phase in the calcium response curve which is discussed in chapter four.

CHAPTER 4

MATHEMATICAL TOOLS

4.1 Introduction

The third goal for this project is to develop mathematical tools for studying brain cell dynamics. Given the recent mathematical advancements in neuroscience, new ways of studying one of the most complicated organs in the body (the brain) have been developed. Our understanding of neuronal communication in the processes involved in development, maintenance, and disorders of the nervous systems has been significantly improved.

Neurons communicate via electro-chemical signalling. One of the most prominent examples of neuronal communication is neurotransmission. Electrical stimulation of the presynaptic neuron causes the release of glutamate which then binds to the NMDA receptor on the post synaptic membrane which may either be at slightly depolarized or resting membrane voltages. The channel then opens and allows positively charged ions such as Na^+ and Ca^{2+} into the cells. This influx of positive charge causes an increase in membrane potential which, if sufficiently high, will cause the cell to fire an action potential which is seen as a spike if the membrane potential is being measured. This in turn causes the release of glutamate from the axon terminal and the signal travels within the neuronal circuit. In a healthy brain, synchronization within and between neural micro-circuits is an important mechanism for neural signalling and information processing(72).

A growing number of tools have been developed allowing the simulation of spiking neuronal networks. Increasing evidence suggests that an improved understanding of the synchronization process would be achieved by studying the bidirectional signalling between astrocytes and neurons. Astrocytes are connected via gap junctions and form a large functional syncytium within neuronal networks. Although astrocytes cannot fire action potentials, they respond to neuronal activity by an increased intracellular calcium concentration. These astrocytic responses to neuronal signalling introduces the concept of the tripartite synapse, where the astrocyte (third element) monitors and responds to synaptic activity. In this chapter, a dynamic, functional model of neurons and astrocytes within the neural circuit and the effect that astrocyte density has on neural synchrony will be discussed.

4.2 Modeling each phase after glutamate stimulation

The goal of this chapter is to describe some of the mathematical tools that have been developed to study neuronal interactions. In addition to developing a model to show the effect of astrocytes on neural synchrony, we have been able to use mathematical equations to model the distinct phases in the calcium response curve when brain cells are stimulated with glutamate. When graphed, the cellular response to glutamate can be considered in three sections: the cells' natural state which is characterized by small baseline oscillations; the immediate response to the stimulus which results in a sharp upward peak, and the recovery of the cells from the stimulus seen as a decrease in fluorescence. In Figure 4-1, a discrete logistic equation is used to model the random oscillatory behavior of cells before any stimulation takes place. Discrete logistic equation:

$$x_{t+1} = 3.7X_t(1 - X_t) + 0.3 \quad \text{Eqn. 4-1}$$

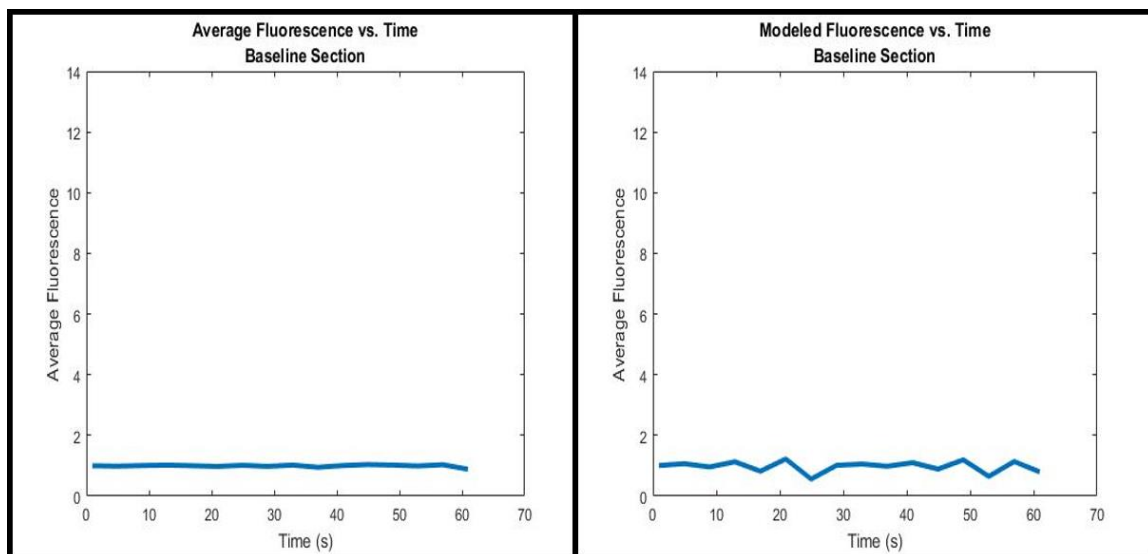


Figure 4-1: Plots of (a) averaged baseline response, (b) baseline response modeled by $x_{t+1}=3.7x_t(1-x_t) +0.3$. For all equations, x_t is the fluorescence at any given time, t , and t_i is the time since the introduction of the stimulus.

This equation is a pseudo-random generation of numbers; each number being determined by the previous value. X_t is the fluorescence at any given time t . T_i is the time since the introduction of the stimulus.

The second part of the response curve is the increase in fluorescence due to glutamate stimulation. The equation of a straight line ($y = mx + b$) where m is the slope of the line and b is the y intercept, is used to model this part and the results are shown in Figure 4-2.

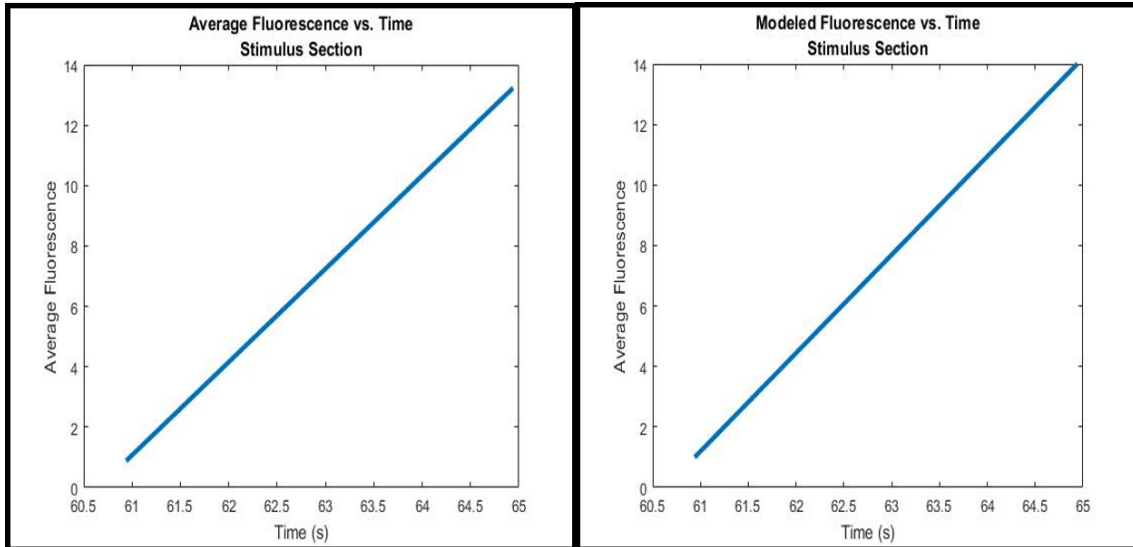


Figure 4-2: Plots (a) averaged immediate response to the glutamate, (b) response to glutamate modeled by $x_t=13t_i-12$. For all equations, x_t is the fluorescence at any given time, t , and t_i is the time since the introduction of the stimulus.

The third and final part of the response curve is the recovery period characterized by a rapid decrease in fluorescence which we have used the exponential decay equation to model. This is shown in Figure 4-3

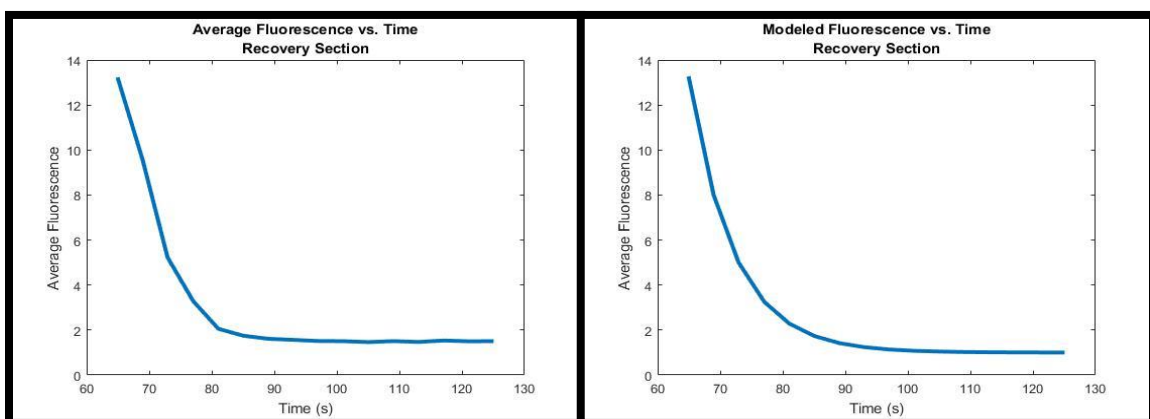


Figure 4-3: Plots (a) averaged fluorescence during the recovery period, and (b) recovery period modeled by $x_t=14e^{-0.14t_i}+1$. For all equations, x_t is the fluorescence at any given time, t , and t_i is the time since the introduction of the stimulus.

The actual baseline oscillations in mixed neuronal cultures that are more dynamic and chaotic than astrocyte cultures are shown in Figure 4-4.

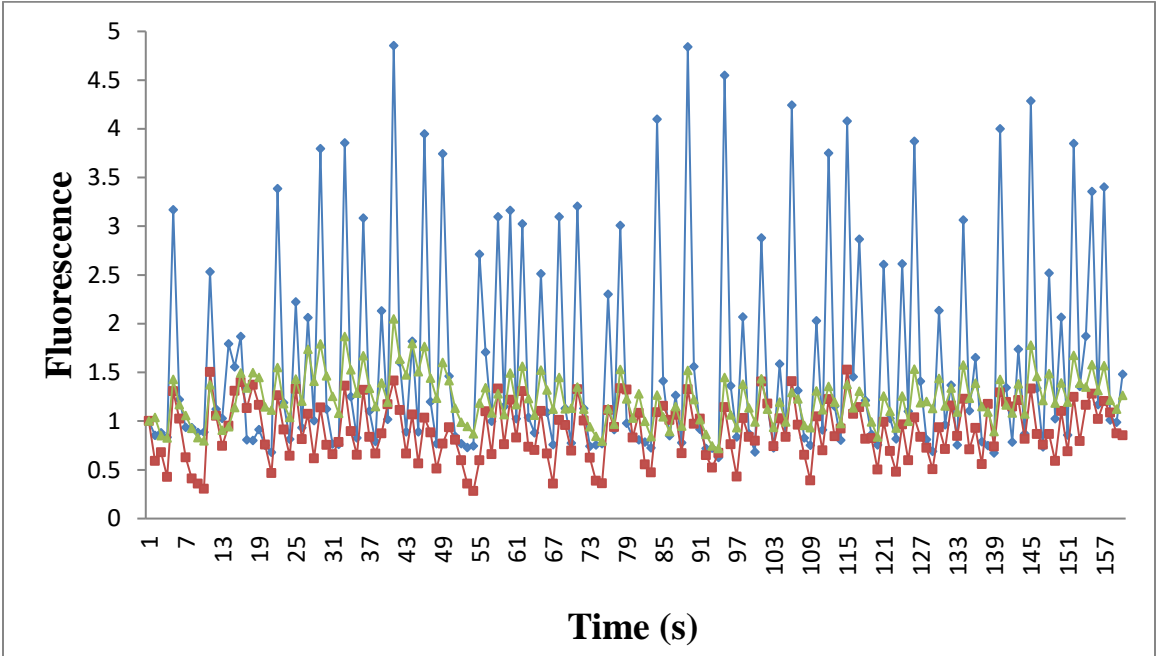
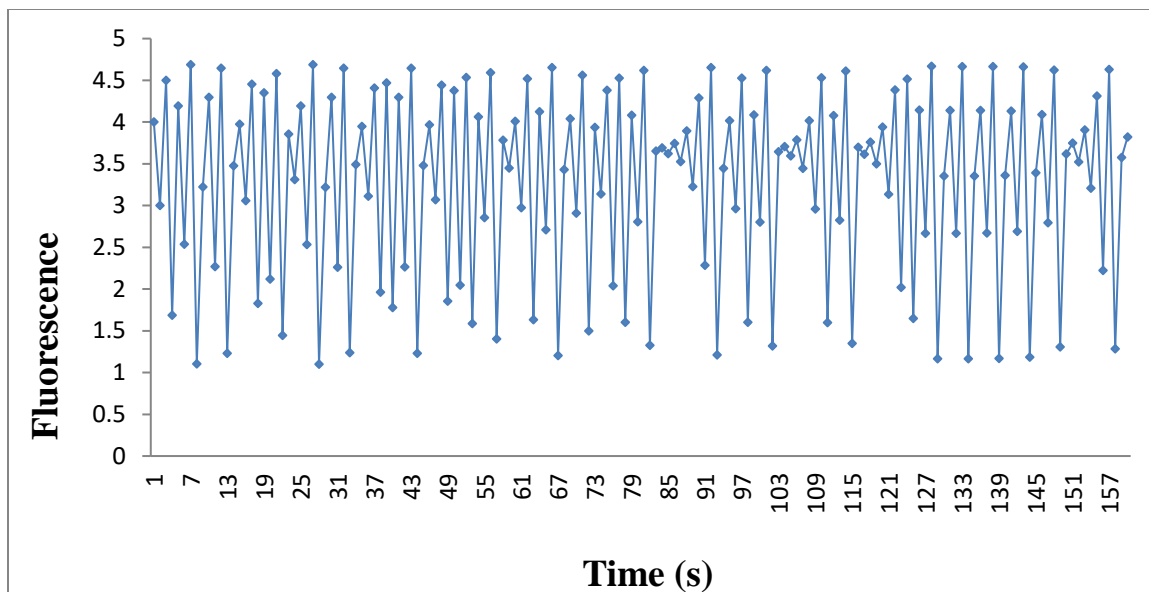


Figure 4-4: Baseline oscillation recorded in mixed neuronal cultures

After running the discrete logistic equation (Eqn. 4-1) 160 times the following graph is obtained (Figure 4-5).



Ionomycin is added to brain cell cultures to obtain a sustained fluorescence maximum.

One equation that can be used to describe this phenomenon is:

$$f(t) = a(1 - e^{-b(t-t_0)}) + b \quad \text{Eqn. 4-2}$$

Where a , b and c are curve fit parameters, t is any given time and t_0 is the time since the introduction of the stimulus. Figure 4-6 shows the type of wave form derived when Eqn. 4-2 is plotted.

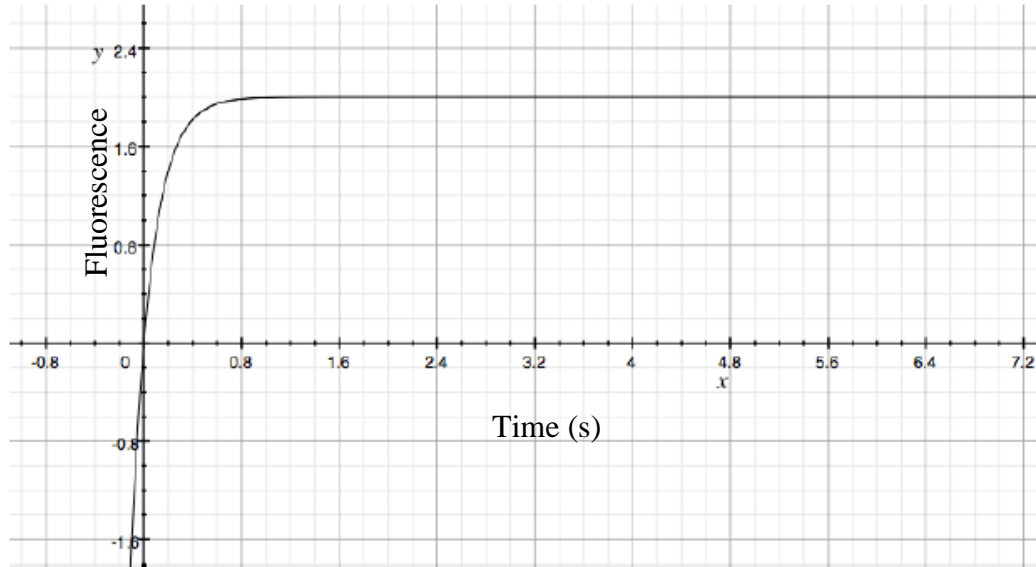


Figure 4-6: Graph showing waveform derived from Eqn. 4-2

During a calcium imaging experiment, the rising slope of the signal is typically different from the falling slope (calcium influx occurs more rapidly than efflux). One model for all three stages of the curve collectively is the Landau function:

$$f(t) = \frac{a}{2\pi} e^{-b(t+e^{ct})} + d \quad \text{Eqn. 4-3}$$

Where a , b , c , and d are curve fit parameters. Figure 4-7 shows the type of wave form derived from this equation.

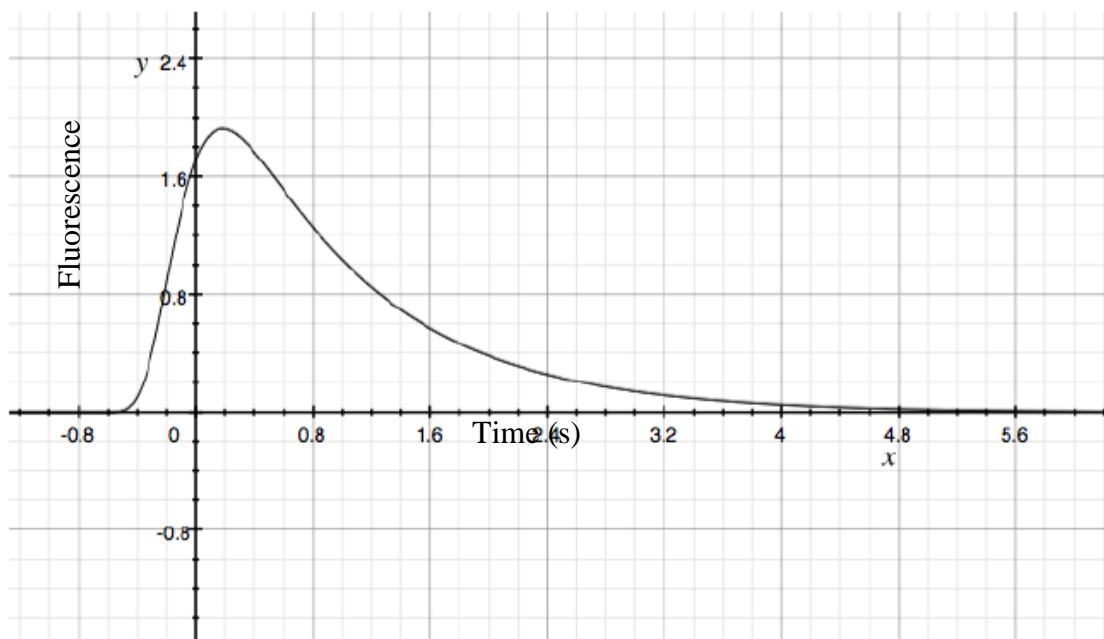


Figure 4-7: Graph showing wave- form derived from Eqn. 4-50.

In addition to the segmented analysis, some more mathematical modelling tools can be found in Appendix C.

CHAPTER 5

CELLULAR INTERACTION WITH NOVEL BIOMATERIALS

5.1 Introduction

The brain is arguably one of the most important organs of the body and as such, the human body has developed many intrinsic protective mechanisms. Unfortunately, the brain can be negatively affected by many conditions such as stroke, hypoxia, neurodegenerative diseases, cancer, and acute trauma which causes a loss of neuronal populations and neurological symptoms ensue. Presently, most treatment options modify disease symptoms but are not able to restore the lost neuronal populations or stop neurodegenerative processes.

Biomaterials demonstrate great promise for use as tools in a wide range of biomedical applications. For applications in neuroscience, these materials have been used to enable and augment targeted delivery therapeutic agents such as drug or proteins to the brain (82). Biomaterial scaffolds can be used as bridges, cell carriers, and targeted drug delivery vehicles, for transporting regenerative and therapeutic agents to damaged neuronal circuits. With the advancements in nanotechnology and material science, scientists are confident in the possibility of developing treatments for damage that is confined to localized neuronal populations or neural circuits. This has stimulated the search and development of drug delivery systems and tissue engineering approaches of neuronal damage repair (82).

Highly specific interactions with neural networks can be accomplished using nanomaterials (83). Nanotechnology based clinical tools are in their preliminary stages of development because of the complexity of neural networks and the central nervous system at large. Nanotechnology is the study of materials and/or devices with the smallest functional dimension on the nanometer scale (~1-100nm). There are two key applications for nanomaterials in neuroscience: platform nanotechnologies and tailored nanotechnologies (83). Platform nanotechnologies serve as building blocks for addressing neuroscience questions and tailored nanotechnologies are designed to complete materials used in treating neurological diseases.

5.2 Biomaterials Used in Neuroscience

Neurological disorders such as traumatic brain injuries, stroke, and epilepsy result in neuronal loss and disruption of the brain parenchyma. Current treatment strategies are limited in that they can only mitigate the degeneration process or alleviate the symptoms but do not reverse the condition. In contrast, regenerative cell-based therapies offer long-term hope for many patients. Bioactive scaffolds are likely to reinforce the success of cell replacement therapies by providing a microenvironment that facilitates the survival, proliferation, differentiation, and connectivity of transplanted and/or endogenous cells.

5.2.1 Quantum Dots

Quantum dots (QD) are nanocrystalline structures made of semiconductor material typically consisting of about 10-50 atoms (84). A remarkable feature of quantum dots is the size dependence of their emission wavelength. The electrons and electron holes within the semiconducting material are confined within the region of the crystalline structure. Due to this confinement, the electrons and the electron holes can be modeled

quantum mechanically as particles confined by an infinite potential of diameter equal to the size of the crystal (85). Another important feature of quantum dots is their narrow emission and broad absorption spectra allowing multiplexing of different colored quantum dots. This feature implies that multiple colors of quantum dots may be used with a single excitation source. A quantum dot usually consists of a core semiconducting material (heavy metal) surrounded by an intermediate unreactive shell typically made of zinc sulfide, which not only protects the crystalline structure of the core but can also boost the quantum yield. The outer coating can be made of bioactive molecules such as antibodies tailored to specific functions (Figure 5-1).

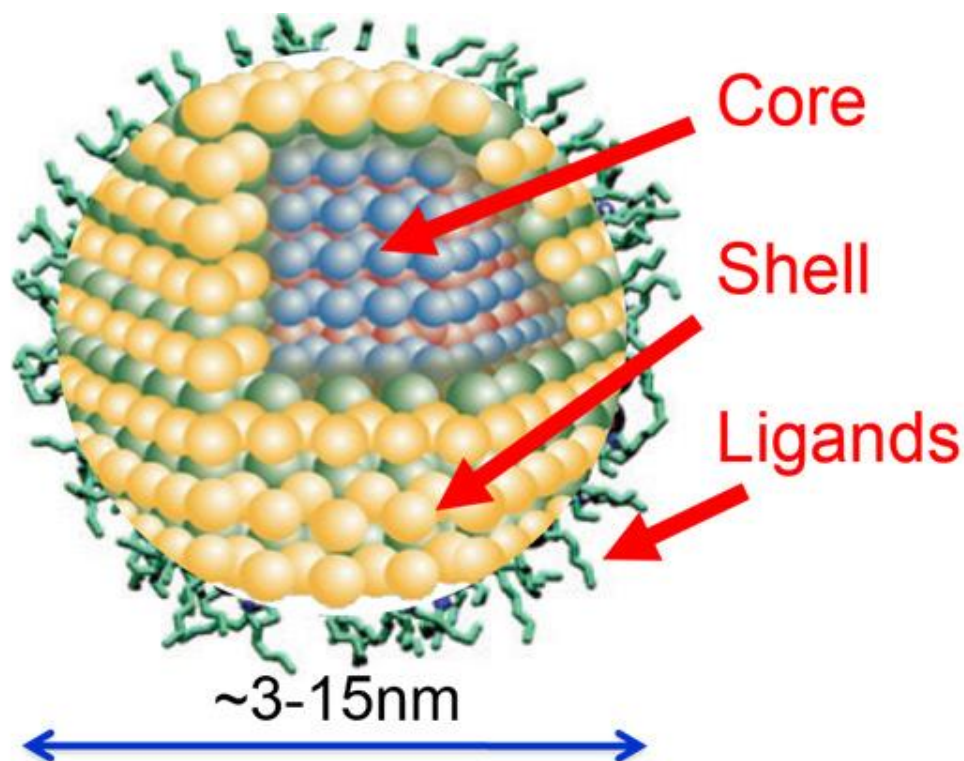


Figure 5-1: Diagram showing structure of semiconductor fluorescent quantum dot nanocrystal (86)

Due to their nanoparticle size, quantum dots are emerging as a powerful tool to track living cells *in vitro* and *in vivo*. They can also be functionalized with biomolecules, allowing for specific targeting of cells, which may aid in development of more accurate biological models.

These properties make quantum dots potentially new tools in neuroscience and neuroscience specific tools are being developed. These nanoparticles are particularly suited for studying neurons and glia as they can be used to visualize, measure, and track specific molecular events over longer periods of time than traditional imaging techniques with minimal photo bleaching. Because of their relatively small size, they can be used to track intra and intercellular events that otherwise evades larger imaging molecules (86). Recently, many neuroscience specific tools are being developed. Vu et al. used β Nerve Growth Factor (β NGF) functionalized quantum dots to promote neurite outgrowth in pheochromocytoma 12 (PC12) cells (87). Quantum dots can be used to track and visualize functional responses in neurons, but this new material is highly toxic therefore are not used if an alternative exists.

5.3 Copper Homeostasis in the CNS

Copper (Cu) is an essential trace element involved in red blood cell development, collagen formation, maintenance of both immune and nerve cells. Cu also functions as a cofactor in a number of enzyme dependent metabolic reactions (88). During infection, Cu facilitates the production of interleukin-2 by activated lymphocytic cells (89). Tiny amounts of copper are needed for healthy brain development and synthesis of neurotransmitters essential for neural signal transduction. Due to its reactivity, the presence of copper within a system can facilitate the development of reactive oxygen

species in a Fenton-like reaction causing cell death and oxidative stress. This is especially deleterious to organs to the brain as neurons are post-mitotic cells and become terminally differentiated early in development thus making it almost impossible to replace dead cells(90). As a result, copper metabolism within the body must be tightly regulated to supply sufficient Cu to target areas but also to prevent Cu induced oxidative stress (91). Cu deficiency and over expression can severely diminish brain function. Certain neurodegenerative diseases are associated with impaired Cu homeostatic mechanism such as Menkes disease, Wilson's disease, and Alzheimer's disease (91).

The presence of several copper-containing enzymes in astrocytes suggests that astrocytes are crucial in regulating Cu metabolism in the brain. Their location (between neuronal elements and capillary endothelial cells) gives them the ability to transport Cu from the blood brain barrier to the parenchymal brain cells (92). Astrocytes store and export Cu efficiently to the neurons and although the mechanism is not fully understood, there is evidence suggesting that in the normal brain, Cu uptake is facilitated by the copper transporter receptor 1(Ctr1) and other presently unidentified transporters. Thus far, the accepted K_M value for copper uptake is $10\mu\text{M}$ and the expression of Ctr1 on astrocytes exposed to copper suggests that this receptor is responsible for high affinity copper uptake (93) (Figure 5-2)

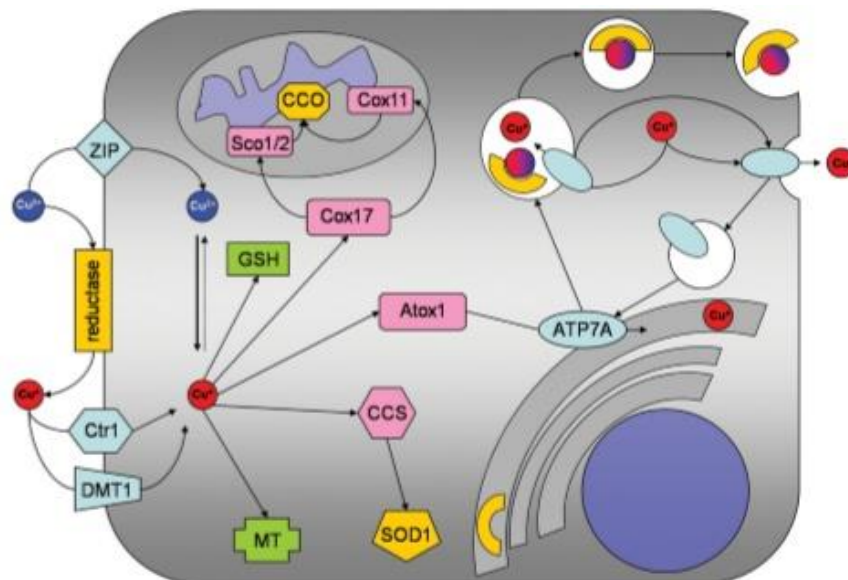


Figure 5-2: Diagram showing summary of copper uptake in astrocytes (93)

Ctr1 receptors and other Ctr1 independent mechanisms are responsible for the uptake of Cu in astrocytes. Some of these mechanisms include the divalent metal transport 1 (DMT1) or the members of the ZIP family of metal transporters(93). Cu is then transported to various cellular regions via copper chaperones (CCS) to superoxide dismutase 1 (SOD1) or Cox17 to Sco1/2or Cox11 for subsequent incorporation into cytochrome c oxidase and by antioxidant protein 1 (Atox1) to ATP7A. ATP7A then transports copper into the trans-Golgi network to be incorporated into copper-dependent enzymes. When the cellular copper level rises above a certain threshold, ATP7A translocates reversibly via vesicles to the plasma membrane to export copper.

Exposure of astrocytes in culture to excess Cu causes the cellular glutathione (GSH) levels to increase and initiates metallothionein synthesis(93). This suggests that excess Cu is stored in the form of GSH and metallothioneins in astrocytes. This stored Cu is then released via ATP7A to supply the neurons (Figure 5-3).

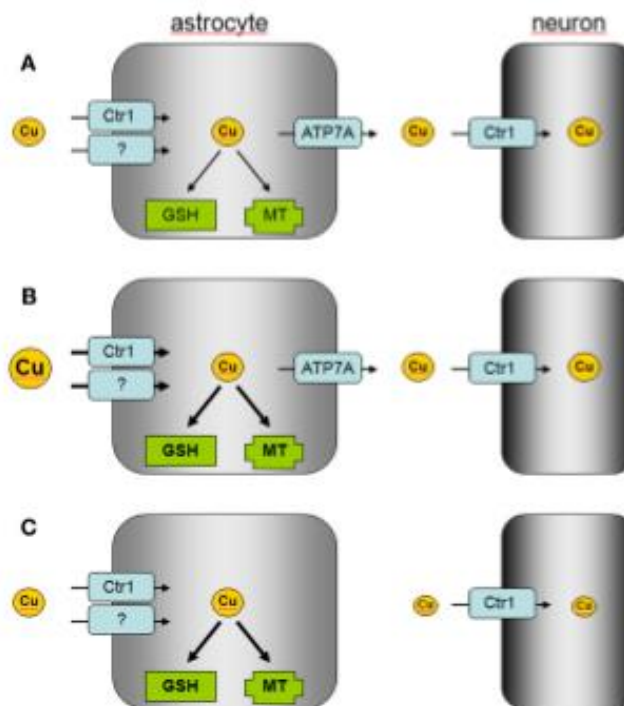


Figure 5-3: Diagram of proposed model of astrocytic copper supply to neurons (93)

Astrocytes can be considered as a therapeutic target for disturbances in brain copper homeostasis as they are able to efficiently uptake, store, and export copper

5.3.1 Copper containing High Aspect Ratio Structures

Our lab has recently developed a copper containing high-aspect ratio structure (CuHARS) synthesized in an aqueous solution with sizes ranging from nano- to the micrometer as confirmed by electron microscopy. We have discovered that over time, and under biological conditions typically used in cell culturing, these structures are formed. CuHARS are made up of a copper metal component (40%) and the amino acid dimer cystine as the organic component (60%) as indicated by the thermo-gravimetric analysis in (results not shown) and by scanning electron microscopy (SEM) (94). These structures, once

generated, are stable without agglomeration, for months-years under refrigeration when stored in water.

5.3.2 Biocompatibility of CuHARS

Many biomedical applications utilizing different biomaterials such as drug delivery would require substantial amounts of the material to be administered to the cells or brain region of interest. As a result, it is important that the cytotoxic effect of moderate to high concentrations of these materials is being investigated. The discovery of this material has opened the possibility of creating functionalized biomaterials with growth factors (for neuronal recovery and regeneration) or antibodies for targeted delivery in the brain. Interactions between the HARS and different cell types have been studied and as a result, we are interested in evaluating the biocompatibility of this material. In this study, we investigated the cytotoxic effects of the CuHARS material on PC12 cells as a model for neuronal development. One property of PC12 cells is their quantifiable, rapid, and reversible response to nerve growth factor (NGF). On exposure to NGF, PC12 cells develop neurite-like extensions up to 1cm in length⁽⁹⁵⁾ . We examine and quantify the specific effects that our HARS biocomposite have on cultured PC12 cells and study their ability to respond to the biological cue NGF as compared with control cells. The main objective of this study was to examine the cytotoxicological effects of our previously developed copper containing biocomposite which is intended for use in neurological cell culture systems.

The protocols used for synthesizing the CuHARS, cell culture and studying the cytotoxic effects of the materials on cells are outlined in APPENDIX A. In these studies, this method was used to evaluate the potential adverse effects of the biocomposite material

in PC12 cells. The assay was done after exposure for 6, 12, 24 and 48 hours. Exposure to increasing concentrations of CuHARS biocomposite resulted in a dose-dependent diminishing viability of PC12 cells using MTT method. At very low to moderate concentrations, cell viability was not significantly affected, however at a concentration of 50 μ g/ml cell viability significantly decreased. The metabolic activity of PC12 cells decreased in a concentration dependent manner (Figure 5-4).

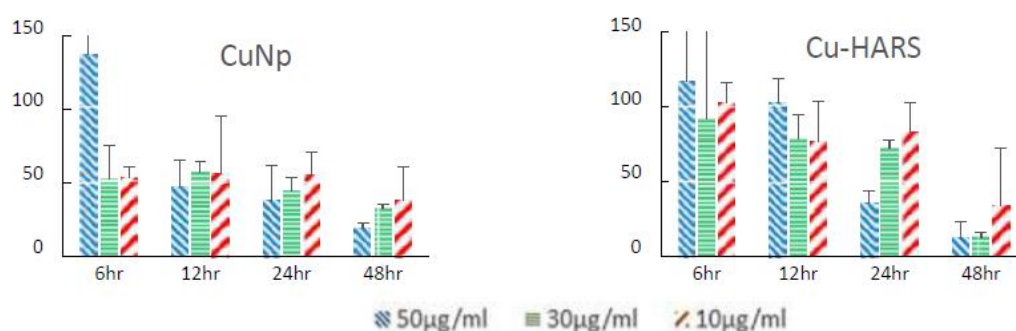


Figure 5-4: Effect of varying CuHARS concentration on mitochondrial toxicity of PC12 cells A) Copper Nanoparticle (CuNP) treatment. B) CuHARS treatment. Y: Axis values=Relative Absorbance normalized to the controls (no treatment).

As mentioned previously, astrocytes are a viable target for treatment with copper. The first step in using any biomaterial as a therapeutic agent is to study the biocompatibility of the material within the target environment which in this case is the brain. The cytotoxic activity of CuHARS was tested with primary astrocytes derived from Sprague –Dawley newborn rat pups (age \leq 48hours). It was found that the metabolic activity of the primary astrocytes also decreased in a concentration dependent manner

5.3.3 Functionalization of CuHARS using Layer by Layer Assembly

Drug delivery systems are developed for targeted delivery and controlled release of drugs. Our lab is interested in using the self-assembled biohybrid CuHARS material as a drug delivery vehicle, as it is a biocompatible material which is fully degraded overtime in cellular media (96). The main goal of this section is to describe the functionalization of the CuHARS with ionomycin. The CuHARS are negatively charged materials. In using the Layer by Layer method, the CuHARS can be functionalized by adding alternating layers of oppositely charged materials with washing steps between. We used a polycationic (positively charged) material called poly-lysine to coat the CuHARS materials then we would like to attempt to add another layer of the ionophore A21387 to the PLL labelled material. The protocol utilized for this process can be found in Appendix A. To confirm that the CuHARS were successfully coated with PLL we used microscopy to observe the reverse coffee ring effect in the coated material. When a drop of liquid containing particulates dries on a solid surface, suspended particulate matter is deposited in a ring-like fashion which is known as the coffee ring effect (102). The CuHARS material, because it does not form particulates does not exhibit this effect. The unlabeled CuHARS are more evenly distributed throughout the well. We observed that the PLL labelled CuHARS were generally found at the edge of the well more than the uncoated CuHARS. Figure 5-5 is a schematic of the observed distribution of CuHARS throughout the entire well and Figure 5-6 are Bright-

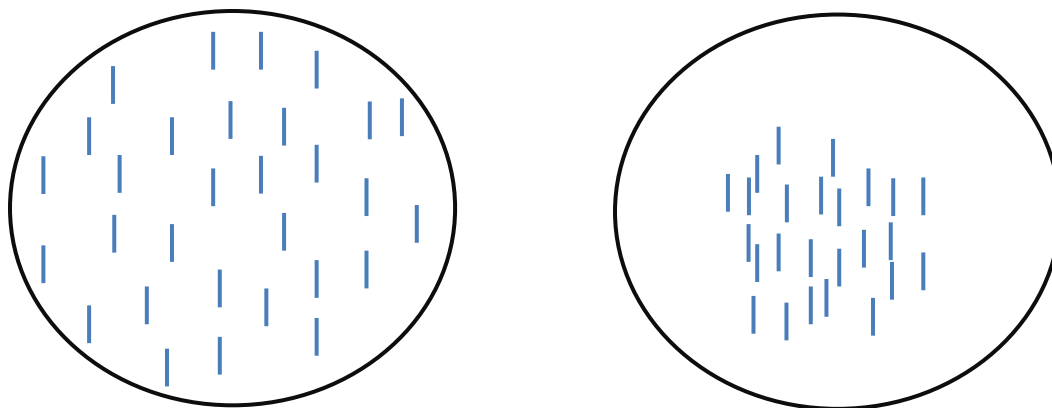


Figure 5-5: Schematic illustrating distribution of CuHARS throughout individual wells in the 48 well cell culture treated plate. Left) PLL coated CuHARS, Right) Uncoated CuHARS

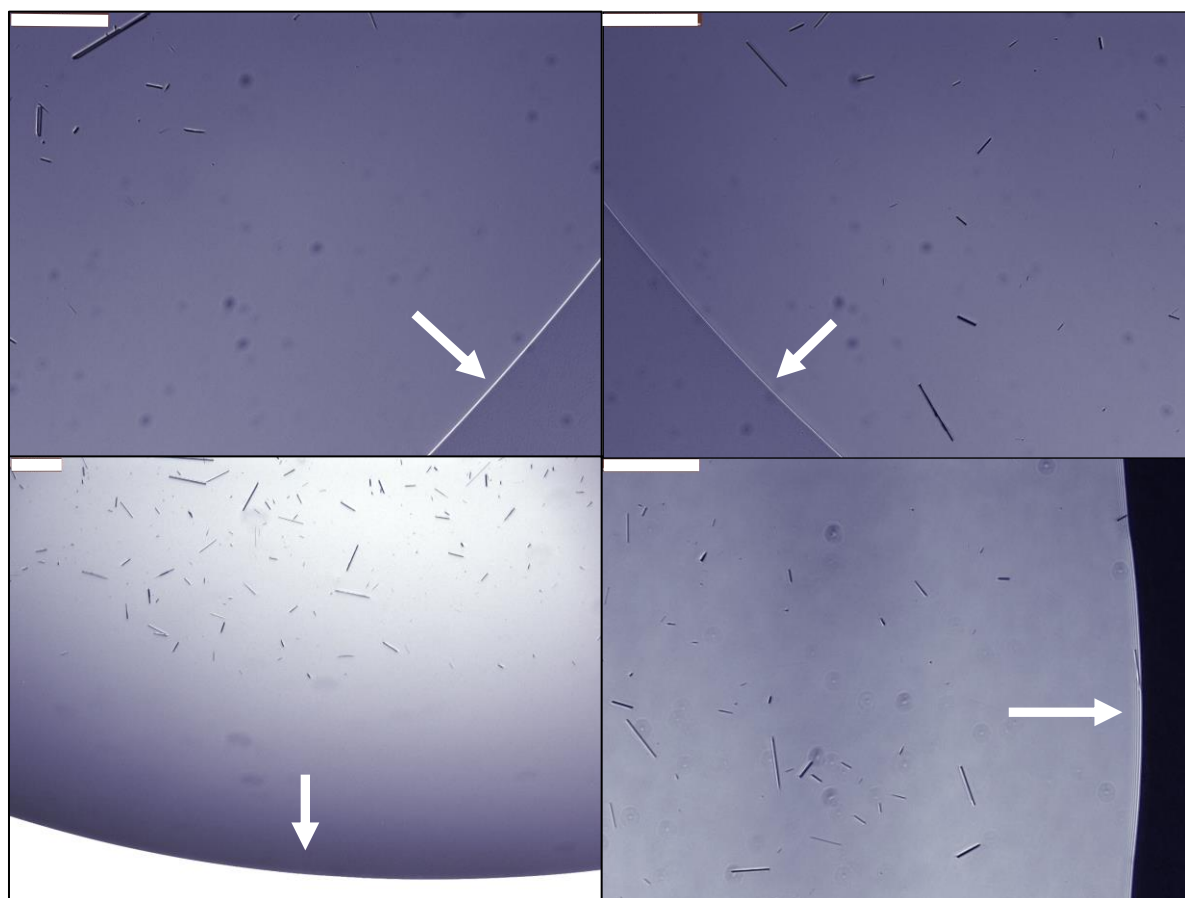


Figure 5-6: Images showing PLL coated and uncoated CuHARS association with edge of the well in a 48 well cell culture treated well. Left) (Top and bottom) Uncoated CuHARS, Right) (Top and bottom) PLL coated CuHARS. White arrows = edge of the droplet. Scale Bars = 100µm

Once the droplet has fully dried images of the middle of the droplet were taken. We found that the coated CuHARS were less dense in the images than the uncoated CuHARS. The uncoated CuHARS are more motile than the coated CuHARS. They are also more evenly dispersed throughout the droplet, therefore when they dry more uncoated CuHARS are found in the middle of the dried droplet. Results are shown in Figure 5-7.

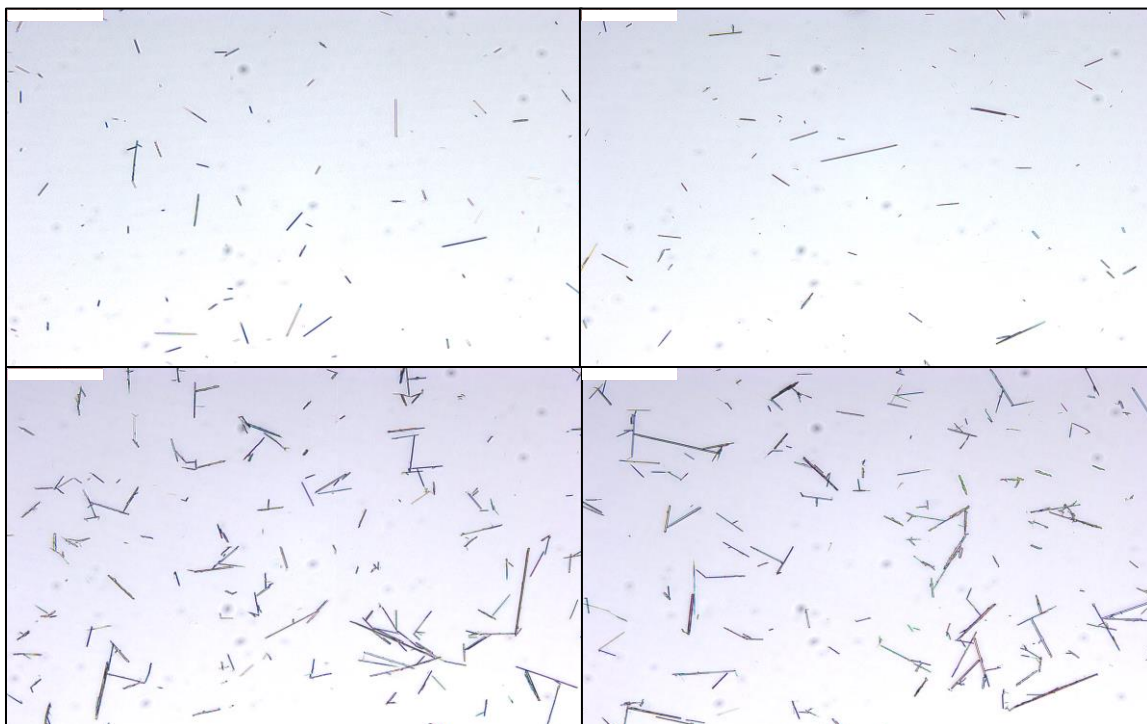


Figure 5-6: Images showing dried PLL coated and uncoated CuHARS association with middle of the well in a 48 well cell culture treated well. Bottom Panel: Uncoated CuHARS, Top Panel: PLL coated CuHARS. Scale Bars = 100 μ m

Image analysis software such as Image J and Image ProPlus can be used to find the number of object within a field after defining what an object is. This can be used to quantify the CuHARS association with cells, middle of droplet. The average distance of CuHARS

to the edge of the droplet can be used to quantify the CuHARS association with the droplet edge.

The antibiotic ionophore A23187 is an ionophorous antibiotic that reduces membrane permeability barriers to biologically important alkali cations such as calcium.

Figure 5-8 shows the structure of A23187.

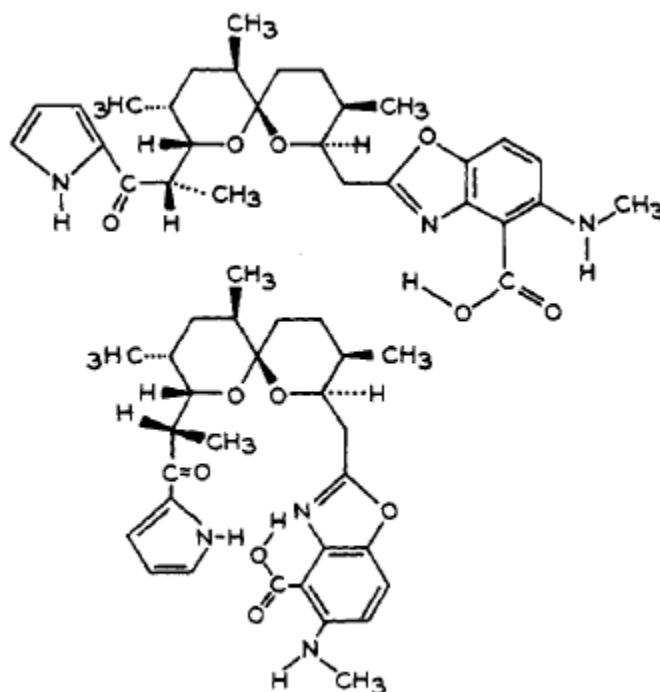


Figure 5-8: Diagram showing the structure of A23187 at the free acid. The two structures are in “open and closed” conformation, respectively (top to bottom) (101)

To confirm that this process is successful, several methods will be utilized. We have observed that uncoated CuHARS are very motile in water under the microscope. This is believed to be due to the electrostatic forces repelling the materials as they are negatively charged. After coating the CuHARS with Poly-L-lysine, which is a positively charged polymer, it is expected that the material will become less motile in a cell culture treated

plate. This was observed under the microscope and movies of the material movement were recorded (results not shown). We also observed how the PLL coated CuHARS interacted with cells. It was expected that the coated materials would be more readily associated with cells as positively charged particles exert attractive forces on the negatively charged cell membrane. The cells were plated at two densities of 10,000 and 20,000 cells per well and two concentrations of CuHARS added. The cells were imaged three hours after the material was added and overall, the PLL coated CuHARS were more readily associated with the cell. Figures 5-9 and 5-10 illustrate the association of PLL coated versus uncoated CuHARS to CRL 2303 cells.

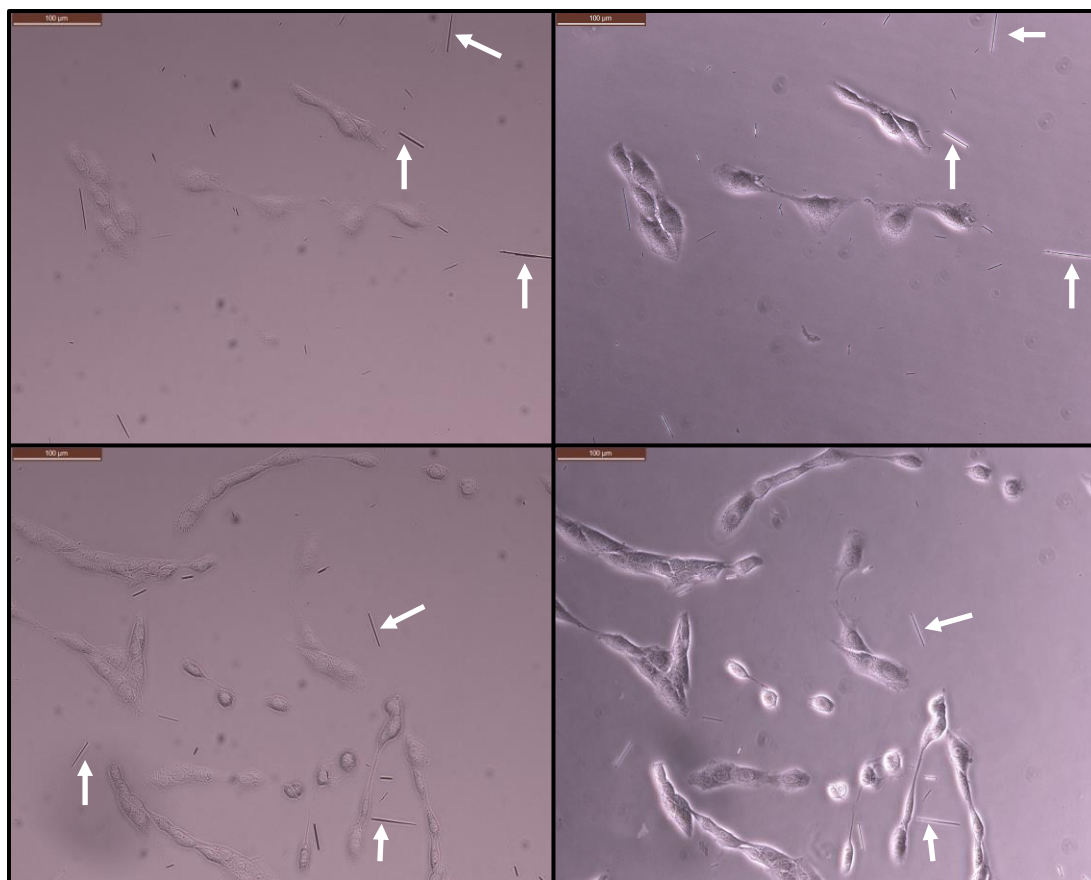


Figure 5-9: Images illustrating Uncoated CuHARS and their association with CRL 2303 cells. Left (Top and bottom) Bright Field images highlighting CuHARS; Right (Top and Bottom) Phase contrast images of the same area of highlighting cells. Scale Bars = 100 μ m. White Arrows = CuHARS

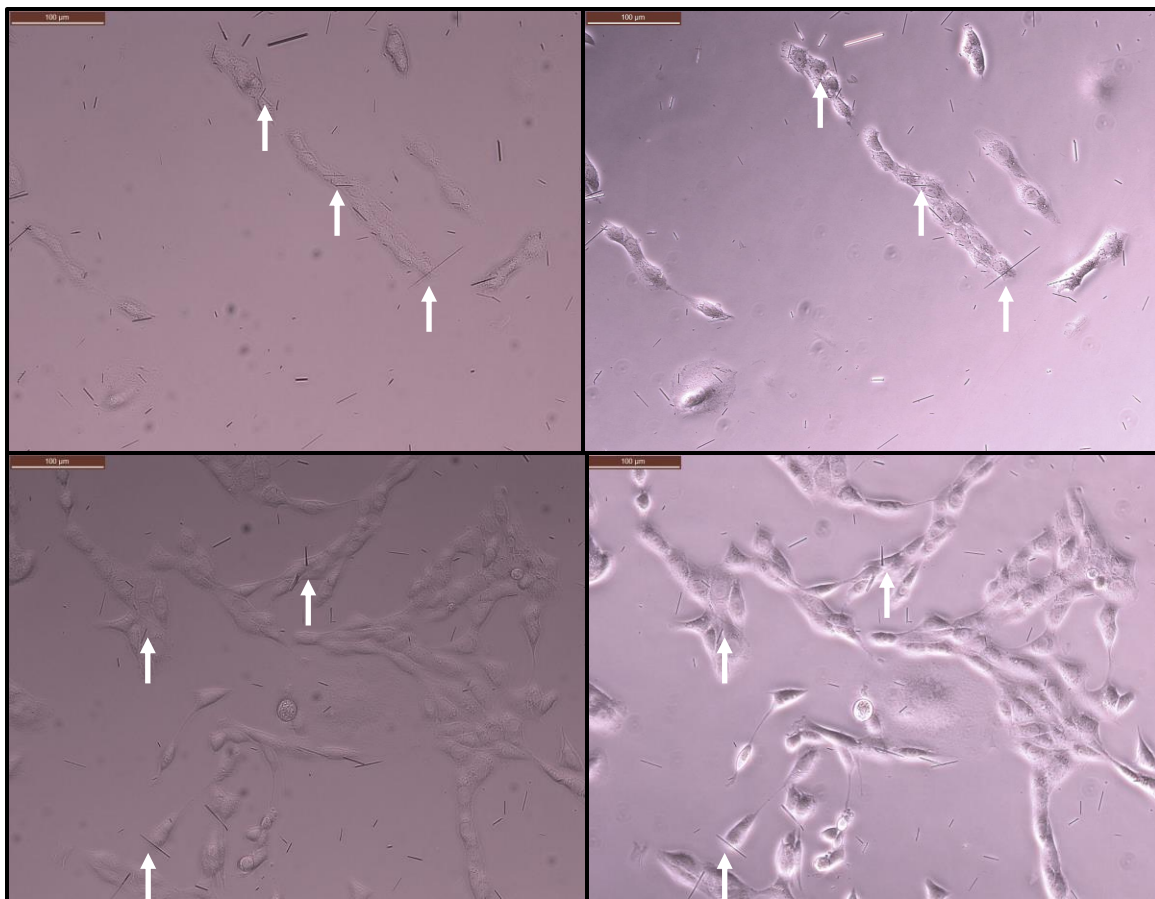


Figure 5-10: Images illustrating PLL-coated CuHARS and their association with CRL 2303 cells. Left (Top and bottom) Bright Field images highlighting CuHARS; Right (Top and Bottom) Phase contrast images of the same area of highlighting cells. Scale Bars = 100µm. White Arrows = CuHARS

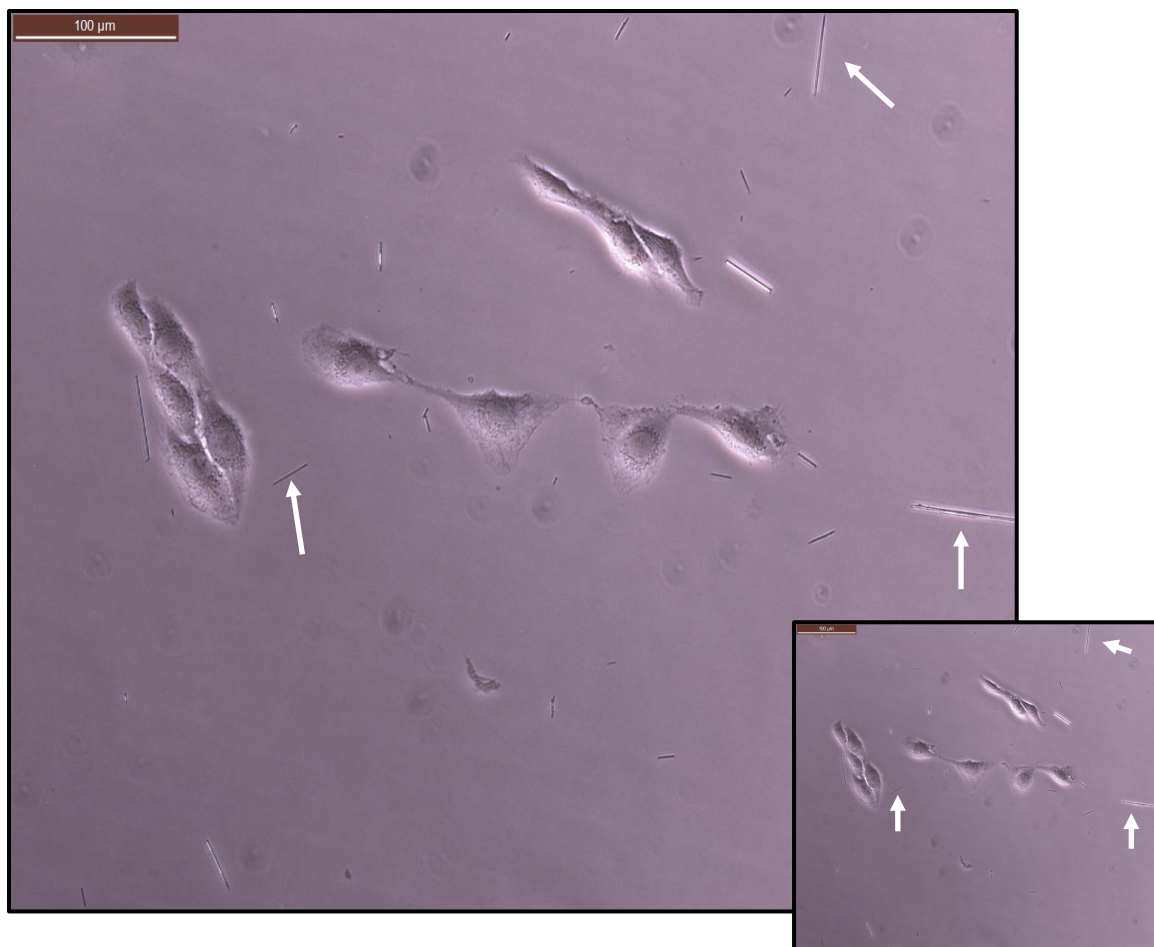


Figure 5-11: Zoomed in Phase image of uncoated CuHARS and their association with CRL 2303 cells. Scale Bars = 100μm. White Arrows = CuHARS

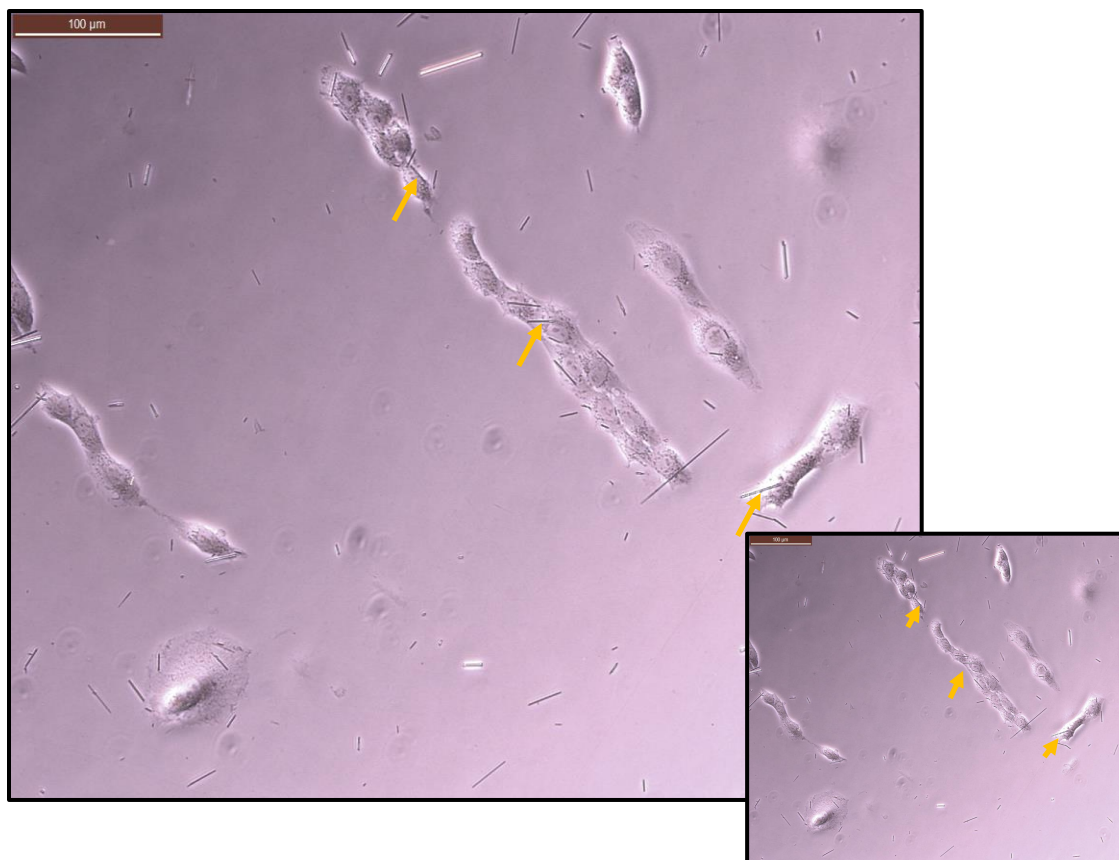


Figure 5-12: Zoomed in Phase image of PLL-coated CuHARS and their association with CRL 2303 cells. Scale Bars = 100μm. Yellow Arrows = CuHARS

CHAPTER 6

CONCLUSIONS AND FUTURE WORK

6.1 Conclusions

An emerging viewpoint in which glia are contributors to calcium processing in the brain has been elucidated by engineering normal cultures and subjecting the cultures to submaximal glutamate stimuli. Tissue engineered microenvironments were constructed to test the effects of the glial cell density have on calcium information processing. Neuronal cultures severely depleted (greater than sixty percent depletion) of glia responded to increasing glutamate additions with large, slightly unsynchronized responses with the greatest area under the curve (AUC) observed which returned to baseline the slowest of the three micro-environments developed. Cultures partially depleted (thirty to sixty percent depletion) of glia, responded to increasing glutamate addition with mid-sized, synchronized responses with lower AUC than cultures with severely depleted glial cells. Mildly depleted cultures behaved similarly to glia rich cultures. The difference between their AUC was not statistically significant. Studying how the brain behaves in altered systems, such as in glia depleted micro-environments adds to a body of work that explores cell loss in the brain and develop more targeted protective strategies.

6.2 Future Work

It is anticipated, this combined experimental/analytical approach will also have utility in understanding additional brain diseases such as glioma and neurodegeneration linked to deregulated homeostatic calcium. To further the investigation of how neuronal calcium information processing is modulated by submaximal glutamate we must also investigate single neuronal responses over time for the different paradigms shown in these studies. Studying individual calcium dynamics could elucidate important aspects of spatiotemporal, synchronized, asynchrony and/or concentration dependent responses when correlated to the averaged calcium dynamics which were investigated throughout the body of this work.

Before a biomaterial can be used for applications in the brain, it is important that an extensive study is done to elucidate all the possible effects this material can have on the brain. Calcium signalling in the brain can affect many neurological process and if dysregulated, may have harmful effects. As a result, future studies should be done to further understand how this material affect the calcium information processing of neural cells. A protocol for this method can be found in Appendix A8. UV spectroscopy will be used to confirm that the CuHARS are successfully coated with the ionophore. After functionalization of CuHARS with ionomycin, the UV absorbance of the supernatant will be used to calculate the concentration using Beer's law.

Beer's Law: $A = \epsilon bc$

Where A = Absorbance

ϵ = molar absorptivity/ Extinction co-efficient: $\epsilon_{278} = 18,200$

b= path length of the sample (path length of cuvette is 1cm)

C= concentration of compound (mol L^{-1})

After each wash, the absorbance of the supernatant will be measured. If the absorbance decreases, we can infer that there is little or no A23187 on the CuHARS. After this is done, the materials can be used to stimulate neuronal cultures in calcium imaging experiments and this would confirm the presence of an ionophore on the material and not in the supernatant.

Calcium Imaging can also be used to confirm that the CuHARS are coated with A23187. If the material is successfully coated with the ionophore, it can be used to stimulate a calcium fluorescent response in cells. Figure 6-1 is a flow chart illustrating the steps needed to successfully functionalize and confirm ionophore coated CuHARS. Blue lines have been completed and red lines will be done in future work.

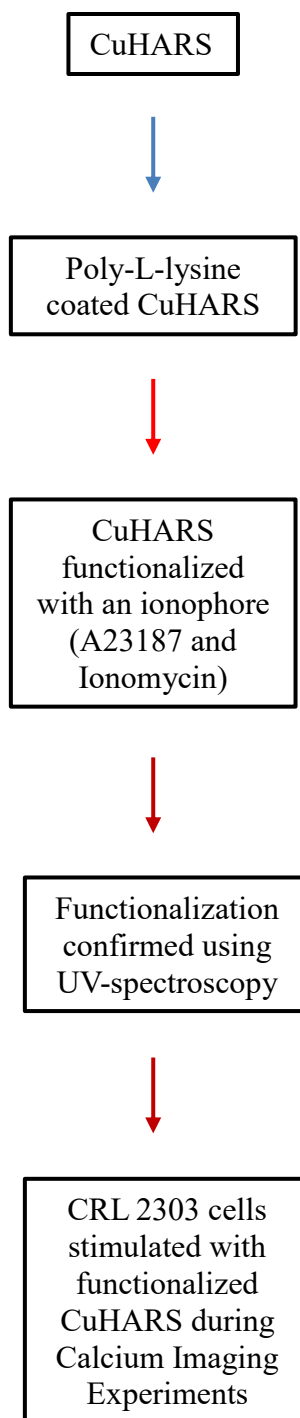


Figure 6-1: Schematic illustrating the steps needed to successfully functionalize and confirm ionophore coated CuHARS. Blue lines have been completed and red lines will be done in future work.

APPENDIX A

CELL CULTURE AND MEDIA

A1 Rat Primary Cervical Disarticulation: IACUC Approved

Pre-treat plates with poly-lysine (PLL) using the following protocol:

25 mg Poly-L-lysine (P-1274), Sigma

1. Prepare 0.01% w/v coating buffer by dissolving 1.4mg PLL into 14 ml distilled water.
2. Sterile filter this solution using a corning syringe filter (μm)
3. Add 300 μl of PLL to each well
4. Let it stand for at least one hour in the tissue culture hood
5. If this needs to be stored for more than 24 hours, add 1ml MEM culture media without antibiotics or serum into each well and store plate in 4°C. The coated plate could be stored safely for one week in this way (97).

If more than seven pups will be sacrificed during the harvest, split the amount into groups of seven. Use a fresh 50 ml tube with 15 ml media and 750 μl penicillin-streptomycin (PS) to collect tissue.

Materials needed for dissection:

1. Large petri dish
2. Diapers
3. Empty yellow-tip containers
4. Plastic bag
5. Cervical Scissors
6. Micro-scissors
7. Curve tip scissors
8. Small tip forceps

9. Large forceps
10. Small spatula
11. Full wash bottle with 70% Isopropyl alcohol
12. 50ml centrifuge tubes with 40ml basal media eagle (BME)
13. 50ml centrifuge tube with 10ml BME and 0.05% PS (one for every 7 pups)
14. Box of gloves
15. 50ml centrifuge tube holder
16. Beaker of ice

Set-up for dissection:

1. Soak the dissection instruments with 70% isopropyl alcohol in a container.
2. Place the “pinkies” (pups) in the yellow container and set on one end of the dissection table.
3. Place three diapers on the dissection table.
4. Place one large petri dish under the microscope and pour ~10ml BME and PS into it.
5. Place another petri dish about seven inches away from the dish under the microscope to be used for waste.
6. Place and keep the plastic bag near the diapers.
7. Place the 50ml centrifuge tube holder on the dissection table next to the alcohol.
8. Place the wash bottle next to the utensils.
9. Keep the basal media, gloves, and other supplies on the cart.
10. Place over-head lighting and stereo scope in position above the centered dish.

Dissection Protocol:

1. Put on a pair of gloves.
2. Remove one pup from the box by pinching the skin above the spine near the lower back and set the pinkie on a diaper.
3. Spray pup with alcohol and pick up again using the pinch method.
4. Quickly set cervical scissors behind ear being cautious of paws and make one very quick and decisive cut. (Dip scissors in alcohol and place it on a clean diaper)
5. Blot the head at point of disarticulation on diaper and discard the body in the plastic bag.
6. Using the micro-scissors, cut the skin in an upward motion then dip scissors in alcohol (This should expose the skull).
7. Cut the skull using the same upward motion (this should expose the brain)
8. Using large forceps, curl back both sides of the skull to better expose the brain then use a spatula to scoop out the brain into the basal media in the petri dish.
9. Remove the cerebellum at the demarcation line and place it in the waste dish.
10. Keep brain in place with large forceps and remove meninges and blood vessels with small forceps. Place the waste into the waste dish.
11. Once all blood vessels and meninges are removed, place tissue into 50 ml tube.
12. Repeat steps 2-11 until all pups are sacrificed.
13. Discard of all waste into freezer room and clean all utensils.

Materials needed for tissue culture:

1. Pre-treated plates with Poly-L-lysine
2. Bucket of ice
3. Neuronal Culture Media
4. Trypsin EDTA

Cell Harvest Protocol:

1. Aspirate harvested brain tissue with a 10ml pipette into a 15 ml tube.
2. Add 4ml of complete NCM and 1ml trypsin brain tissue then triturate about 15 times.
3. Let the brain tissue settle by placing it into a large beaker of ice for 5 minutes.
4. The supernatant will contain the neuronal cells. Remove the supernatant and place it into another sterilized 15 ml centrifuge tube and place on ice.
5. Repeat steps 2-4 two more times.
6. Centrifuge and follow protocol to count and plate cells at a density of ~100,000 cells per well.

A2 Fluo3/AM Loading:**Materials needed for 2ml imaging solution:**

1. 2 μ l Pluronic acid
2. 4 μ l Fluo 3/AM
3. 2ml Locke's Solution (pre-warmed in incubator for at least 15 minutes)

Protocol:

1. Turn off the light of the cell culture hood
2. Warm all components to room temperature prior to experiment.

3. Add 2ml of pre-warmed Locke's solution to a 15 ml centrifuge tube
4. Add 2 μ l pluronic acid to the tube then mix (vortex until soapsuds are observed)
5. Add 4 μ l Fluo3/AM (2mg/ml in DMSO) and cap the tube.
6. Mix the contents of the tube by gently inverting it two or three times.
7. Remove all media from one well then add ~500 μ l of loading solution to the emptied well.
8. Repeat step seven for all the wells to be imaged.
9. Place the cell into the incubator and allow the dye to enter the cells for 45 minutes to an hour.
10. Remove the loading solution and allow the cells to recover in 475 μ l of Locke's solution for 30 minutes then the cells are ready for imaging.

A3. MTT Assay Protocol

1. Dissolve MTT crystals into 10X PBS to get a final concentration of 5mg/ml.
2. Occasionally there may be some particulate material that will not dissolve; this can be removed by filtration or centrifugation.
3. For adherent cells, remove the media from the well and replace it with 100 μ l of MTT solution.
4. Incubate the cells at 37°C for 4 hours in a humidified chamber.
5. Add 100 μ l of 91% isopropanol to each well and mix thoroughly using a pipette.
6. Allow the plate to rest for ten minutes before measuring absorbance.
7. Use the Thermo-Scientific Multiskan spectrum plate reader to read absorbance at 570nm.

A4. Primary Neuronal Culture Media

Material Needed:

1. 25ml Fetal Bovine Serum (FBS)
2. 25ml Horse Serum (HS)
3. 98ml Ham's F-12 K (Without glutamine)
4. 98.25ml Basal Media Eagle
5. 1.25ml PS
6. 1.25ml Glucose solution in sterile distilled water (120mg/ml)
7. 1.25 ml Glutamine in sterile distilled water (20mg/ml)
8. Sterile Filtration Unit

Protocol:

1. Under the cell culture hood, transfer BME into filtration unit.
2. Add thawed FBS and HS to filtration unit
3. Add glucose solution, glutamine solution, PS and Ham's F-12 K.
4. Put the lid on the filtration unit, connect the hose then start vacuum
5. Draw all liquid through then turn off the vacuum.
6. Carefully remove the upper portion of the filtration unit under the hood then place the sterile cap on the bottle.
7. Label the bottle with the name of the media, date, and your initials.

A5. Primary Astrocyte Media

Materials Needed:

1. 12.5ml FBS

2. 12.5ml HS
3. 1.25ml PS
4. 223.75ml Ham's F-12K media with L-glutamine
5. Sterile Filtration Unit

Protocol:

1. Add 100ml Ham's F-12K to vacuum filtration unit
2. Add FBS, HS and PS
3. Add 123.75ml of Ham's F-12K
4. Put the lid on the filtration unit, connect the hose, then start vacuum
5. Draw all liquid through then turn off the vacuum.
6. Carefully remove the upper portion of the filtration unit under the hood then place the sterile cap on the bottle.
7. Label the bottle with the name of the media, date, and your initials.

A5. Primary Microglia Media**Materials Needed:**

1. 25ml FBS
2. 2.5ml PS
3. 222.5ml Dulbecco's Modified Eagle's Medium (DMEM)

Protocol:

1. Add 100ml Ham's F-12K to vacuum filtration unit
2. Add FBS and PS
3. Add 122.5ml DMEM
4. Put the lid on the filtration unit, connect the hose, then start vacuum

5. Draw all liquid through then turn off the vacuum.
6. Carefully remove the upper portion of the filtration unit under the hood then place the sterile cap on the bottle.
7. Label the bottle with the name of the media, date, and your initials.

A6. Locke's Solution

Materials Needed:

1. 2250 mg Sodium Chloride (NaCl)
2. 104.4mg Potassium Chloride (KCl)
3. 75.6mg Sodium Bicarbonate (NaHCO₃)
4. 84.5mg Calcium Chloride (CaCl₂.2H₂O)
5. 252.3 mg Glucose (C₆H₁₂O₆)
6. 1.25ml of 1M Stock Solution (Ph 7.4)
7. 248.75 distilled water (H₂O)

Protocol

1. Dissolve all solid components into 100ml purified water.
2. Add 100ml water to filtration unit
3. Add solution made in step 1 to filtration unit
4. Add Hepes solution
5. Add remaining water
6. Put the lid on the filtration unit, connect the hose, then start vacuum
7. Draw all liquid through then turn off the vacuum.
8. Carefully remove the upper portion of the filtration unit under the hood then place the sterile cap on the bottle.

9. Label the bottle with the name of the media, date, and your initials.

A7. Immunohistochemistry

DAPI Staining

4',6-diamidino-2-phenylindole (DAPI):

The blue fluorescent nucleic acid stain that preferentially binds to adenosine-thymine (AT) rich regions in double stranded DNA (dsDNA). When DAPI is bound to the dsDNA a ~20-fold fluorescence increase is observed (98). The excitation maximum for bound DAPI is ~358nm and the emission maximum is 461nm. It is possible to excite the dye with a xenon or mercury-arc lamp or with a UV laser. DAPI can also be used in flow cytometry systems utilizing UV excitation sources (99). The protocol used to stain the cells is as followed:

1. Equilibrate the sample briefly with phosphate-buffered saline (PBS).
2. Dilute the DAPI stock solution to 300 nM in PBS. Add 300 μ L of this dilute DAPI staining solution to the well, making certain that the cells are completely covered.
3. Incubate for 1–5 minutes.
4. Rinse the sample several times in PBS.
5. View the sample using a fluorescence microscope with appropriate filters.

A8. Biocompatibility testing using Calcium Imaging

1. Once the cells are harvested from the cortical region of the rat pup brains and resuspended in fresh astrocyte media, count the cells using a hemocytometer.

2. Plate the cells in 48 multi-well plates (cell culture treated, CellStar) at an optimal density (for calcium imaging) of 20,000 cells per well. Plate enough cells for experimentation for eighteen days.
3. Add the material upon plating or 24 hours after the cells are plated
4. Place the cell in an incubator to be maintained in 37 degrees Celsius (°C), five percent carbon dioxide, and 100% humidity incubation.
5. At four *days in vitro*, remove one plate and perform calcium imaging as described in chapter 3.
6. Repeat step five every four to five days while continuously adding media to ensure that the media in the well does not dry up.

APPENDIX B

MAT LAB CODE

The data retrieved from the InCyt Im software will be in the following format.

```

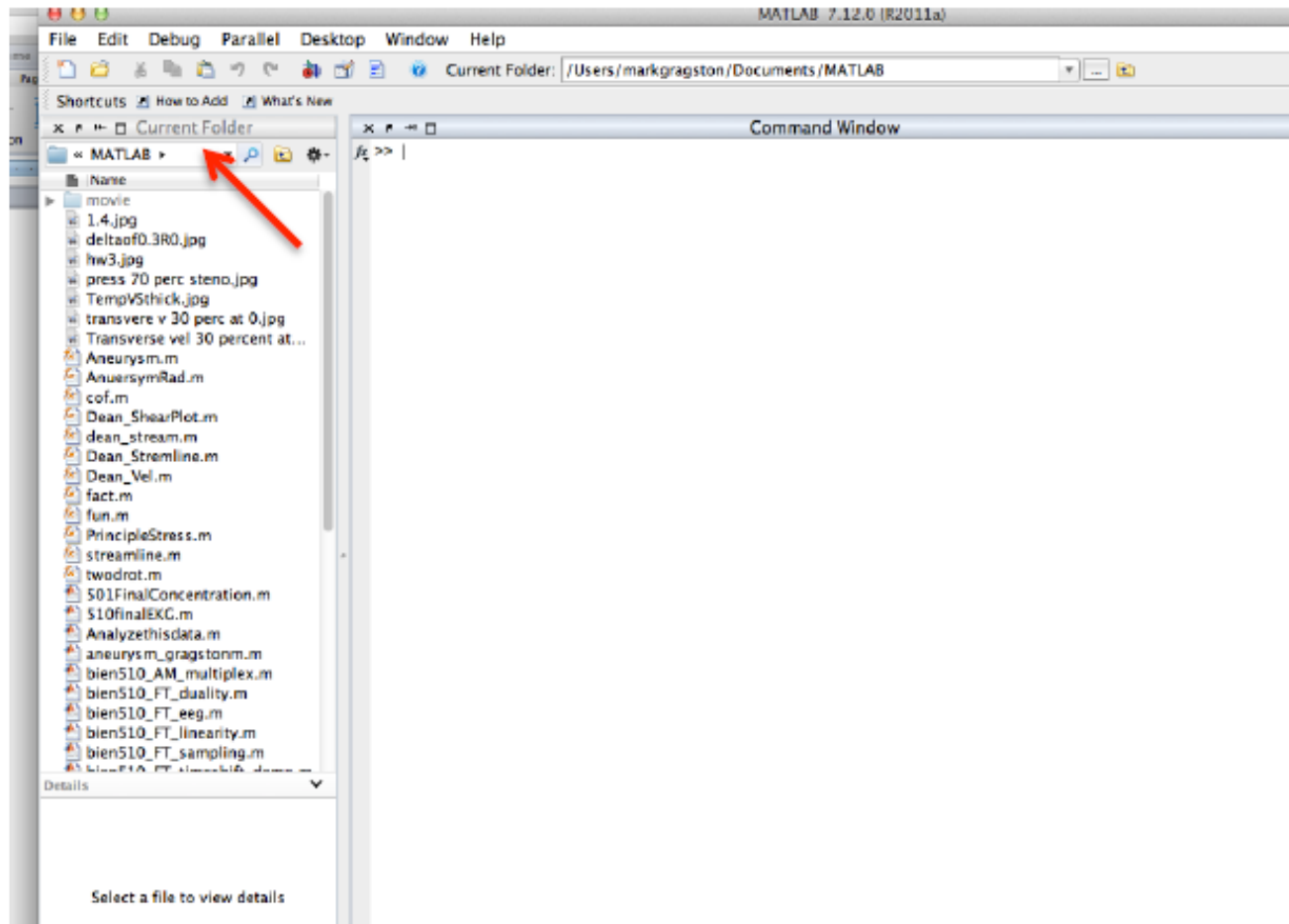
Reserved
Ion: Ca++
Wavelength_Used: 480
Other_Wavelength: 460
Exposure_Time: 147
Minimum_Fluorescence: 0.000000
Maximum_Fluorescence: 4095.000000
Image_Width: 640
Image_Height: 480
Number_of_Time_Points: 30
Number_of_Objects: 5
Object_Areas [in_pixels]:
object 1 813.000000
object 2 453.000000
object 3 1025.000000
object 4 1989.000000
object 5 1541.000000
Event_Times
    74.640
    76.406
Horizontal_Binning=1
Vertical_Binning=1
Reserved
DATA_AFTER_THIS_LINE
Time[seconds] Object[01] Object[02] Object[03] Object[04] Object[05]
0.1700 12162 533 2148 18437 429
4.1670 12509 593 2238 19865 567
8.1750 12209 601 2626 20122 771
12.1730 12729 682 2619 20183 886
16.1800 12425 832 2742 21282 929
20.1770 12699 779 2834 21023 989
24.1810 12492 648 2855 21031 1018
28.1780 12761 811 2940 20090 1084
32.1860 12646 744 2841 19797 987
36.1840 12850 784 2689 19666 879
40.1910 13465 789 2772 19757 982
44.1890 13527 748 2574 18570 728

```

B1. Area Under the Curve

Instructions:

1. Ensure that you set the path in Matlab.



The red arrow above shows how to change the folder in which Matlab is working.

2. Select the folder that contains the code. The code will allow for the file path of the data to be defined whether the data is in the same folder as the code.
3. Open the .m file and find the following block of code.

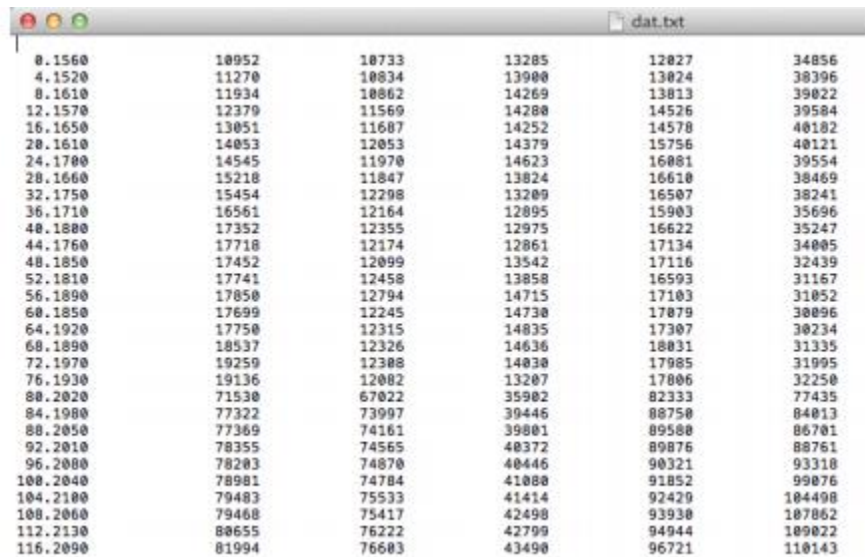
```

33 %-----PUT FILENAME BELOW-----
34 %-----VVVVVV-----
35 - data_file=fopen('dat.txt','r'); %Open the file to be read
36 - formatSpec = '%f %f %f %f %f %f'; %Format of File to be read
37 - size_data = [6 Inf]; %Output is 2 by INF array
38 - data = fscanf(data_file,formatSpec,size_data); %Read in the file
39 - fclose(data_file); %Close the file
40 - data = data'; %Transpose
41

```

4. Replace the dat.txt portion with the datafile's name and extension (usually .txt). (In the

above example, I have the data and code in the same path. Thus, I didn't need to specify a path like ~\Documents\Matlab\data.txt.) In the above picture, look at line 36. The %f is needed for each column of data. So, the code above assumes that there are six columns of numbers of floating type. It corresponds to the data shown in the picture. You of You will not always have six columns of data; therefore, you will need to add or delete some of the %fs on the code:



| | | | | | |
|----------|-------|-------|-------|-------|--------|
| 0.1560 | 10952 | 10733 | 13285 | 12027 | 34856 |
| 4.1520 | 11270 | 10834 | 13900 | 13024 | 38396 |
| 8.1610 | 11934 | 10862 | 14269 | 13813 | 39022 |
| 12.1570 | 12379 | 11569 | 14280 | 14526 | 39584 |
| 16.1650 | 13051 | 11687 | 14252 | 14578 | 40102 |
| 20.1610 | 14053 | 12053 | 14379 | 15756 | 40121 |
| 24.1700 | 14545 | 11970 | 14623 | 16001 | 39554 |
| 28.1660 | 15218 | 11847 | 13824 | 16610 | 38469 |
| 32.1750 | 15454 | 12298 | 13209 | 16507 | 38241 |
| 36.1710 | 16561 | 12164 | 12095 | 15903 | 35696 |
| 40.1800 | 17352 | 12355 | 12975 | 16622 | 35247 |
| 44.1760 | 17718 | 12174 | 12861 | 17134 | 34005 |
| 48.1850 | 17452 | 12099 | 13542 | 17116 | 32439 |
| 52.1810 | 17741 | 12458 | 13858 | 16593 | 31167 |
| 56.1890 | 17050 | 12794 | 14715 | 17103 | 31052 |
| 60.1850 | 17699 | 12245 | 14730 | 17079 | 30096 |
| 64.1920 | 17750 | 12315 | 14835 | 17307 | 30234 |
| 68.1890 | 18537 | 12326 | 14636 | 18031 | 31335 |
| 72.1970 | 19259 | 12308 | 14030 | 17985 | 31995 |
| 76.1930 | 19136 | 12002 | 13207 | 17006 | 32250 |
| 80.2020 | 71530 | 67022 | 35902 | 02333 | 77435 |
| 84.1900 | 77322 | 73997 | 39446 | 08750 | 84013 |
| 88.2050 | 77369 | 74161 | 39801 | 09500 | 86701 |
| 92.2010 | 78355 | 74565 | 40372 | 09876 | 88761 |
| 96.2000 | 78203 | 74870 | 40446 | 90321 | 93310 |
| 100.2040 | 78901 | 74784 | 41000 | 91852 | 99076 |
| 104.2100 | 79483 | 75533 | 41414 | 92429 | 104498 |
| 108.2060 | 79468 | 75417 | 42498 | 93930 | 107062 |
| 112.2130 | 80655 | 76222 | 42799 | 94944 | 109022 |
| 116.2090 | 81994 | 76603 | 43490 | 96721 | 110143 |

Also, look at line 37 The number '6' will be changed to the number of columns of data you have. 3) Save the modified code. Run it. It will ask you to specify the lower and upper bounds of integration.

B2. Calcium Imaging Data

This code is to gather header information

```
function HDR = Calcium HDR(Filename)
```

```

%% Import data from text file.
% Script for importing data from the following text file:
%
%     F:\R1C2_250glu_500g_750g.DAT
%
% To extend the code to different selected data or a different
text file,
% generate a function instead of a script.

% Auto-generated by MATLAB on 2018/06/01 14:38:51

%% Initialize variables.
filename = Filename;
delimiter = '\t';

%% Format for each line of text:
% column1: text (%s)
% column2: text (%s)
% column3: text (%s)
% column4: text (%s)
% column5: text (%s)
% column6: text (%s)
% For more information, see the TEXTSCAN documentation.
format Spec = '%s%s%s%s%s%s%[\n\r]';

%% Open the text file.
fileID = fopen(filename, 'r');

%% Read columns of data according to the format.
% This call is based on the structure of the file used to
generate this
% code. If an error occurs for a different file, try regenerating
the code
% from the Import Tool.
dataArray = textscan(fileID, formatSpec, 'Delimiter', delimiter,
'TextType', 'string', 'ReturnOnError', false);

%% Close the text file.
fclose(fileID);

%% Post processing for unimportable data.
% No unimportable data rules were applied during the import, so
no post
% processing code is included. To generate code which works for
% unimportable data, select unimportable cells in a file and
regenerate the
% script.

%% Create output variable
RawData = [dataArray{1:end-1}]; % Get raw data

% Data to find
ToFind =
{'Experiment_Code', 'Ion', 'Wavelength_Used', 'Other_Wavelength', 'Exposure
_Time', ...

```

```

'Minimum_Fluorescence','Maximum_Fluorescence','Image_Width',...
    'Image_Height','Number_of_Time_Points','Number_of_Objects'};

    for idx = 1:size(ToFind,2)

        ToFindCol = false(1,size(RawData,2)); % Pre-allocate for
speed

        ToFindRow = contains(RawData(:,1),ToFind{idx}); % Find rows
for header info
        ToFindCol(2:end) = arrayfun(@(Col)
~isempty(RawData{ToFindRow,Col}),2:size(RawData,2)); % Find the column
of header info

        if idx <= 2
            HDR.(ToFind{idx}) = RawData{ToFindRow,ToFindCol}; % Store
the header info
        else
            HDR.(ToFind{idx}) =
str2double(RawData{ToFindRow,ToFindCol}); % Store the header info
        end

    end

    %% Find Object Areas

    Object_AreasRow = find(contains(RawData(:,1),'object')); % Find
rows for header info
    Object_AreasCol = nan(size(Object_AreasRow,1),1); % Pre-allocate
for speed
    HDR.Object_Areas = nan(1,size(Object_AreasRow,1)); % Pre-allocate
for speed

    for idx = 1:size(Object_AreasRow,1)
        Object_AreasCol(idx) = find(arrayfun(@(Col)
~isempty(RawData{Object_AreasRow(idx),Col}),3:size(RawData,2)))+2; %
Find the column of header info

        HDR.Object_Areas(idx) =
str2double(RawData{Object_AreasRow(idx),Object_AreasCol(idx)}); % Save
data to HDR variable
    end

    %% Find # of Events and Event Times

    Number_of_EventsRow = find(contains(RawData(:,1),'Event_Times'));
% Find rows for header info
    Number_of_EventsCol = false(1,size(RawData,2)); % Pre-allocate
for speed

```

```

    Number_of_EventsCol(1,2:end) = arrayfun(@(Col)
~isempty(RawData{Number_of_EventsRow,Col}),2:size(RawData,2)); % Find
the column of header info

    HDR.Number_of_Events =
str2double(RawData{Number_of_EventsRow,Number_of_EventsCol}); % Save
data to HDR variable

    HDR.Events = nan(1,HDR.Number_of_Events); % Pre-allocate for
speed
    EventsCol = nan(1,HDR.Number_of_Events); % Pre-allocate for speed

    for idx = 1:HDR.Number_of_Events
        EventsCol(idx) = find(arrayfun(@(Col)
~isempty(RawData{Number_of_EventsRow+idx,Col}),1:size(RawData,2))); %
Find the column of header info

        HDR.Events(idx) =
str2double(RawData{Number_of_EventsRow+idx,EventsCol(idx)}); % Save
data to HDR variable
    end

    HDR = orderfields(HDR); %Alphabetize the header information

end

```

Code for the other function used to gather the data

```

function[Time, ObjectData] = CalciumData(Filename,HDR)

%% Import data from text file.
% Script for importing data from the following text file:
%
%   F:\R1C2_250glu_500g_750g.DAT
%
% To extend the code to different selected data or a different
text file,
% generate a function instead of a script.

% Auto-generated by MATLAB on 2018/06/01 14:38:51

%% Initialize variables.
filename = Filename;
delimiter = '\t';

%% Format for each line of text:
%   column1: text (%s)
%   column2: text (%s)
%   column3: text (%s)
%   column4: text (%s)
%   column5: text (%s)
%   column6: text (%s)

```

```

% column7: text (%s)
% For more information, see the TEXTSCAN documentation.
formatSpec = '%s%s%s%s%s%s%s%[\n\r]';

%% Open the text file.
fileID = fopen(filename,'r');

%% Read columns of data according to the format.
% This call is based on the structure of the file used to
generate this
% code. If an error occurs for a different file, try regenerating
the code
% from the Import Tool.
dataArray = textscan(fileID, formatSpec, 'Delimiter', delimiter,
'TextType', 'string', 'ReturnOnError', false);

%% Close the text file.
fclose(fileID);

%% Post processing for unimportable data.
% No unimportable data rules were applied during the import, so
no post
% processing code is included. To generate code which works for
% unimportable data, select unimportable cells in a file and
regenerate the
% script.

%% Create output variable
RawData = [dataArray{1:end-1}]; % Get raw data

% Data to find

DataStartRow =
find(contains(RawData(:,1),'DATA_AFTER_THIS_LINE'))+2; % Find the row
for the first data point
DataStopRow = DataStartRow-1 + HDR.Number_of_Time_Points; % Find
the row for the last data point

TimeCol = find(contains(RawData(DataStartRow-1,:), 'Time')); %
Find rows for header info

TimeDouble = arrayfun(@(Rows)
str2double(RawData{Rows,TimeCol}),DataStartRow:DataStopRow)'; % Store
time values

% TimeTypeRaw = RawData{DataStartRow-1,TimeCol};
% TimeTypeStr = cell2mat(regexp(TimeTypeRaw,'[a-zA-
Z]*(?=)'),'match');
% TimeType = str2func(TimeTypeStr);
% Time = TimeType(TimeDouble); % Change time from double to
duration

Time = TimeDouble; % Keep time as double if an error is thrown

```

```

    ObjectData =
nan(HDR.Number_of_Time_Points,HDR.Number_of_Objects); % Pre-allocate
for speed

    for Col = 1:HDR.Number_of_Objects
        ObjectData(:,Col) = arrayfun(@(Rows)
str2double(RawData{Rows,Col+TimeCol}),DataStartRow:DataStopRow)'; %
Store object values
    end

    subplot(2,1,1)
    plot(Time,ObjectData) %Plot ObjectData vs. Time
    RangeOfGraph = get(gca, 'ylim'); %Determine max and min for y-
axis
    xlabel('Time (seconds)') %X-axis label = Time(seconds)
    ylabel('R.O.I. Fluorescence Values') %Y-axis label = ROI
Fluorescence values
    grid on %Turn on grid for plot
    title('Fluorescence vs. Time') %Give plot a title
    hold on

    for Index2 = 1:HDR.Number_of_Objects %Produce input for legend
(indexes appropriately with # of ROIs present)
        names{Index2} = ['Object ' num2str(Index2)]; %Add Object
1,2,3...N to legend of plot
    end
    legend(names, 'Location', 'NorthEastOutside') %Determine legend
location relative to plot

    for Index3 = 1:size(HDR.Events,2) %Add marker (vertical line)
wherever an event occurs
        line([HDR.Events(Index3) HDR.Events(Index3)] ,RangeOfGraph)
%create vertical line at specific time point
    end

    Average_Waveform = NaN(size(ObjectData,1),1); %Preallocate for
speed
    for Index4 = 1:size(ObjectData,1)
        Summation_Row = 0; %Preallocate Summation_Row
        for Index5 = 1:size(ObjectData,2)
            Summation_Row = Summation_Row+ObjectData(Index4,Index5); %Sum
Row
        end
        Average_Row = Summation_Row/size(ObjectData,2); %Average the
row
        Average_Waveform(Index4,1) = Average_Row; %Create
average_waveform matrix which is average_row instanced
size(ObjectData,1) times
    end
    hold off

    subplot(2,1,2)
    plot(Time,Average_Waveform, 'Linewidth',2) %plot average_waveform

```

```

    DomainOfGraph1 = get(gca, 'xlim'); %Determine max and min on x-
axis
    RangeOfGraph1 = get(gca, 'ylim'); %Determine max and min on y-
axis
    xlabel('Time (seconds)') %X-axis label = Time(seconds)
    ylabel('R.O.I. Fluorescence Values') %Y-axis label = ROI
Fluorescence values
    grid on %Turn on grid for plot
    title('Fluorescence vs. Time') %Give plot a title
    legend('Average', 'Location', 'NorthEastOutside') %Determine
legend location relative to plot
    hold on

    for Index6 = 1:size(HDR.Events,2) %Add marker (vertical line) to
graph whenever event occurs
        line([HDR.Events(Index6) HDR.Events(Index6)] ,RangeOfGraph1)
%create verticl line at specific time point
    end

    hold off
    % line(DomainOfGraph1,[1.2*Average_Waveform(1)
1.2*Average_Waveform(1)]) %Plot threshold line for 1.2*Baseline of
average_waveform
    % hold off %End holding so if this function is ran again in the
same sitting, it will not keep the waveforms on the plot

    % names{HDR.Number_of_Objects+1} = 'Average'; %After Object N,
add average_waveform to plot legend

end

```

APPENDIX C

MORE MATHEMATICAL TOOLS

C.2 Dynamic Models of Neuron: Astrocyte Interaction

C2.1 The Neuron Model

$$C \frac{dv_j(t)}{dt} = -\bar{g}_{Ca} m_\infty(v_j(t)) (v_j(t) - v_{Ca}) - \bar{g} K w_j(t) (v_j(t) - v_k) - \bar{g}_L (v_j(t) - v_L) + i_j(t) \quad \text{Eqn. C-1}$$

$$\frac{dw_j(t)}{dt} = \phi \left[\frac{w_\infty(v_j(t) - w_j(t))}{\tau_w(v_j(t))} \right] \quad \text{Eqn. C-2}$$

$$i_j(t) = i_j^{\text{constant}}(t) + i_j^{\text{noise}}(t) + i_j^{\text{slow}}(t) \quad \text{Eqn. C-3}$$

$$\frac{di_j^{\text{slow}}(t)}{dt} = \varepsilon_j (v^* - v_j(t) - \alpha_j i_j^{\text{slow}}(t)) \quad \text{Eqn. C-4}$$

A modified version of the Morris-Lecar equation is used as the basic model for each neuron (73).

where w_j is an auxiliary variable and is the fraction of open K^+ channels. The channel conductances \bar{g}_{Ca} , \bar{g}_K , and \bar{g}_L for the Ca^{2+} , K^+ and leak currents are constants. The functions $m_\infty(v_j(t))$, $w_\infty(v_j(t))$ and $\tau_w(v_j(t))$ control the dynamics of the ion channels and are defined by the following equations:

$$m_\infty(v_j(t)) = 0.5 \left[1 + \tanh\left(\frac{v_j(t) - \hat{v}_1}{\hat{v}_2}\right) \right] \quad \text{Eqn. C-4}$$

$$w_\infty(v_j(t)) = 0.5 \left[1 + \tanh\left(\frac{v_j(t) - \hat{v}_3}{\hat{v}_4}\right) \right] \quad \text{Eqn. C-5}$$

$$\tau_w(v_j(t)) = \frac{1}{\cosh\left(\frac{(v_j(t) - \hat{v}_3)}{2\hat{v}_4}\right)} \quad \text{Eqn. C-6}$$

$i_j(t)$ is the applied current to the j th neuron. This contains a constant background current $i_j^{constant}(t)$, a slow, fluctuating current $i_j^{slow}(t)$ (71), and a noisy current ($i_j^{noise}(t)$) with amplitude D_n and correlation τ_n which models the unavoidable noise found within physiological systems. ε_j and α_j control the bursting behavior of the j th neuron. Because of the constant slow currents $i_j^{slow}(t)$, the neuron displays dynamic behavior.

The following equations are the compact form of Eqns. 4-1 to 4-8.

$$\frac{dv_j}{dt} = F(v_j, w_j, i_j) \quad \text{Eqn. C-7}$$

$$\frac{dw_j}{dt} = G(v_j, w_j) \quad \text{Eqn. C-8}$$

Where,

$$F(v_j, w_j, i_j) = -\bar{g}_{Ca} m_\infty(v_j(t)) (v_j(t) - v_{Ca}) - \bar{g}_K w_j(t) (v_j(t) - v_K) - \bar{g}_L (v_j(t) - v_L) + i_j(t) \quad \text{Eqn. C-9}$$

$$G(v_j, w_j) = \phi(w_\infty) \left(\frac{v_j(t) - w_j(t)}{\tau_w(v_j(t))} \right) \quad \text{Eqn. C-10}$$

A mathematical model of a neuronal network consisting of two neurons (M-L) connecting via gap junctions has been developed and is described in the following equations (74):

$$\frac{dv_1}{dt} = f(v_1, w_1, i_1) + g_{se}(v_2 - v_1) \quad \text{Eqn. C-11}$$

$$\frac{dv_2}{dt} = f(v_2, w_2, i_2) + g_{si}(v_1 - v_2) \quad \text{Eqn. C-12}$$

$$\frac{dw_1}{dt} = G(v_1, w_1) \quad \text{Eqn. C-13}$$

$$\frac{dw_2}{dt} = G(v_2, w_2) \quad \text{Eqn. C-14}$$

The variables g_{se} and g_{si} are the maximal conductances for excitatory or inhibitory synaptic connections (gap junctions). These numbers are always positive and can be referred to as coupling constants. g_{se} is used to change the excitation level and an increase in g_{se} causes an enhancement of the coupling strength between neurons and can therefore also affect neural synchrony.

C2.2 The Astrocyte Model

It has been proven that astrocytes play an active role in synaptic activity. These cells have numerous receptors but do not have adequate voltage-gated sodium channels to exhibit electrical excitability. Excitation of astrocytes takes place via calcium influx. Increased intracellular calcium concentration in astrocytes causes the release of glutamate, ATP and other neuroactive chemicals that are involved in controlling the synaptic activity of nearby neurons(75). Figure C-1 shows the main mechanism for neuron-astrocyte interactions which will be modelled mathematically.

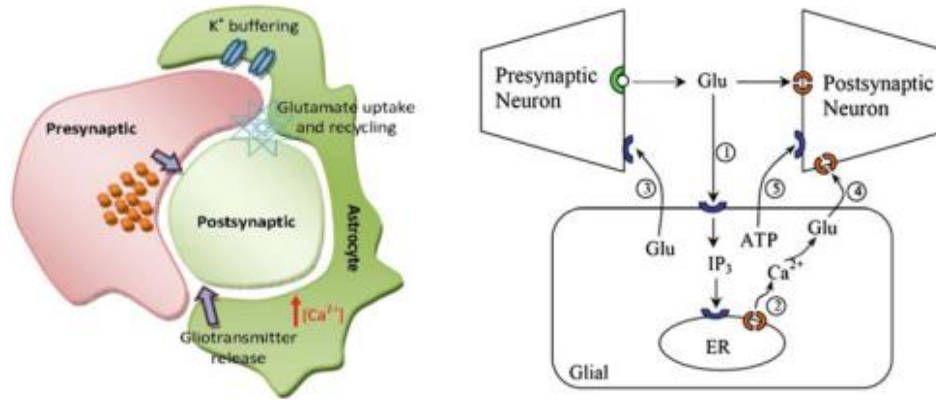


Figure C-1: A schematic of the main pathways for neuron–astrocyte interactions: (1) Release of glutamate from the presynaptic neuron activates astrocytic receptors and (2) induces an increase in intracellular Ca^{2+} levels. (3) The release of glutamate from astrocyte activates presynaptic receptors and regulates neurotransmitter release, while (4) activation of postsynaptic receptors directly depolarizes neurons. (5) Stimulation of astrocyte elicits also the release of ATP which, in turn, inhibits nearby neurons(76)

A dynamic model introduced by Postnov *et al.* (77, 78) is used to describe the intracellular calcium waves produced by astrocytes. This model is shown in the following equations:

$$\tau_c \frac{dc}{dt} = -c - c_4 f(c, c_e) + (r + \beta S_m) \quad \text{Eqn. C-15}$$

$$\varepsilon_c \tau_c \frac{dc_e}{dt} = f(c, c_e) \quad \text{Eqn. C-16}$$

$$f(c, c_e) = c_1 \frac{c^2}{1 + c^2} - \left(\frac{c_e^2}{1 + c_e^2} \right) \left(\frac{c^4}{c_2^4 + c^4} \right) - c_3 c_e \quad \text{Eqn. C-17}$$

$$\tau_{S_m} \frac{dS_m}{dt} = (1 + \tanh [S_{S_m}(z - h_{S_m})]) * (1 - S_m) - \frac{S_m}{d_{S_m}} \quad \text{Eqn. C-18}$$

$$\tau_{G_m} \frac{dG_m}{dt} = (1 + \tanh [S_{G_m}(z - h_{G_m})]) * (1 - G_m) - \frac{G_m}{d_{G_m}} \quad \text{Eqn. C-19}$$

The variables, c and c_e denotes the astrocyte cytoplasmic calcium concentration and the calcium concentration within the endoplasmic reticulum respectively. The parameters ε_c and τ_c are used to define the characteristic time for calcium oscillation. The influx of calcium is modulated by the production of secondary messenger (S_m) IP₃. The movement of calcium between the ER and the cytoplasm is defined by the non-linear function $f(c, c_e)$. During simulations, the control parameters $r, \beta, \tau_c, \tau_{S_m}, \tau_{G_m}, S_{S_m}, S_{G_m}, h_{S_m}, h_{G_m}, d_{S_m}, d_{G_m}$ are set to the values listed in Table C-1. These values are taken from Amiri et al. (74).

Table C-1: Parameter values used in the simulations (74)

| | | | | | | | | | |
|----------------|--------|--------------|--------|-----------------|-------|---------------|---------------------------|-----------------|-------|
| c_1 | 0.13 | c_2 | 0.9 | c_3 | 0.004 | c_4 | $\frac{1}{\varepsilon_c}$ | r | 0.02 |
| β | 1 | τ_{S_m} | 10 | h_{S_m} | 0.015 | d_{S_m} | 0.071 | τ_c | 2 |
| S_{S_m} | 100 | a | 2 | ε_c | 0.01 | D_n | 10^{-5} | τ_n | 5 |
| \bar{g}_{Ca} | 1 | \bar{g}_k | 2 | \bar{g}_L | 0.5 | \emptyset | 1.107 | \hat{v}_2 | 0.15 |
| \hat{v}_4 | 0.145 | v^+ | -0.217 | σ_s | 0.02 | β_s | 0.05 | \emptyset_s | 0.2 |
| v_{Ca} | 1 | v_k | -0.7 | v_L | -0.5 | \hat{v}_1 | -0.01 | \hat{v}_3 | 0.1 |
| α_i | 0.0001 | g_{si} | 0.0051 | C | 1 | i_j^{const} | 0.02 | ε_j | 0.002 |

C2.3 Modeling Astrocyte Interactions with Two Coupled Neurons

The two Morris-Lecar neuron model is extended to add the modulating activity of astrocytes on signal strength. For the sake of mathematical simplicity, the two neurons are connected via gap junctions. Neuron-astrocyte interactions are modeled by a chemical

synapse to model the tripartite synapse. The concentration of neurotransmitter in the synaptic cleft is modeled by the following equation:

$$[T]_j = \frac{1}{1 + \exp\left(-\frac{v_j(t) - \theta_s}{\sigma_s}\right)}, \quad j = 1,2 \quad \text{Eqn. C-20}$$

where θ_s and σ_s are half-activation voltage and steepness of the sigmoid function, respectively. The input of an astrocyte (z) is concentration of the neurotransmitter ($[T]_j$) released by activated neuron, and it triggers the IP_3 production. This is defined by:

$$z = a \sum_{j=1}^2 [T]_j \quad \text{Eqn. C-21}$$

The variable a is greater than zero and is an amplifying parameter. The output of the astrocyte is as follows:

$$i_j^{ast} = \lambda_j \cdot G_m, \quad j = 1,2 \quad \text{Eqn. C-22}$$

Astrocyte interactions can either have excitatory or inhibitory effects on neurons. For this model, excitatory effects of astrocytes on neurons are indicated by positive signs and inhibitory effects, negative signs. To illustrate these interactions of astrocytes with neighboring neurons “ $+i^{ast}$ ” and “ $-i^{ast}$ ” is added to Equation 4-3. The complete equations for the current of the neuron are as follows:

$$i_1(t) = i_j^{constant}(t) + i_j^{noise}(t) + i_j^{slow}(t) + i_j^{ast}(t) \quad \text{Eqn. C-23}$$

$$i_2(t) = i_j^{constant}(t) + i_j^{noise}(t) + i_j^{slow}(t) - i_j^{ast}(t) \quad \text{Eqn. C-24}$$

$$i_j^{ast}(t) = \lambda_j \cdot G_m \text{ and } \lambda_j > 0$$

The coupled Morris-Lecar model is also modified to include the astrocyte outputs as follows:

$$\frac{dv_1}{dt} = f(v_1, w_1, i_1 - i_1^{ast}(t)) \quad \text{Eqn. C-25}$$

$$+ g_{se}(v_2 - v_1) + i_1^{ast}(t)$$

$$\frac{dv_2}{dt} = f(v_2, w_2, i_2 - i_2^{ast}(t)) + \quad \text{Eqn. C-26}$$

$$g_{si}(v_1 - v_2) + i_2^{ast}(t)$$

C2.4 Computational Analysis of Neural Synchrony

To mathematically analyze the effect of astrocytes on neural synchrony, one must first define the concept of synchronization. Two theorems have been provided by Labourian et al. and Wang et al. to describe neural synchrony(79). Amiri et al. went on to use these theorems to also describe neural desynchronization in the presence of astrocytes. The theorem simply states that if two neurons are strongly coupled, they can be synchronized regardless of the initial conditions and parameter values(74). The physiological situation in which astrocyte contribution to synaptic regulation is considered.

Results of this simulation is shown in Figure C-1. The top panel shows the increase of coupling level, g_{se} , and the middle panel demonstrates the membrane potential of the coupled neurons. In this simulation, it is assumed that the astrocyte begins to interact with the coupled neurons at $t = 7000$ s. It is shown here that the astrocyte modifies the synaptic currents by providing appropriate feedback actions. Consequently, runaway excitation is compensated, and normal asynchronous behavior is again resumed quickly.

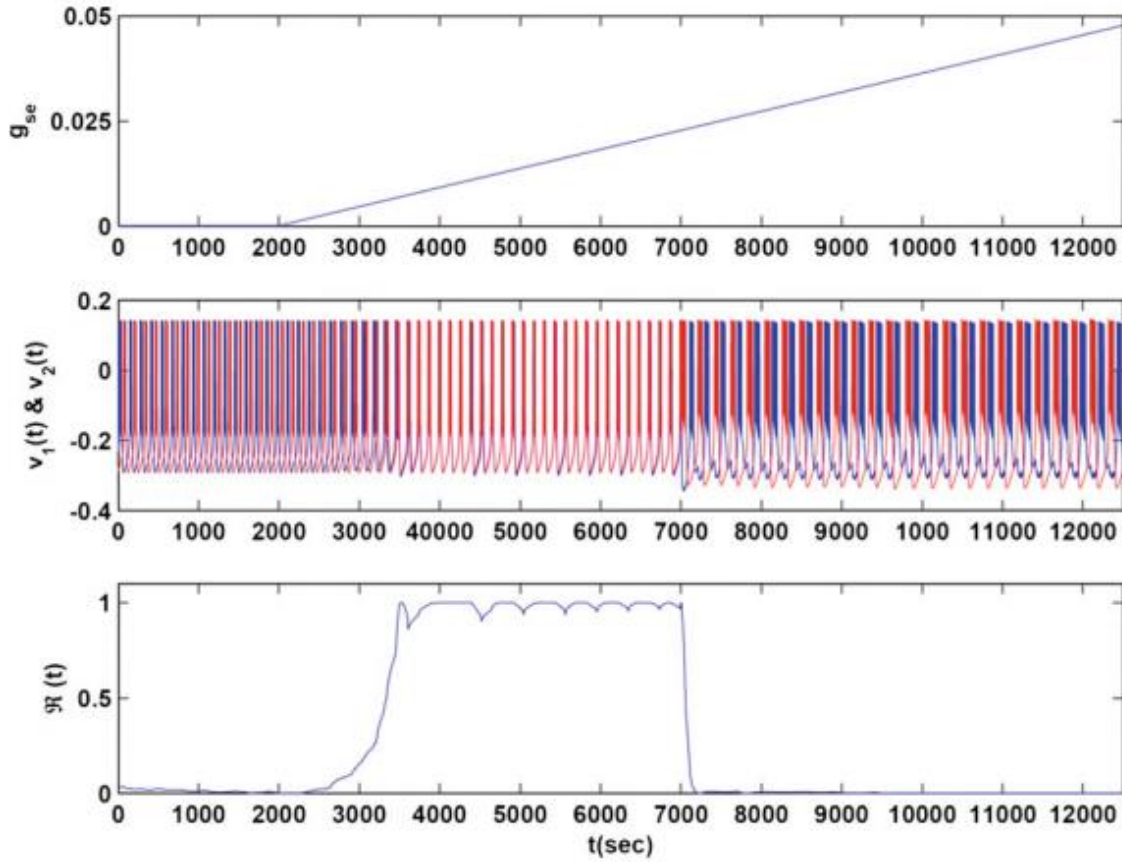


Figure C-2: The effect of varying coupling strength (g_{se}) in two coupled neurons in which the interaction of astrocyte with the individual neurons is included for $t > 7000$ s.

In this case, astrocyte provides balanced excitation and inhibition to coordinate synaptic interactions. The bottom panel shows the synchronization index. It is apparent that the concurrent firing of neurons is disturbed by feedback from astrocyte.

C2.4 Neural Population Model

The minimal, two M-L neuron mathematical model can be extended to a model consisting of 50 pyramidal neurons (PY) and 50 interneurons (IN) that are arranged in a rectangular grid with dimensions 0.1×0.1 spatial units. The feed forward inhibition of pyramidal neurons by adjacent interneurons is considered within this model. The total synaptic current of the j th neuron from the other neurons within the population is given as follows (80):

$$i_j^{sys}(t) = g_{se}(v_j(t) - v_{se}) \sum_{i,exc} g_i(t) + g_{si}(v_j(t) - v_{si}) \sum_{i,inh} g_i(t) \quad \text{Eqn. C-27}$$

g_{se} and g_{si} are the conductances of the excitatory and inhibitory synapses, v_{se} and v_{si} are excitatory and inhibitory reversal potentials and the sum is taken with respect to the index i running over excitatory and inhibitory synapses. The current for individual neurons within the population is as follows:

$$i_j(t) = i_j^{const}(t) + i_j^{slow}(t) + i_j^{sys}(t) + i_j^{noise}(t) \quad \text{Eqn. C-28}$$

The excitatory synapse conductance (g_{se}) is used to control the level of excitation within the system. The local field potential of the neuronal population is measured as follows:

$$v_o(t) = \left(\frac{R_e}{4\pi}\right) \sum_j \left(\frac{i_{vj}(t)}{r_j}\right) \quad \text{Eqn. C-29}$$

R_e is the extracellular resistance and is assumed to be homogeneous. To normalize the output signal, $v_o(t)$, we use:

$$R_e = 4\pi \sum_j r_j \cdot i_{vj}(t) \quad \text{Eqn. C-30}$$

$\sum_j r_j \cdot i_{vj}(t)$ is the sum of the ionic currents and r_j is the distance between the j th and the electrode used to measure the currents. A low pass filter is then used to filter the output signal $v_o(t)$ as follows:

$$\frac{dv_j}{dt} = v_0 - 0.1v_f(t) \quad \text{Eqn. C-31}$$

As a result, when the neurons are synchronized, the output of the filter has a high amplitude and in an asynchronous population, the output is very noisy.

C2.5 Astrocyte model for the neural population

The dynamic model developed based on the Li-Rinzel model(81). This model is illustrated by the following equations:

$$\frac{d[IP_3]}{dt} = \frac{(IP_3^* - IP_3)}{\tau_{IP_3}} + r_{IP_3}[T] \quad \text{Eqn. C-32}$$

$$\frac{d[Ca^{2+}]}{dt} = J_{chan} - J_{pump} + J_{leak} \quad \text{Eqn. C-33}$$

$$\frac{dq}{dt} = \alpha_q(1 - q) - \beta_q q \quad \text{Eqn. C-34}$$

$[Ca^{2+}]$ is the cytosolic calcium concentration, q is the fraction of activated IP_3 receptors and IP_3^* is the equilibrium IP_3 concentration. J_{chan} , J_{pump} and J_{leak} are the calcium influx from the ER to the cytosol, the pump flux from the cytoplasm to ER, and the leakage flux from the ER to cytosol, respectively. These values are given in the following expressions:

$$J_{chan} = c_1 v_1 p_\infty^3 n_\infty^3 q^3 ([Ca^{2+}]_{ER} - [Ca^{2+}]) \quad \text{Eqn. C-35}$$

$$J_{leak} = c_1 v_1 ([Ca^{2+}]_{ER} - [Ca^{2+}]) \quad \text{Eqn. C-36}$$

$$J_{pump} = \frac{v_3 [Ca^{2+}]^2}{[Ca^{2+}] + k_3^2} \quad \text{Eqn. C-37}$$

$$p_\infty = \frac{[IP_3]}{[IP_3] + d_1} \quad \text{Eqn. C-38}$$

$$n_\infty = \frac{[Ca^{2+}]}{[Ca^{2+}] + d_5} \quad \text{Eqn. C-39}$$

$$\alpha_q = a_2 d_2 \frac{[IP_3] + d_1}{[IP_3] + d_3} \quad \text{Eqn. C-40}$$

$$\beta_q = a_2 [Ca^{2+}] \quad \text{Eqn. C-41}$$

$$[Ca^{2+}]_{ER} = \frac{c_0 - [Ca^{2+}]}{c_1} \quad \text{Eqn. C-42}$$

$[Ca^{2+}]_{ER}$ is the concentration of calcium within the endoplasmic reticulum (ER).

C2.6 Astrocyte -Neuron interaction for the neural population

The model for astrocyte- neuron interactions for the neural population is as follows:

$$\frac{df}{dt} = \frac{-f}{\tau_{Ca^{2+}}} + (1 - f)K\emptyset([Ca^{2+}] - [Ca^{2+}]_{th}) \quad \text{Eqn. C-43}$$

Where \emptyset is the Heaviside function and K is the scaling factor. To model astrocyte coupling, the differential equation for IP_3 concentration is modified by adding the intracellular coupling term J_G .

$$J_G = \sum_j k_{gj}([IP_3]_j - [IP_3]_i) \quad \text{Eqn. C-44}$$

k_{gj} denotes the coupling co-efficient for gap-junctional diffusion from the j th astrocyte.

Astrocytes within a neural circuit have similar k_{gj} . The output of the astrocyte is:

$$i^{ast} = \gamma \cdot f \quad \text{Eqn. C-45}$$

The full expression for the current of the j th pyramidal neuron is:

$$i_j^{PY}(t) = i_j^{const}(t) + i_j^{slow}(t) + i_j^{sys}(t) + i_j^{noise}(t) - i_j^{ast}(t) \quad \text{Eqn. C-46}$$

The full expression for the current of the j th interneuron is:

$$i_j^{IN}(t) = i_j^{const}(t) + i_j^{slow}(t) + i_j^{sys}(t) + i_j^{noise}(t) + i_j^{ast}(t) \quad \text{Eqn. C-47}$$

The values of the parameters used for the simulations are shown in Table 4-2.

Table C-2: Parameters used in the simulation of the extended neural population model(8)

| | | | | | |
|----------------|----------------------|----------------|--------------------------|-------------|--------------------|
| v_1 | $6s^{-1}$ | k_3 | $0.1 \mu\text{M}$ | d_3 | $0.94 \mu\text{M}$ |
| IP_3^* | $0.16\mu\text{M}$ | v_2 | $0.11 s^{-1}$ | d_1 | $0.13 \mu\text{M}$ |
| c_1 | 0.185 | v_3 | $0.9 \mu\text{M s}^{-1}$ | d_2 | $1.05 \mu\text{M}$ |
| r_{IP_3} | 7.2mMs^{-1} | \bar{g}_k | 2 | \bar{g}_L | 0.5 |
| c_1 | 0.185 | v^* | -0.22 | σ_s | 0.02 |
| \bar{g}_{Ca} | 1 | v_k | -0.7 | v_L | -0.5 |
| \hat{v}_4 | 0.145 | θ_s | 0.2 | α_s | 0.1 |
| v_a | 1 | \bar{g}_{si} | 0.1 | $[Ca]_{th}$ | 0.2 |

Simulation results of the proposed model under different conditions are presented. All the simulations were implemented in Simulink (MATLAB).

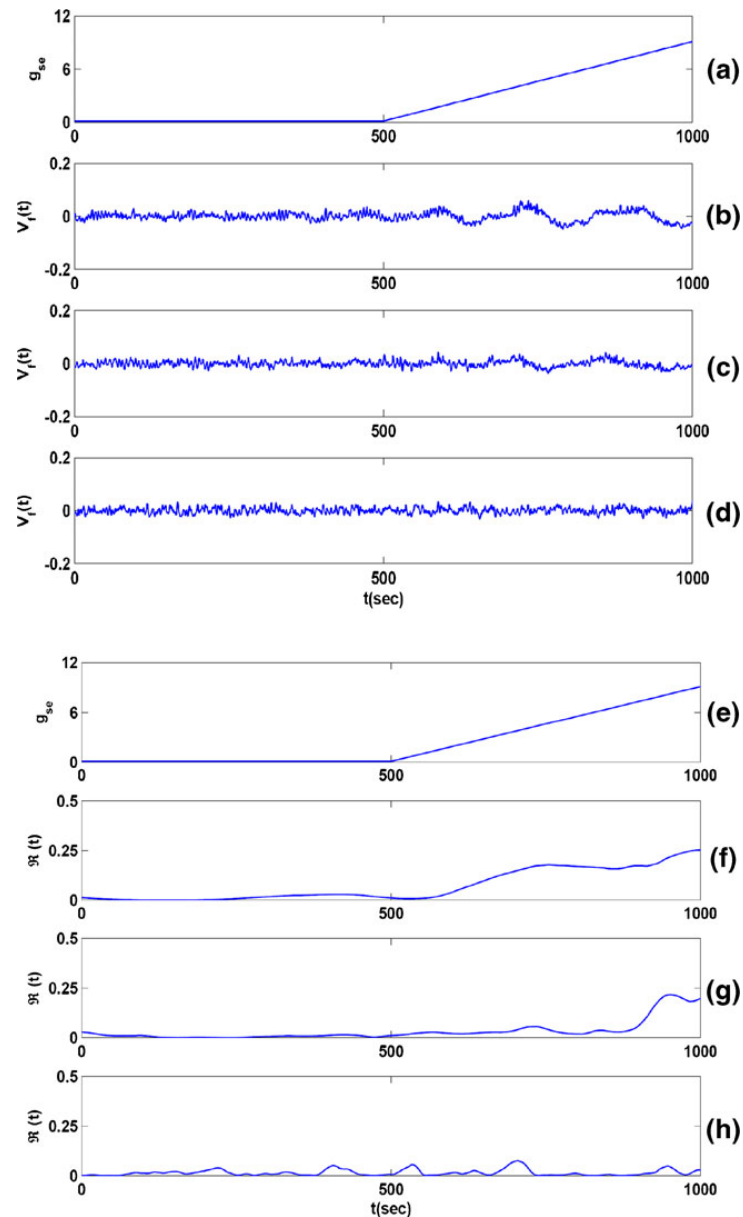


Figure C-3: The effect of increasing astrocyte-neuron interactions in the neural population model. (a) and (e) show the profile of increasing coupling strength g_{se} . (b)–(d) show the LFP recorded by the measurement electrode and (f)–(h) show the synchronization index for the different level of astrocyte-neuron interactions. (b) and (f) show the results of simulation for the neuronal population of Fig. 3(a) which is a neuronal network without astrocyte or equivalently $\gamma_1=0, \gamma_2=0$. In this case, increasing g_{se} leads to the neurons in the population get synchronized. (c) and (g) are for the extended neuronal networks in which astrocyte neuron interactions are also considered. For these simulations $\gamma_1=0.25$ and $\gamma_2=0.2$. In this case, due to the astrocyte neuron interaction, neuronal synchrony has been decreased compared to (b) and (f). In (d) and (h), the astrocyte-neuron interactions are again increased by setting $\gamma_1=0.7$ and $\gamma_2=0.6$ which leads to the asynchronous firing of the neurons.

BIBLIOGRAPHY

1. Organization WH. Neurological Disorders, public health challenges. 2006.
2. Cotrina ML, Nedergaard M. Astrocytes in the aging brain. *J Neurosci Res.* 2002;67(1):1-10.
3. Bruce-Keller AJ. Microglial-neuronal interactions in synaptic damage and recovery. *J Neurosci Res.* 1999;58(1):191-201.
4. Sejnowski TJ, Churchland PS, Movshon JA. Putting big data to good use in neuroscience. *Nat Neurosci.* 2014;17(11):1440-1.
5. *Fundamental Neuroscience.* Larry Squire DB, Floyd E. Bloom, Sascha du Lac, Anirvin Ghosh, Nicholas C. Spitzer, editor: Elsevier; 2012. 1152 p.
6. Bezzi P, Volterra A. A neuron-glia signalling network in the active brain. *Curr Opin Neurobiol.* 2001;11(3):387-94.
7. Haydon PG. GLIA: listening and talking to the synapse. *Nat Rev Neurosci.* 2001;2(3):185-93.
8. Amiri M, Hosseinmardi N, Bahrami F, Janahmadi M. Astrocyte-neuron interaction as a mechanism responsible for generation of neural synchrony: a study based on modeling and experiments. *J Comput Neurosci.* 2013;34(3):489-504.
9. Robertson JM. The Astrocentric Hypothesis: proposed role of astrocytes in consciousness and memory formation. *J Physiol Paris.* 2002;96(3-4):251-5.

10. Helmut Kettenmann FK, Alexei Verkhratsky. Microglia: New Roles for the Synaptic Stripper. *Neuron*. 2013;77:10-8.
11. Wake H, Moorhouse AJ, Jinno S, Kohsaka S, Nabekura J. Resting microglia directly monitor the functional state of synapses in vivo and determine the fate of ischemic terminals. *J Neurosci*. 2009;29(13):3974-80.
12. Ullian EM, Sapperstein SK, Christopherson KS, Barres BA. Control of synapse number by glia. *Science*. 2001;291(5504):657-61.
13. Del Puerto A, Wandosell F, Garrido JJ. Neuronal and glial purinergic receptors functions in neuron development and brain disease. *Front Cell Neurosci*. 2013;7:197.
14. Schousboe A. Transport and metabolism of glutamate and GABA in neurons are glial cells. *Int Rev Neurobiol*. 1981;22:1-45.
15. Fontainhas AM, Wang M, Liang KJ, Chen S, Mettu P, Damani M, et al. Microglial morphology and dynamic behavior is regulated by ionotropic glutamatergic and GABAergic neurotransmission. *PLoS One*. 2011;6(1):e15973.
16. DeCoster MA. Calcium dynamics in the central nervous system. *Adv Neuroimmunol*. 1995;5(3):233-9.
17. Grienberger C, Konnerth A. Imaging calcium in neurons. *Neuron*. 2012;73(5):862-85.
18. Simms BA, Zamponi GW. Neuronal voltage-gated calcium channels: structure, function, and dysfunction. *Neuron*. 2014;82(1):24-45.
19. Hall GACaJE. *Textbook of Medical Physiology*. 11 ed: Elsevier Saunder; 2006.
20. Roberts BJHaJL. *From Molecules to Networks: An Introduction to Cellular and Molecular Neurosciences*. Elsevier Science. 2004.
21. Catterall WA. Voltage-gated calcium channels. *Cold Spring Harb Perspect Biol*. 2011;3(8):a003947.

22. Clapham DE. Calcium signaling. *Cell*. 2007;131(6):1047-58.
23. Wheeler D.G. GRD, Ma H., Barrett C.F., Owen S.F. Safa P., Tsien R.W. Ca(V)1 and Ca(V)2 channels engage distinct modes of Ca(2+) signaling to control CREB-dependent gene expression. *Cell*. 2012;149:1112-24.
24. Bliss TVP, Collingridge GL. A Synaptic Model of Memory - Long-Term Potentiation in the Hippocampus. *Nature*. 1993;361(6407):31-9.
25. Rosenmund C, Feltz A, Westbrook GL. Calcium-dependent inactivation of synaptic NMDA receptors in hippocampal neurons. *J Neurophysiol*. 1995;73(1):427-30.
26. Tong G, Shepherd D, Jahr CE. Synaptic desensitization of NMDA receptors by calcineurin. *Science*. 1995;267(5203):1510-2.
27. Mennerick S, Zorumski CF. Postsynaptic modulation of NMDA synaptic currents in rat hippocampal microcultures by paired-pulse stimulation. *J Physiol*. 1996;490 (Pt 2):405-17.
28. Brasnjo G, Otis TS. Neuronal glutamate transporters control activation of postsynaptic metabotropic glutamate receptors and influence cerebellar long-term depression. *Neuron*. 2001;31(4):607-16.
29. Wanjerkhede SM, Bapi RS. Role of CAMKII in reinforcement learning: a computational model of glutamate and dopamine signaling pathways. *Biol Cybern*. 2011;104(6):397-424.
30. Silva AJ. Molecular and cellular cognitive studies of the role of synaptic plasticity in memory. *J Neurobiol*. 2003;54(1):224-37.
31. Upreti C, Zhang XL, Alford S, Stanton PK. Role of presynaptic metabotropic glutamate receptors in the induction of long-term synaptic plasticity of vesicular release. *Neuropharmacology*. 2013;66:31-9.
32. Niswender CM, Conn PJ. Metabotropic glutamate receptors: physiology, pharmacology, and disease. *Annu Rev Pharmacol Toxicol*. 2010;50:295-322.

33. Singh P, Hockenberry AJ, Tiruvadi VR, Meaney DF. Computational investigation of the changing patterns of subtype specific NMDA receptor activation during physiological glutamatergic neurotransmission. *PLoS Comput Biol.* 2011;7(6):e1002106.
34. Kroemer G, Galluzzi L, Vandenabeele P, Abrams J, Alnemri ES, Baehrecke EH, et al. Classification of cell death: recommendations of the Nomenclature Committee on Cell Death 2009. *Cell Death Differ.* 2009;16(1):3-11.
35. Kerr JF, Wyllie AH, Currie AR. Apoptosis: a basic biological phenomenon with wide-ranging implications in tissue kinetics. *Br J Cancer.* 1972;26(4):239-57.
36. Orrenius S, Gogvadze V, Zhivotovsky B. Calcium and mitochondria in the regulation of cell death. *Biochem Biophys Res Commun.* 2015;460(1):72-81.
37. Danese A, Patergnani S, Bonora M, Wieckowski MR, Previati M, Giorgi C, et al. Calcium regulates cell death in cancer: Roles of the mitochondria and mitochondria-associated membranes (MAMs). *Biochim Biophys Acta.* 2017;1858(8):615-27.
38. Joza N, Susin SA, Daugas E, Stanford WL, Cho SK, Li CY, et al. Essential role of the mitochondrial apoptosis-inducing factor in programmed cell death. *Nature.* 2001;410(6828):549-54.
39. Sattler R, Tymianski M. Molecular mechanisms of calcium-dependent excitotoxicity. *J Mol Med (Berl).* 2000;78(1):3-13.
40. Olney JW. Excitotoxicity: an overview. *Can Dis Wkly Rep.* 1990;16 Suppl 1E:47-57; discussion -8.
41. Kass IS, Lipton P. Mechanisms involved in irreversible anoxic damage to the in vitro rat hippocampal slice. *J Physiol.* 1982;332:459-72.
42. DeCoster MA, Schabelman E, Tombran-Tink J, Bazan NG. Neuroprotection by pigment epithelial-derived factor against

- glutamate toxicity in developing primary hippocampal neurons. *J Neurosci Res.* 1999;56(6):604-10.
43. Barreto-Chang OL, Dolmetsch RE. Calcium imaging of cortical neurons using Fura-2 AM. *J Vis Exp.* 2009(23).
 44. Kim WT, Rioult MG, Cornell-Bell AH. Glutamate-induced calcium signaling in astrocytes. *Glia.* 1994;11(2):173-84.
 45. Kelly KC. Use of Randomized Submaximal Glutamate Stimulus to Interpret Glial Effects on Neuronal Calcium Dynamics. *Neurochemistry and Neuropharmacology Open Access.* 2015;1(1).
 46. Tsien RY, Pozzan T, Rink TJ. Calcium homeostasis in intact lymphocytes: cytoplasmic free calcium monitored with a new, intracellularly trapped fluorescent indicator. *J Cell Biol.* 1982;94(2):325-34.
 47. Paredes RM, Etzler JC, Watts LT, Zheng W, Lechleiter JD. Chemical calcium indicators. *Methods.* 2008;46(3):143-51.
 48. Alonso MT, Chamero P, Villalobos C, Garcia-Sancho J. Fura-2 antagonises calcium-induced calcium release. *Cell Calcium.* 2003;33(1):27-35.
 49. Marambaud P, Dreses-Werringloer U, Vingtdoux V. Calcium signaling in neurodegeneration. *Mol Neurodegener.* 2009;4:20.
 50. Danbolt NC. Glutamate uptake. *Prog Neurobiol.* 2001;65(1):1-105.
 51. Coulter DA, Eid T. Astrocytic regulation of glutamate homeostasis in epilepsy. *Glia.* 2012;60(8):1215-26.
 52. Cavus I, Kasoff WS, Cassaday MP, Jacob R, Gueorguieva R, Sherwin RS, et al. Extracellular metabolites in the cortex and hippocampus of epileptic patients. *Ann Neurol.* 2005;57(2):226-35.
 53. Ben-Ari Y. Limbic seizure and brain damage produced by kainic acid: mechanisms and relevance to human temporal lobe epilepsy. *Neuroscience.* 1985;14(2):375-403.

54. Fahn S. Description of Parkinson's disease as a clinical syndrome. *Ann N Y Acad Sci.* 2003;991:1-14.
55. Surmeier DJ, Schumacker PT, Guzman JD, Ilijic E, Yang B, Zampese E. Calcium and Parkinson's disease. *Biochem Biophys Res Commun.* 2017;483(4):1013-9.
56. Rajkowska G, Stockmeier CA. Astrocyte pathology in major depressive disorder: insights from human postmortem brain tissue. *Curr Drug Targets.* 2013;14(11):1225-36.
57. Braun K, Antemano R, Helmeke C, Buchner M, Poeggel G. Juvenile separation stress induces rapid region- and layer-specific changes in S100ss- and glial fibrillary acidic protein-immunoreactivity in astrocytes of the rodent medial prefrontal cortex. *Neuroscience.* 2009;160(3):629-38.
58. Soisson SM, MacDougall-Shackleton B, Schleif R, Wolberger C. Structural basis for ligand-regulated oligomerization of AraC. *Science.* 1997;276(5311):421-5.
59. Daniel B, DeCoster MA. Quantification of sPLA(2)-induced early and late apoptosis changes in neuronal cell cultures using combined TUNEL and DAPI staining. *Brain Res Protoc.* 2004;13(3):144-50.
60. Zaheer A, Mathur SN, Lim R. Overexpression of glia maturation factor in astrocytes leads to immune activation of microglia through secretion of granulocyte-macrophage-colony stimulating factor. *Biochem Biophys Res Commun.* 2002;294(2):238-44.
61. Martin DP, Wallace TL, Johnson EM, Jr. Cytosine arabinoside kills postmitotic neurons in a fashion resembling trophic factor deprivation: evidence that a deoxycytidine-dependent process may be required for nerve growth factor signal transduction. *J Neurosci.* 1990;10(1):184-93.
62. Hui CW, Zhang Y, Herrup K. Non-Neuronal Cells Are Required to Mediate the Effects of Neuroinflammation: Results from a Neuron-Enriched Culture System. *PLoS One.* 2016;11(1):e0147134.

63. Schott S, Bruning A. Induction of apoptosis in cervical cancer cells by the duplex drug 5-FdU-ECyd, coupling 2'-deoxy-5-fluorouridine and 3'-C-ethinylcytidine. *Gynecol Oncol.* 2014;135(2):342-8.
64. Ebada SS, Edrada RA, Lin W, Proksch P. Methods for isolation, purification and structural elucidation of bioactive secondary metabolites from marine invertebrates. *Nat Protoc.* 2008;3(12):1820-31.
65. Riss TL, Moravec RA, Niles AL, Duellman S, Benink HA, Worzella TJ, et al. Cell Viability Assays. In: Sittampalam GS, Coussens NP, Brimacombe K, Grossman A, Arkin M, Auld D, et al., editors. *Assay Guidance Manual.* Bethesda (MD)2004.
66. Zhang YF, Li X, Peng LL, Wang GH, Ke KF, Jiang ZL. Novel glycine-dependent inactivation of NMDA receptors in cultured hippocampal neurons. *Neurosci Bull.* 2012;28(5):550-60.
67. Finkel TH, Pabst MJ, Suzuki H, Guthrie LA, Forehand JR, Phillips WA, et al. Priming of neutrophils and macrophages for enhanced release of superoxide anion by the calcium ionophore ionomycin. Implications for regulation of the respiratory burst. *J Biol Chem.* 1987;262(26):12589-96.
68. Liu C, Hermann TE. Characterization of ionomycin as a calcium ionophore. *J Biol Chem.* 1978;253(17):5892-4.
69. Lautens M, Colucci JT, Hiebert S, Smith ND, Bouchain G. Total synthesis of ionomycin using ring-opening strategies. *Org Lett.* 2002;4(11):1879-82.
70. Sather W, Dieudonne S, MacDonald JF, Ascher P. Activation and desensitization of N-methyl-D-aspartate receptors in nucleated outside-out patches from mouse neurones. *J Physiol.* 1992;450:643-72.
71. DeCoster MA, Koenig ML, Hunter JC, Tortella FC. Calcium dynamics in neurons treated with toxic and non-toxic concentrations of glutamate. *Neuroreport.* 1992;3(9):773-6.

72. Luo M, Wu Y, Peng J. Washout filter aided mean field feedback desynchronization in an ensemble of globally coupled neural oscillators. *Biol Cybern.* 2009;101(3):241-6.
73. Morris C, Lecar H. Voltage oscillations in the barnacle giant muscle fiber. *Biophys J.* 1981;35(1):193-213.
74. Amiri M, Montaseri G, Bahrami F. On the role of astrocytes in synchronization of two coupled neurons: a mathematical perspective. *Biol Cybern.* 2011;105(2):153-66.
75. Silchenko AN, Tass PA. Computational modeling of paroxysmal depolarization shifts in neurons induced by the glutamate release from astrocytes. *Biol Cybern.* 2008;98(1):61-74.
76. Newman EA. New roles for astrocytes: regulation of synaptic transmission. *Trends Neurosci.* 2003;26(10):536-42.
77. Postnov DE, Ryazanova LS, Sosnovtseva OV. Functional modeling of neural-glia interaction. *Biosystems.* 2007;89(1-3):84-91.
78. Postnov DE, Koreshkov RN, Brazhe NA, Brazhe AR, Sosnovtseva OV. Dynamical patterns of calcium signaling in a functional model of neuron-astrocyte networks. *J Biol Phys.* 2009;35(4):425-45.
79. Huang D, Yamauchi K, Inden Y, Jun Y, Zheng J, Ida H, et al. Use of an artificial neural network to localize accessory pathways of Wolff-Parkinson-White syndrome with 12-lead electrocardiogram. *Medical Informatics & the Internet in Medicine.* 2005;30(4):277-86.
80. Amiri M, Bahrami F, Janahmadi M. Functional contributions of astrocytes in synchronization of a neuronal network model. *J Theor Biol.* 2012;292:60-70.
81. Li YX, Rinzel J. Equations for InsP₃ receptor-mediated [Ca²⁺]_i oscillations derived from a detailed kinetic model: a Hodgkin-Huxley like formalism. *J Theor Biol.* 1994;166(4):461-73.

82. Orive G, Anitua E, Pedraz JL, Emerich DF. Biomaterials for promoting brain protection, repair and regeneration. *Nat Rev Neurosci.* 2009;10(9):682-92.
83. Silva GA. Neuroscience nanotechnology: progress, opportunities and challenges. *Nat Rev Neurosci.* 2006;7(1):65-74.
84. Azzazy HM, Mansour MM, Kazmierczak SC. From diagnostics to therapy: prospects of quantum dots. *Clin Biochem.* 2007;40(13-14):917-27.
85. Brus LE. Electron-electron and electron-hole interactions in small semiconductor crystallites: The size dependence of the lowest excited electron state. *Chem Phys* 1984;80:4403-9.
86. Pathak S, Cao E, Davidson MC, Jin S, Silva GA. Quantum dot applications to neuroscience: new tools for probing neurons and glia. *J Neurosci.* 2006;26(7):1893-5.
87. Vu TQ, Maddipati R, Blute TA, Nehilla BJ, Nusblat L, Desai TA. Peptide-conjugated quantum dots activate neuronal receptors and initiate downstream signaling of neurite growth. *Nano Lett.* 2005;5(4):603-7.
88. Arredondo M, Nunez MT. Iron and copper metabolism. *Mol Aspects Med.* 2005;26(4-5):313-27.
89. Percival SS. Copper and immunity. *Am J Clin Nutr.* 1998;67(5 Suppl):1064S-8S.
90. Aranda-Anzaldo A. The post-mitotic state in neurons correlates with a stable nuclear higher-order structure. *Commun Integr Biol.* 2012;5(2):134-9.
91. Scheiber IF, Mercer JF, Dringen R. Metabolism and functions of copper in brain. *Prog Neurobiol.* 2014;116:33-57.
92. Scheiber IF, Dringen R. Astrocyte functions in the copper homeostasis of the brain. *Neurochem Int.* 2013;62(5):556-65.

93. Dringen R, Scheiber IF, Mercer JF. Copper metabolism of astrocytes. *Front Aging Neurosci.* 2013;5:9.
94. Kelly KC, Wasserman JR, Deodhar S, Huckaby J, DeCoster MA. Generation of Scalable, Metallic High-Aspect Ratio Nanocomposites in a Biological Liquid Medium. *Jove-J Vis Exp.* 2015(101).
95. Tischler AS, Greene LA. Nerve growth factor-induced process formation by cultured rat pheochromocytoma cells. *Nature.* 1975;258(5533):341-2.
96. Karan A, Darder M, Kansakar U, Norcross Z, DeCoster MA. Integration of a Copper-Containing Biohybrid (CuHARS) with Cellulose for Subsequent Degradation and Biomedical Control. *Int J Environ Res Public Health.* 2018;15(5).
97. Ni M, Aschner M. Neonatal rat primary microglia: isolation, culturing, and selected applications. *Curr Protoc Toxicol.* 2010;Chapter 12:Unit 12 7.
98. Kubista M, Akerman B, Norden B. Characterization of interaction between DNA and 4',6-diamidino-2-phenylindole by optical spectroscopy. *Biochemistry.* 1987;26(14):4545-53.
99. DAPI Counterstaining Protocols 2006 [Available from: <https://www.thermofisher.com/us/en/home/references/protocols/cell-and-tissue-analysis/dapi-protocol/basic-dapi-counterstaining-protocols.html#prot7>].
100. Eng LF, Ghirnikar RS, Lee YL. Glial fibrillary acidic protein: GFAP-thirty-one years (1969-2000). *Neurochem Res.* 2000;25(9-10):1439-51.
101. Douglas R. Pfeiffer, Peter W. Reed, and Henry A. Lardy. Ultraviolet and Fluorescent Spectral Properties of the Divalent Cation Ionophore A23187 and Its Metal Ion Complexes. *Biochemistry.* 1974;13(4007-14)
102. Peter J. Yunker , Tim Still1, Matthew A. Lohr and A. G. Yodh. Suppression of the coffee-ring effect by shape-dependent capillary interactions. *Nature.* 2011;476(308-11)

